Analysis of Electric Disturbances from the Static Frequency Converter of a Pumped Storage Station

Sebastian P. Rosado

Thesis submitted to the Faculty of the Virginia Polytechnic Institute and State University in partial fulfillment of the requirements for the degree of

Master of Science

in

Electrical Engineering

Dr. Yilu Liu, Chair

Dr. Arun G. Phadke

Dr. Jaime de la Ree Lopez

August 9, 2001

Blacksburg, Virginia

Keywords: power quality, power system transients, power system harmonics, power transformers, synchronous machines, variable speed drives, frequency conversion, power system modeling

Analysis of Electric Disturbances from the Static Frequency Converter of a Pumped Storage Station

Sebastian P. Rosado

Abstract

The present work studies the disturbances created in the electric system of a pumped storage power plant, which is an hydraulic generation facility where the machines can work as turbines or pumps, by the operation of a static frequency converter (SFC). The SFC is used for starting the synchronous machines at the station when in the pump mode. During the starting process several equipment is connected to the SFC being possible to get affected by the disturbances generated. These disturbances mainly include the creation of transient overvoltages during the commutation of the semiconductor devices of the SFC and the introduction of harmonics in the network currents and voltages. This work analyzes the possible effects of the SFC operation over the station equipment based on computer simulations. For this purpose, the complete system was modeled and the starting process simulated in a computer transient simulator program. The work begins with a general review of the effects of electric disturbances over high voltage equipment and in particular of the disturbances generated by power electronics conversion equipment. Then the models for the different kind of equipment present in the system are discussed and formulated. The control system that governs the operation of the SFC during the starting process is analyzed later as well as the operation conditions. Once the model of the system is set up, the harmonic analysis of the electric network is done by frequency domain and time domain methods. Time domain methods are also employed for the analysis of the commutation transient produced by the SFC operation. Finally, the simulation results are used to evaluate the impact of the SFC operation on the station equipment, especially on the generator step up transformer.

Acknowledgments

There are too many people that helped me in one way or another to complete my Masters. In the department of Electrical Engineering at Virginia Tech I would like to thank everyone in the center for power engineering, especially my advisor Dr. Yilu Liu for her guidance during this two years. Thanks also to the other members of my committee Dr. Arun Phadke and Dr. Jaime de la Ree for the knowledge shared during this time, Dr. Virgilio Centeno and my lab partners for many useful technical (or not) discussions and their friendship, and Dr. Xuzhu Dong for his help during the development of part of this work. I am also grateful to the Fulbright Commission and the Organization of American States for sponsoring my master studies.

Most of all I would like to thank all my family, especially my parents for their unconditional support. And thanks God for allowing me reach this goal.

Table of Contents

List of Illustrations

List of Tables

1 Introduction

1.1 Object of the Study

The purpose of this study is to analyze the electric disturbances produced by the static frequency converter (SFC) starting a synchronous machine in a pumped storage station. The SFC is used during the start up process of the machine when used as a motor for pumping the water in the lower reservoir to the upper reservoir of the facility. In addition to the SFC starting, there are some other ways to start the synchronous motor; the most suitable alternative can be a simultaneous starting with a synchronous generator, called back-to-back, that provides the necessary voltage source of variable frequency. Although this last alternative is possible and is frequently used, the SFC has demonstrated to be more convenient from an operative an economic point of view [1]. On the other side, the operation of the SFC creates disturbances in the voltage at the machine and other connected equipment. Therefore, the magnitude and possible effects of those disturbances must be analyzed and the safety of the system assessed. This is especially necessary if, as in the case of the system under study, problems in the high voltage equipment connected to the SFC have been detected.

This study analyzes the disturbances created by the SFC and their possible effects over the high voltage equipment making special emphasis in the generator step up (GSU) transformer connecting each synchronous generator to the high voltage transmission system. This emphasis is originated in several failures that took place in these transformer that created serious economic losses to the company operating the facility. The study is based on simulations of the complete system under study done on a computer; the electromagnetic transient program PSCAD/EMTDC was used as simulation tool. Field measurements on the actual facility are used to validate the model and other considerations necessary for the analysis of the problem.

1.2 Description of the Facility under study

A simplified diagram of the electric configuration of the facility under study is shown in Figure 1.1. The station is connected to the high voltage transmission network through three 345 kV transmission lines. The high voltage (HV) bus bar and switching equipment is of the gas insulated system (GIS) type. There exist six synchronous machines operating at 16.5KV. A GSU transformer is connected to each machine converting the voltage form generation to transmission level allowing delivering the energy produced at the station while being used to feed the synchronous machines when working at the pump mode. The six 300 MVA, 16.5/345 kV GSU transformers are connected to the 345 kV GIS via oil-filled 345 kV cables of 630 m length. The transformers constructive characteristics are of the special three-phase type, namely, multi-tank units constructed with separate core and coil assemblies at each phase and connected with a common tank top cover. The GIS bus bars are of the single-phase type. Zinc Oxide surge arresters are provided at the end of the connecting buses in the GIS to protect the switchgear from incoming surges. There are no surge arresters connected at the HV side of the GSU transformer other than arresters at the GIS; therefore, this arresters connected after the 630 m cable are the only overvoltage protection existing at the HV side of the transformer.

For the synchronous machine starting process there are two alternatives. One possibility is to start two machines together, one working as generator and another working as motor, providing the generator the variable frequency, variable voltage required by the machine starting as a motor. The other alternative is to feed the starting synchronous motor from an independent source. In this case a static frequency converter is used as the variable frequency, variable voltage required for starting the synchronous machine. Starting the pump by the SFC has some advantages from the operative point of view like simplicity and the availability of the other machines to work independently. In the facility object of this study two SFCs are fed from the auxiliary bus of the station (not shown in Figure 1.1) and can be connected to each of the starting buses at 16.5 kV allowing (theoretically) for a simultaneous start of two machines. Once the SFC is connected to the desired machine, there is no isolation from the GSU transformer and transmission cable. Therefore, the GSU transformer

is connected to the SFC output voltage, but do not have any load connected to its high voltage (HV) side besides the 345 kV transmission cable.

In has been detected that three 345 kV GSU transformers failed successively in the pumped storage plant object of this study in recent years resulting in a considerable economic loss due to unavailability of delivering energy from the plant. These series of faults originated major concern in the company owing the facility and originated a series of investigations that include this work.

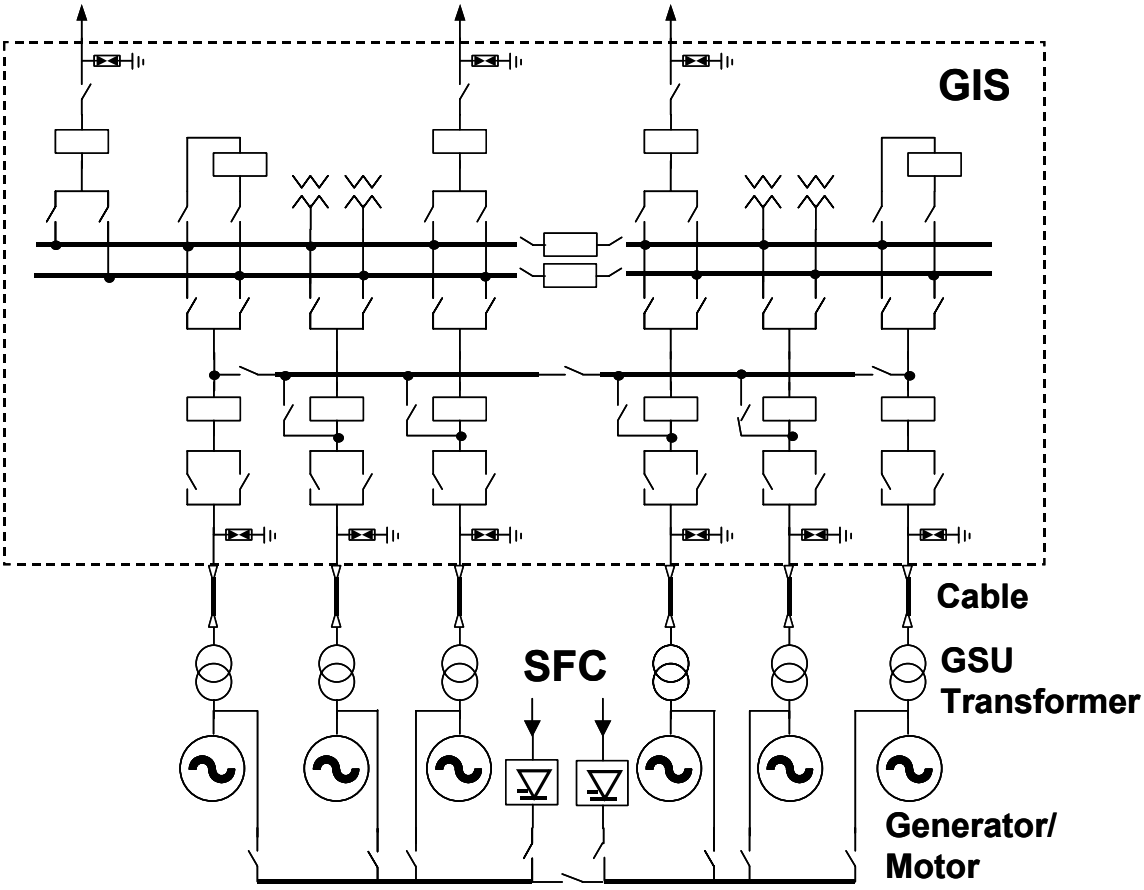

Figure 1.1. Simplified on-line diagram of the pumped storage generation station used during this study

An important characteristic of the operation of a pumped storage station is the relatively high number of switching of the HV equipment. In regular generation stations the

main power equipment, such as the GSU transformers, are connected or disconnected for long periods of time that can be of several months. In a pumped station, due to the frequent changes in the operation modes of the synchronous machines from generator to motor the number of switching events can reach a few per day. This frequent connection-disconnection introduces high requirements over the equipment insulation that needs to be analyzed.

2 Effects of Disturbances on the Electric Equipment

The electric disturbances affecting power equipment are primarily classified according to their time evolution and magnitude. Table 2.1 shows a general classification of the different kind of disturbances existing in an electric energy system. The danger that each type of disturbance can create on the equipment depends on its time evolution and relative magnitude to the rated parameters of the system. Therefore, the possibility of existence and characteristics of each kind of disturbance, and the proper countermeasures to mitigate their effects must be analyzed in detail.

Table 2.1 General classification of electric disturbances

Type of disturbance		**Causes**	**Characteristics**
Temporary	Overvoltages	Improper operation Resonance, Ferro-resonance Faults	Duration: From hundreds of msec to sec Magnitude: 1.1~1.3 pu
	Overcurrents	Overloads Protection Failure	Wide magnitude and duration range
Transients	Switching Transients	Switching Energization of HV equipment	Duration: hundreds of μsec Magnitude: 1.1~2 pu
	Very Fast Transients	Switching on special kind of equipment like GIS	Duration: μsec Magnitude: 1.1~2 pu
	Lighting	Atmospheric phenomena	Duration: μsec Magnitude: can be much larger than U_{rated}
Waveform Distortion	Harmonics Inter-harmonics Notching Noise	Non-linearity of equipment Non-linear loads Power electronic operation	Duration: Permanent Magnitude: wide range, harmonics can be larger than fundamental frequency magnitudes

2.1 Temporary Overvoltages and Overcurrents

This type of disturbance is a temporary increment of an electric magnitude over the limits the equipment is designed to withstand. It is generally a rated frequency oscillatory phenomenon undamped or weakly damped. The most common cause of this kind of disturbance is the resonance phenomena. The resonance is produced when the inductive and capacitive reactance in a portion of the electric system are roughly equal creating magnification of voltage or current according to the circuit configuration. Ferro-resonance creates amplification of the magnitudes based on the non-linearity of the ferro-magnetic core of electric machines [2]. The necessary capacitors for the resonant effect can be capacitor banks or the distributed capacitances of ungrounded cables or transmission lines. Ferro-resonance can lead to transformer overheating due to saturation that creates high current peaks and high flux density. The core saturation produces large harmonic components that increase the effect of the phenomenon. Usually there is an exciting phenomenon that starts the ferro-resonance effect. This can be a fault, or an undesired operation condition like a failed switching opening only one phase in a multi-phase system, or loss of grounding. Other mechanisms that can create temporary overvoltages are Ferranti effect, load rejection, over-excitation of synchronous machines, etc.

Overcurrents are produced when the rated current capacity of the system is exceeded. This can be created by a non-desired operation condition or by improper setting or working of the protection systems. The effect of an overcurrent is the overheating of the equipment circulated by that current that can lead to thermal degradation of the insulation and failure.

2.2 Switching Transients - Very Fast Transients

Switching transients result from switching operations in the power system or faults. The resulting voltage waveform has short duration and is highly damped, and its magnitude range is wide, being possible to be several times the rated voltage of the system. Phenomena like current chopping, pre-strike or re-strike can contribute to the increment of the effects of switching transients [3]. The most typical events that create switching overvoltages are: line energization and reclosing, fault inception and clearing, switching of capacitive and small

inductive currents and special switching operations like the switching of series capacitors or resonant circuits.

The effects of switching overvoltages on the equipment can be quite complex. Specifically, the windings of power transformers behave in a complex manner. As a result of this kind of transients, the voltage distribution along the winding can get a quite non-linear distribution producing regions where the dielectric stresses concentrate creating harmful conditions. Moreover, partial resonances can be generated inside the winding coil producing large voltage stresses at certain location of the windings [4]. These two effects can lead to failures in the transformer coil. As the phenomena has a large non-uniform distribution, harmful conditions can be reached even if the voltage on the whole winding is smaller than the machine design parameters as the basic insulation level (BIL). Therefore, the surge arresters may not properly protect the equipment against this situation. It is also possible that the switching voltage excites interaction between the different equipment in the system, like resonance, leading to an increment in the overvoltages.

Due to the constructive characteristics of GIS, especially the smaller insulation distances compared with conventional substations, the switching transient acquires special characteristics [5]. The time duration is very short and the frequencies involved very high, on the range of MHz, being named very fast transients (VFT), which are also characterized by its relatively frequent occurrence. The VFT waveform consists of a voltage step with a very short rise time superimposed with three major frequency clusters, one in the range of about 5 MHz, other in the range between 5 and 30 MHz and the other in the range of 100 MHz. Due to its high frequency characteristics, the VFT waveform propagation in the system is generally highly attenuated. Therefore, the equipment that is mostly affected by VFT is the one directly connected to the GIS.

The effects of VFT on the transformer windings are closely related with the characteristics that the overvoltage acquire [6]. The effects of VFT are similar to the ones created by regular switching transients, but due to its shorter duration and steepness the consequences are magnified. The stresses over certain parts of the transformer winding like the ends can be very large. Figure 2.1 is taken from [5] and shows the voltage distribution in a tapped winding transformer under VFT conditions where at certain frequencies the voltage at a portion of the tap winding, U_2, is larger than the total voltage U_1.

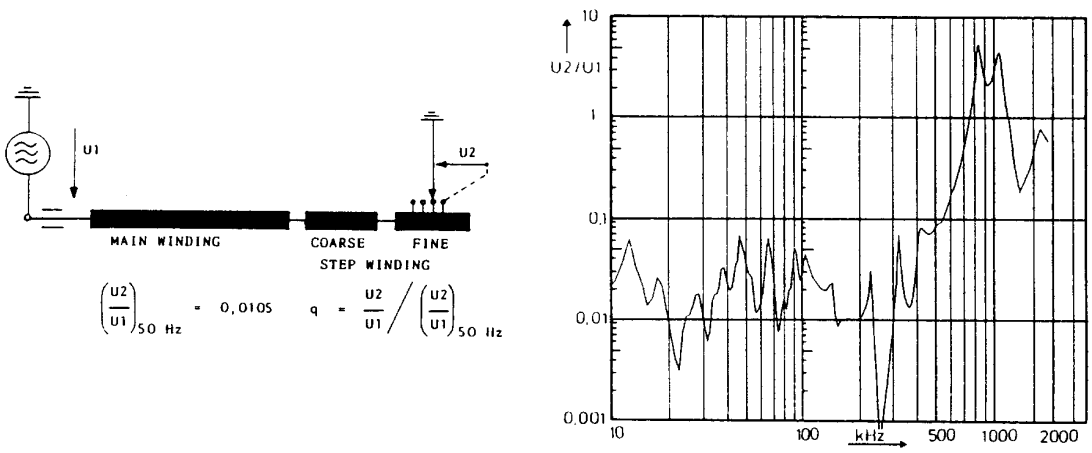

Figure 2.1 Voltage ratio between one step of a tapped winding and the whole HV winding vs. frequency (taken from [5])

2.3 Lightning

Lighting strikes can create large phase to phase or phase to ground overvoltages. Lightning overvoltages can be classified as direct stroke, when the strike directly impacts on the equipment; back flashovers, caused by strokes that impacted on a tower or grounding cable; and induced voltages, caused by strokes that have impacted on nearby equipment. The lightning overvoltage has duration between 1 and 100 μsec and the front wave lasts between 1 and 5 μsec. The lightning stroke can be modeled as a current source rather than a voltage source. The magnitude of the lightning current can be quite well approximated by Anderson's formula [7],

$$P_I = \frac{1}{1+\left(\frac{I}{31}\right)^{2.6}} \qquad (2\text{-}1)$$

where P_I is the probability of exceeding the lightning current I in kA.

The harmful effects of lightning overvoltages have been reduced to a reasonable level by proper design of the high voltage facilities, which include the use of surge arresters and other shielding devices. In case the overvoltages created by this phenomenon reaches the equipment terminals, the main effects are a consequence of the large magnitude of the

voltage. In a transformer this can creates failure of the main insulation, which is the insulation between windings. Also the distribution over the winding can produce stresses along the insulation due to the large magnitude of the voltage applied. Lightning overvoltages can also create similar effects than switching transients.

2.4 Waveform Distortion

These phenomena affect the shape of the voltage waveform in the permanent regime. A common cause of voltage distortion are harmonics, which are currents or voltages of a frequency that is an integer multiple of the fundamental frequency. Harmonic distortion is generated basically by the non-linear behavior of the system components. The harmonic composition of a waveform is generally analyzed through Fourier series [8]. The characterization of the harmonic content of a waveform can be done by the magnitude and phase of each harmonic component. A convenient way to characterize the harmonic content is by the total harmonic distortion indicator, which can be calculated by,

$$THD = \frac{\sqrt{\sum_{h=2}^{h\max} M_h^2}}{M_1} \qquad (2\text{-}2)$$

Where M_h is the rms value of the hth harmonic component h of the quantity M.

Harmonics in power system results in additional losses in the equipment circulated by the harmonic currents. The losses in most of the electrical equipment, such as rotating machines and transformers, are dependent on the frequency of the circulating current. Harmonic components are actually currents of frequency larger than the rated one. It is also possible that there exist some resonance between the system components at certain harmonic frequency. If this is the case, the harmonic currents and voltages are magnified producing large stresses over the equipment [9].

Interharmonics are components of the current and voltages with a frequency that is not an integer of the fundamental frequency. The causes if this kind of distortion can be of the same type of the harmonic sources, but the variability of the regime is generally also present in this case. Moreover, the effects are similar to the ones created by harmonics.

Notching are periodic disturbances that appear in the voltage waveform mainly created by the commutation in power electronics conversion equipment. Because the disturbance is periodic, it can be characterized by the harmonic content they create. Noise in power systems is basically a distortion that cannot be classified as any of the other types [10].

3 Disturbances Generated by Power Electronics Conversion Equipment

Equipment for energy conversion based on power electronic devices generates two main kinds of disturbances: commutation transients and harmonics. These disturbances produce three main effects on power transformers and other high-voltage connected equipment:

1) insulation failures due to transient overvoltages generated during the commutation of the semiconductor devices,
2) overvoltages excited by resonances occurring at some of the harmonic frequencies (these harmonics are generated by the converter operation), and
3) transformer overheating and consequent loss of life due to the harmonic components of the current.

This chapter discusses in detail these disturbances and their effects on the equipment, especially on power transformers.

3.1 Commutation Transients

Commutation transients are produced by power electronics conversion equipment when the current in the converter is switched from one branch to the other. Because of physical constraints, the current cannot instantly switch from one branch to other. Therefore, two thyristors that were previously connected to points of different voltage value are simultaneously in conduction making a short circuit. This short circuit creates a sudden voltage change in the circuit that affects the voltage waveform creating notching. Moreover, the large variation of the current can create overvoltages in the inductances in the circuit being these real or produced by stray effects. The mechanism on how transients are generated during commutation at power electronics inverter circuit has been widely described in the literature [3].

The term silicon controlled rectifier (SCR) generally refers to rectifying devices with a certain control capability, like thyristors, GTOs, etc. To protect the SCRs against commutation transients, they are generally provided with snubber circuits and other protection devices, such as saturation reactors, that attenuate the effects of the transient over the SCR and therefore over other connected equipment [11]. The snubber circuit generally consists of an RC series circuit connected in parallel with the SCR being the main purpose to limit the voltage rise time over the SCR avoiding non-desired tripping by high dv/dt. The parameters of that snubber circuit, capacitance and resistance, must be carefully evaluated to achieve the desired levels of protection. Design methods have been proposed on how to calculate these parameters [12]. Surge arresters are employed to limit the maximum value of the overvoltage that can reach the devices in the SFC or at the equipment connected to the converter.

The effects of adjustable speed drives over electric motors have been widely investigated due to the close relation between this equipment in all kind of facilities [13], [14]. The effectsof surges created by the operation of power electronic converters over power transformers in HV systems has been studied mainly for high voltage direct transmission applications [15]. The effect of steep-fronted waves generated by electric drives is similar to the effect of steep-fronted waves produced by switching transients; this last effect has been discussed in 2.2. For example non-linear distribution of the voltage over the electric machine winding with stressful concentrations on the turns close to the terminals is a general effect of this type of disturbance. Different types of converters generate transients with different characteristics, and therefore more or less harmful consequences over the equipment [13]. Those consequences depend on the characteristics of the generated waveform rather than the source. In any case, to analyze the possible harm of a voltage transient, not only the maximum peak but also other parameters such as rise time, magnitude step or frequency of the wave shape must be considered. Figure 3.1, which is taken from [16], shows a generic transient voltage waveform and a set of parameters that need to be considered for the evaluation of the possible effects of that waveform.

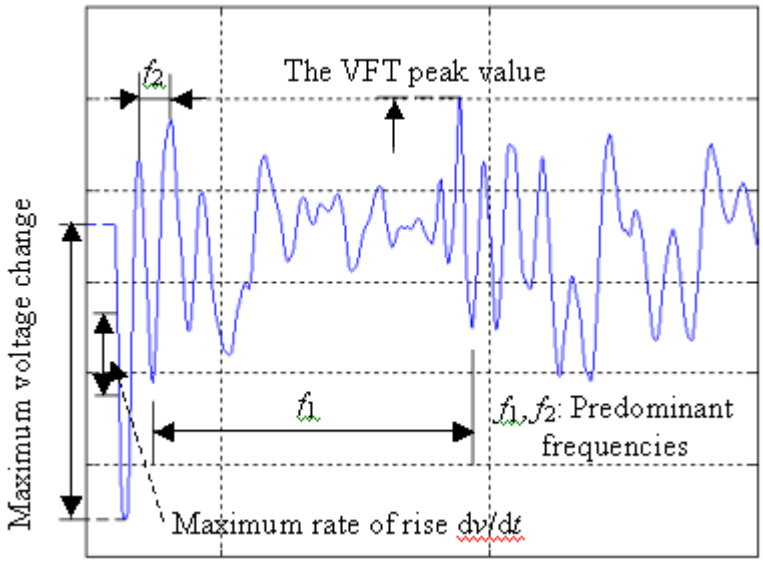

Figure 3.1 relevant parameters in the study of the effect of a transient waveform

3.2 Resonance at Harmonic Frequencies

The harmonic presence in power systems is generally characterized by a set of signals with a wide range of frequencies. Therefore, there are true possibilities that there exist a natural resonance between the system components close to one of the harmonic frequencies. If this is the case, the magnitude of the currents and/or voltages at that particular frequency will increase over the values existing of the other harmonics and can be larger even than the fundamental frequency magnitudes. In this case, despite the source of harmonics could be not large, the magnification of one of the components can considerable increment the voltage creating harmful overvoltages over the equipment. Or in a similar way, the current of certain harmonic order can be increased in a way that creates important overheating on the equipment. The relation among the different system parameters, mainly inductance and capacitance, is the key on the existence of resonance in that system. The inductance or capacitance can be the design parameters of the equipment or just created by stray phenomena. In this last case the evaluation of possible resonance becomes more difficult.

A simple an easy way to detect resonance at other than the fundamental frequency is by mean of a frequency scan that is a description of the frequency response of the system to a variable frequency source [9]. This description is basically the impedance seen from the point

where that response is analyzed, called the driving point. The frequency scan permits to easily identify frequencies where resonance is produced and the results of frequency scans over the study system will be presented in chapter seven.

3.3 Overheating in Power Transformers due to Harmonics

The presence of harmonic currents in an electric circuit increases the losses in the equipment where they circulate. The losses in most of the equipment depend in a certain way on the frequency of the circulating current, generally, the higher the frequency, the larger the losses for the same current magnitude. Therefore, the increasing frequency of the harmonic components will contribute in an appreciable way to the amount of losses. This is particularly true in transformers, which are the key component in this study. A first classification of the transformer losses separate them into no-load losses P_{NL}, which are losses existing even if the transformer has no load, and load losses P_{LL}, which are related to the transformer load current [17]

$$P_{loss} = P_{NL} + P_{LL} \tag{3-1}$$

Some of the electric phenomena that take place in a transformer, including the losses, can be represented in a simplified way by the equivalent circuit of the transformer. Figure **3.2** shows the equivalent circuit of a two winding transformer. The electric parameters are normally referred to the primary or secondary sides of the transformer; in this discussion we will name it generally with the sub-index 1 or 2 as the parameters of the primary or secondary winding.

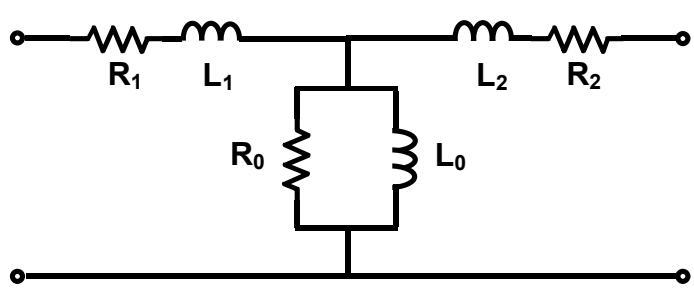

Figure 3.2 Equivalent circuit of a two winding transformer

The resistances R_1 and R_2 represent the electric losses in the primary and secondary winding respectively. The losses due to the Joule effect and the ones due to the eddy current effect compose the winding losses. Because the windings are generally made of copper these are designated as the copper losses. The losses in each winding can be expressed as,

$$P_{cu} = P_{\Omega} + P_{EC} \tag{3-2}$$

Where P_{Ω} and P_{EC} represent the joule and eddy current losses respectively.

The eddy current losses depend on the square of the frequency of the current. Therefore, the copper losses at a frequency different from the fundamental one are given by;

$$P_{cu} = I^2 R_{DC} + I^2 R_{EC} \left(\frac{f_h}{f_1} \right)^2 \tag{3-3}$$

Where R_{DC} is the resistance of the winding measured with a DC current, R_{EC} is the equivalent resistance due to the eddy current effect in the winding, f_h is the frequency at which the losses are calculated, and f_1 is the rated frequency of the transformer. As both terms on the left are proportional to the square of the current, a new resistance, called the resistance in AC at the f_h frequency is defined,

$$R_{AC} = R_{DC} + R_{EC} \left(\frac{f_h}{f_1} \right)^2$$

or in an equivalent way,

$$R_{AC} = R_{DC} \left(1 + P_{EC(pu)} \left(\frac{f_h}{f_1} \right)^2 \right) \tag{3-4}$$

where $P_{EC(pu)}$ is the coefficient of eddy current losses in per unit, and is defined as,

$$P_{EC(pu)} = \frac{R_{EC}}{R_{DC}}$$

The winding losses P_{cu} are part of the load losses, the same are other losses designated generally as other stray losses P_{OSL}. The no load losses are mainly the ones originated in the magnetic core P_{Fe}.

$$P_{LL} = P_{cu} + P_{OSL}$$

$$P_{NL} = P_{Fe}$$

The total transformer losses are then according to (5-1),

$$P_{loss} = P_{cu} + P_{Fe} + P_{OSL} \tag{3-5}$$

When the current circulating the transformer has a sine shape, the losses can be expressed as

$$P_{loss} = I^2 R_{DC} + I^2 R_{EC} + P_{Fe} + P_{OSL} \tag{3-6}$$

and under a non-sinusoidal regime

$$P_{loss} = \sum_h I_h{}^2 R_{DC} + \sum_h I_h{}^2 R_{EC} \left(\frac{f_h}{f_1} \right)^2 + \sum_h P_{Feh} + \sum_h P_{OSLh} \tag{3-7}$$

The two first terms in the equation correspond to winding losses and have been previously discussed. Therefore, the discussion will continue on proper values of the last two terms.

The superposition principle is not valid for the calculation of the losses in the iron core as is demonstrated in [18]; therefore, the summation symbol in equation (5-7) is not exactly valid and only represents the total amount of losses produced under the presence of harmonics. As it is shown in that work, the losses in the iron core depend on the harmonic content of the magnetic induction inside the core iron in a complex way mainly related to the shape of the induction waveform and the maximum value it achieves. In the transformer core, the magnetic induction is related to the voltage by the expression,

$$B = K \int V(t) dt$$

Where K is a constant and V(t) is the time evolution of the voltage. According to this expression the decomposition in harmonic components of the voltage can be employed to obtain the harmonic components of the magnetic induction B. If the voltage is a sine type wave, the induction will be also the same type of function and no harmonic components will be present.

The losses in the iron core are basically due to hysteresis and eddy current effects in the magnetic core. The eddy current losses as in the case of the windings depend on the square of the frequency. The hysteresis losses dependence with the frequency is not related in a simple direct way like the eddy current losses. The relations for the losses in a ferro-magnetic material and the frequency are presented in [19]. Moreover, as it was said above, the iron core losses depend on the wave shape and the peak value of the magnetic induction and not only on the magnitude of the harmonic components. Nevertheless, if the harmonic distortion is relatively low there is a simple way to approximate the increment in the losses under non-sinusoidal applied voltage. When the amount of distortion is such that,

$$0.95 < \frac{V_{rms}}{1.11 V_{avg}} < 1.05 \tag{3-8}$$

Where V_{rms} and V_{avg} are the RMS and the average voltage applied to the winding under consideration. Then, the iron core losses for a distorted wave shape can be calculated according to [20] as;

$$P_M = P \cdot \left(p_1 + p_2 \left(\frac{V_{rms}}{1.1 V_{avg}} \right)^2 \right) \tag{3-9}$$

Where P is the iron core losses at a sinusoidal waveform, p_1 is the relative losses due to hysteresis, and p_2 is the losses due to eddy current effects affected by the voltage waveform. In the case the voltage distortion is high, the computation of the iron core losses become quite complex. For those cases, calculation procedures based on experimental data have been proposed [21].

The other stray losses P_{OSL} are due to several electromagnetic phenomena that take place in the whole transformer, which means the transformer structures and tank walls. There is still a discussion on how these losses depend on the frequency [22], but according to [23], the stray losses variation with frequency can be expressed as:

$$P_{OSL} = P_{OSLR} \sum_{h=1}^{h\max} \left[\frac{I_h}{I_R} \right]^2 h^{0.8} \tag{3-10}$$

Where P_{OSLR} is the other stray losses value at rated load and frequency, I_R is the rated load current.

3.4 Transformer derating, K factor and other non-sine wave evaluation factors

The transformer under non-sinusoidal conditions (current and or voltage) experiments a reduction in the power that it can deliver. In order to account the conditions under which the transformer is operating some factors were defined that account for the harmonic presence in the transformer current. The simplest factor relates the maximum value of the voltage applied to the transformer with the rms value over the transformer and it is called the crest factor,

$$CF = \frac{V_{peak}}{V_{rms}}$$

This factor indicates the overvoltage over the transformer, but is not useful for determination of the derating due to the harmonic regime. For this purpose another factor has been proposed; the K factor was defined by the Underwriters Laboratory UL [24] an is calculated as,

$$K = \frac{\sum_h I_h^2 \cdot h^2}{I_R^2} \qquad (3\text{-}11)$$

This factor is mainly related with the eddy current losses generated in the windings by the harmonic current. According to equation (5-3) the additional losses due to eddy currents in the winding can be calculated as:

$$P_{EC} = R_{EC} \sum_h I_h^2 h^2$$

or,

$$P_{EC} = P_{EC-R} \frac{\sum_h I_h^2 h^2}{I_R^2}$$

Where $P_{EC\text{-}R}$ is the eddy current losses at rated and sinusoidal current. It is clear from this formula and the K factor definition (5-10) that the K factor relates the eddy current losses at rated conditions to the conditions when the harmonics are present in the circuit.

Other coefficient proposed in [23] to consider the additional losses produced in the transformer under harmonic conditions is the *harmonic loss factor* F_{HL}, which is also based in the additional losses due to harmonics and it is defined as:

$$F_{HL} = \frac{P_{EC}}{P_{EC-0}} = \frac{\sum_{h=1}^{h\max} I_h^2 h^2}{\sum_{h=1}^{h\max} I_h^2}$$

Where P_{EC} is the eddy current losses, including harmonics and $P_{EC\text{-}0}$ is the eddy current losses at the measured current and rated frequency. The harmonic loss factor is related to the K factor by,

$$K = \frac{\sum_{h=1}^{h\max} I_h^2}{I_R^2} \cdot F_{HL}$$

The F_{HL} is analyzed and compared to the K-factor in [25]. It is found there that generally it produces less conservative results, from the derating point of view, than the K-factor.

3.5 Transformer loss of life due to harmonic effects

The reduction in the transformer loss of life is related with the additional increment in the temperature that the harmonics create in the equipment. In [26] the life reduction is related to the temperature of the transformer hottest spot. The temperature increment will lead to a faster degradation in the transformer insulation and a shortage of the equipment life. The transformer operating temperature is given by:

$$\theta_{0F} = \theta_{01} \left(\frac{P_{Hn} + P_{En} + P_{jn}}{P_{H1} + P_{E1} + P_{j1}} \right)^{m1}$$

where θ_{0F} is the final top oil temperature rise in relation of ambient temperature with distorted load and θ_{01} is the temperature rise with linear load. P_{Hn} is the hysteresis losses with distorted conditions and P_{H1} is the losses with linear load. P_{En} and P_{E1} are the eddy current losses in the iron core at distorted and linear conditions respectively, and P_{jn} and P_{j1} are the total winding losses under the two conditions. m1 is a coefficient varying between 1.0 and 0.8 depending on the transformer characteristics. The temperature time evolution is given by the following equation,

$$\theta_0 = \theta_{0F} \left(1 - e^{-\frac{\Delta t}{T_0}} \right) + \theta_{i0}\, e^{-\frac{\Delta t}{T_0}}$$

where θ_0 is the final oil temperature, θ_{i0} is the initial temperature increment; T_0 is the initial temperature; Δt is the time span. The hottest spot temperature rise is given by

$$\theta_{0F} = \theta_{01} \left(\frac{P_{jn}}{P_{j1}} \right)^{m2}$$

where m2 is a coefficient between 1.0 and 0.8 according to the transformer constructive characteristics.

The dependence between the temperature and the transformer loss of life can be calculated as a function of hottest spot temperature. The actual expression that the loss of life follows depends on several factor and constructive characteristics of the equipment. In [26] the following expression is proposed,

$$PV\% = 10^{-\left(\frac{6972.15}{273+\theta_{mQ}} - 13.391\right)} \Delta t 100$$

where PV% is the percent reduction in the loss of life, θ_{mQ} is the total hottest spot temperature and Δt is the time span the hottest spot remains at θ_{mQ}.

4 Modeling of the System

A basic consideration in electromagnetic studies is the range of frequencies to be analyzed. This frequency range rules the type and parameters of the model required for the study. General considerations about power system equipment modeling for transient studies can be found in [3].

Fast and very fat transients produced by switching or lightning are not part of the subject of this study. Moreover, the snubber circuits provided in the SFC remove possible high frequencies and attenuate steep front waves. Therefore, the modeling at this stage will consider frequencies up to around 20 kHz. Unlike transient studies, harmonic studies require accuracy of the model in a lower frequency range. Usually, an upper limit of 5 kHz is more than enough for harmonic analysis, due to the negligible value of the harmonics above the 50th component (3 kHz at 60 Hz). Moreover, phase-angle controlled converters like the SFC in this study generate harmonic components whose magnitude decreases when frequency increases. Regular 60 Hz models are usually accurate enough for harmonic studies. The model used in this study covers the range of frequencies from 5 Hz to 20 kHz. The fifth and seventh harmonic filter was not connected to the auxiliary bus of the station during the different simulations developed for this study. Refer to Appendix A for the complete diagram and additional technical data of the circuit model.

4.1 Supply Network and Starting Transformer

The medium voltage (13.8 kV) auxiliary network model is a voltage source plus its equivalent short circuit impedance behind the source as shown in Figure 4.1. A standard calculation process based on the short circuit parameters at the auxiliary busbar of the Station produces the values shown in Table 4.1. Due to the low relevance of the starting transformer for this study, a simplified model based only on its short circuit values is used. Table 4.1 also shows the starting transformer parameters used in the simulations. It is assumed in the circuit model that a 100 Ω resistance grounds the auxiliary network. This value is not relevant for

the study because the starting transformer is wye-delta connected with the wye isolated from the ground.

Table 4.1 Values for the auxiliary network and starting transformer models

Network	
Rated voltage [KV]	13.8
Max. short circuit power [MVA]	350
Max. short circuit current [KA]	14.64
Min. short circuit impedance [Ω]	j0.541
Transformer	
Primary voltage [KV]	13.8
Secondary voltage [KV]	16.5
Rated power [MVA]	24.5
Short circuit voltage [pu]	0.10

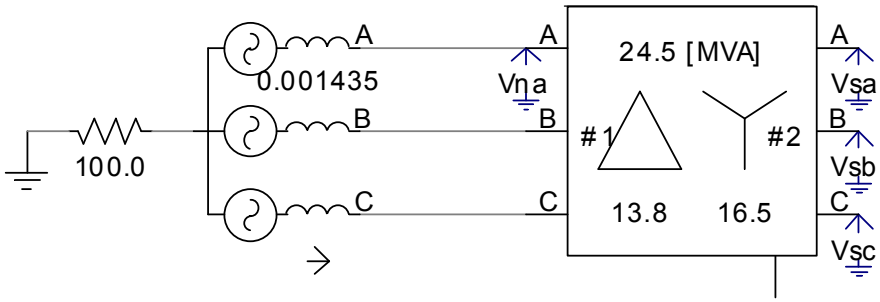

Figure 4.1 PSCAD/EMTDC model of the auxiliary network and starting transformer

4.2 The Synchronous Machine

4.2.1 General considerations about machine modeling

The synchronous machine is the core of the facility under study. It works as a generator producing energy while working in the turbine mode, and as a motor while in the pump mode, sending the water back to the upper reservoir. The electromagnetic configuration of a synchronous machine is represented in Figure 4.2. The stator holds three windings

electrically shifted 120 degrees. The field winding is placed in the rotor and also are the amortisseur windings. Generally a synchronous machine has at least two amortisseur windings.

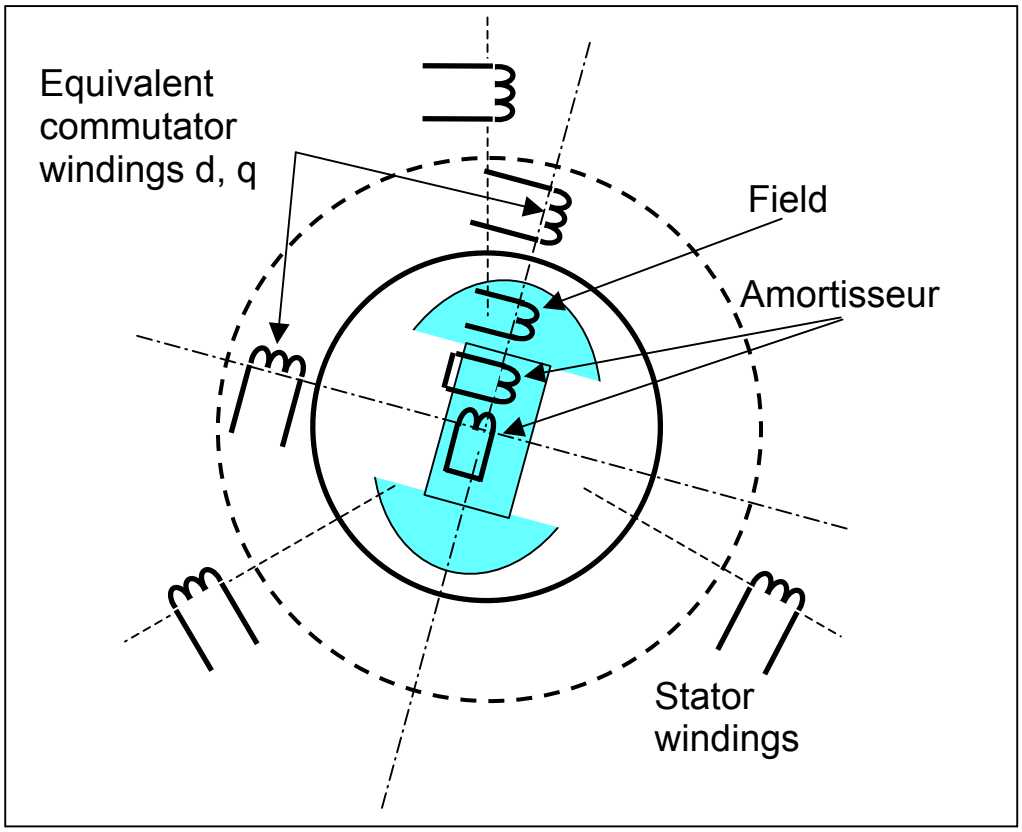

Figure 4.2 Electromagnetic circuit model of the synchronous machine

For control purposes it is a regular practice to model the synchronous machine in rotating coordinates. The modeling of the synchronous machines in rotating coordinates has been extensively covered in the literature [27], [28]. The three-stator windings are reduced to two equivalent windings in the dqo system, and the rotor windings are preserved in its original form since they are originally located in the dqo coordinates. After the transformation the stator winding equations can be written as,

$$\begin{aligned} V_{ds} &= R_s\, i_{ds} + \dot{\psi}_{ds} - \omega_r\, \psi_{qs} \\ V_{qs} &= R_s\, i_{qs} + \dot{\psi}_{qs} - \omega_r\, \psi_{ds} \end{aligned} \qquad (4\text{-}1)$$

Where V_{ds} and V_{qs} are the voltages applied to the stator equivalent windings. R_s is the resistance of the stator winding; ψ_{ds} and ψ_{qs} are the fluxes in the two equivalent stator windings; and ω_r is the machine electrical speed. Moreover, the rotor circuit equations in dqo coordinates are:

$$\begin{aligned} 0 &= R'_{dr}\, i'_{dr} + \dot{\psi}'_{dr} \\ 0 &= R'_{qr}\, i'_{qr} + \dot{\psi}'_{qr} \end{aligned} \tag{4-2}$$

Where R_{dr} and R_{qr} are the rotor equivalent resistances; i_{dr} and i_{qr} are the currents in the equivalent circuit in the d and q axis; and ψ_{dr} and ψ_{qr} are fluxes in the respective windings. And the field winding equation is given by,

$$e'_{fd} = R'_{fd}\, i'_{fd} + \dot{\psi}'_{fd} \tag{4-3}$$

Where R'_{fd}, i_{fd}, e_{fd}, and ψ_{fd} are the excitation winding resistance, current, voltage and flux respectively.

The coupling relation between the several windings that compose the synchronous machine is given by the following set of equations:

$$\begin{aligned} \psi_{ds} &= L_{ds}\, i_{ds} + L_{md}\, i'_{fd} + L_{md}\, i'_{dr} \\ \psi_{qs} &= L_{qs}\, i_{qs} + L_{mq}\, i'_{qr} \\ \psi'_{dr} &= L_{md}\, i_{ds} + L'_{dr}\, i'_{dr} \\ \psi'_{qr} &= L_{mq}\, i_{qs} + L'_{qr}\, i'_{qr} \\ \psi'_{fd} &= L'_{fd}\, i'_{fd} + L_{md}\, i_{ds} + L_{md}\, i'_{dr} \end{aligned} \tag{4-4}$$

Where L_{ds}, L_{qs}, and L'_{fd} are the self-inductances of the stator direct and quadrature windings. The L_{md} and L_{mq} are the mutual inductances in the direct and quadrature axis between stator and rotor. L_{dr} and L_{qr} are the self-inductances in the direct and quadrature windings. And L_{fd} is the self-inductance of the field winding. All these relations of the machine electromagnetic variables can be manipulated and merged in the machine equivalent circuit of Figure 4.3.

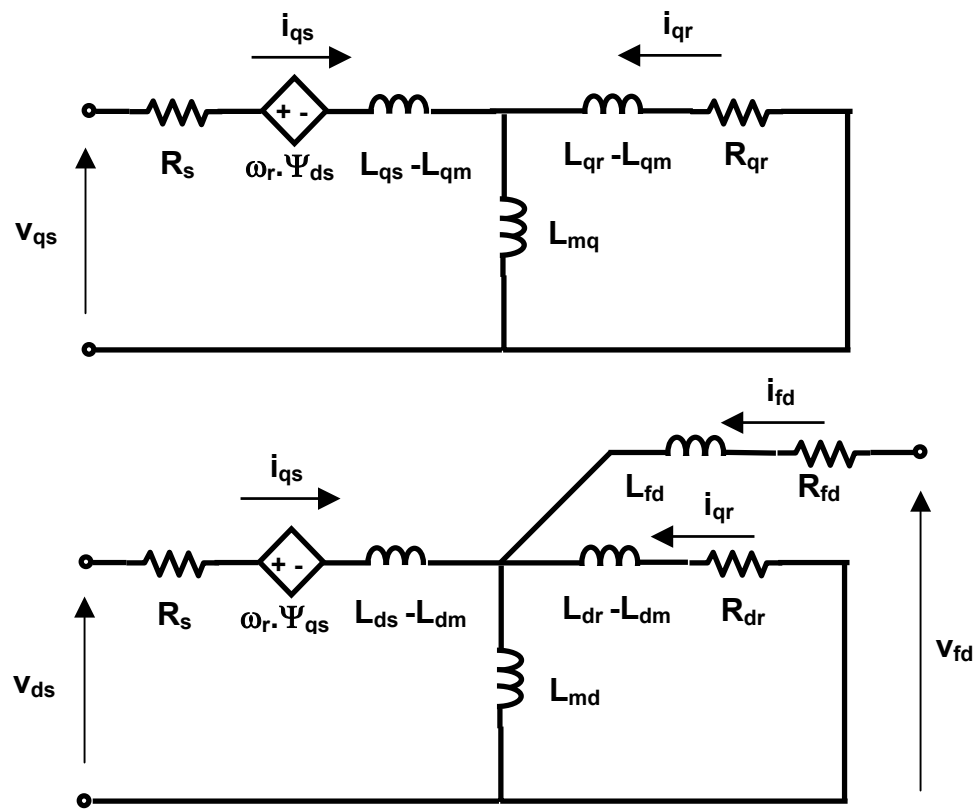

Figure 4.3 Equivalent circuit model of the synchronous machine

4.2.2 Computer model of the Synchronous machine

The synchronous machine models for low-frequency transient analysis (up to 20 kHz) are quite simple [3] and allow for neglecting the distributed capacitances. On the other side, because the synchronous machine in a power system acts as an harmonic source, an harmonic impedance and an harmonic frequency converter [29], [30] its model for simulation purposes must be carefully done [31], [32]. The harmonic source effect is corrected by an appropriate design, and the frequency converter behavior is related with conditions of unbalance or distortion in voltages and currents that generates harmonics of different order due to the rotation of the magnetic field.

In the past, harmonic studies considered a rather simplified model for the synchronous machines. This model employs a reactance and a constant source behind that reactance. The value of the reactance varies with the harmonic under consideration and is

given by the negative sequence reactance referred to the corresponding harmonic expressed as,

$$x_2 = h.\frac{x''_d + x''_q}{2} \qquad (4\text{-}5)$$

Where h is the harmonic order, and x''_d and x''_q are the direct and quadrate axis sub-transient reactances respectively. Although being quite intuitive this model has proven to be rather inadequate for harmonic studies [9]. In the development of this study it was found to introduce artificial resonant frequencies and harmonic amplification; this fact will be shown in more detail later.

EMTDC provides complete synchronous machine models appropriate for harmonic studies [8] that follow the general considerations done in the previous section. These models simulate the various electromagnetic and mechanical phenomena inside the machine making them adequate for using when harmonics must be considered. While the mechanical phenomenon is not of major relevance for this study, besides its influence on the acceleration process, the electromagnetic phenomenon and its frequency dependence characteristic are of prime importance. The *sync_machine* model in the EMTDC version 3.0.6 based on version 2 model *MAC 100* employs the equations and equivalent circuit presented in section 4.2.1. Although these equations were not developed specifically for harmonic studies its generality makes the model appropriate enough for this study. The program routine calculates the equivalent model based on the machine test data. Because some of the required data was not readily available, the estimation of some parameters was necessary in order to fulfill all the simulation data requirements. The machine data needed to complete the computer model used in the study was assumed based on machine theory and typical values taken from the literature [33], [34], and is in shown Table 4.2.

Table 4.2 Synchronous machine parameters assumed for the study

Potier reactance Xp [pu]	0.32
Q-axis reactance Xq [pu]	0.75
Q-axis transient reactance X'q[pu]	0.75
Q-axis sub-transient time constant $T''_q = T'_d$ [sec]	0.052
Inertia constant H [sec]	4.0
Frictional damping [pu]	0.0

In the actual facility, the neutral point of the generator is grounded through a distribution transformer plus a resistor resulting in 1310 Ω grounding resistance, which was considered in the machine model.

4.3 The Static Frequency Converter

4.3.1 General considerations of the SFC modeling

The Static Frequency converter provides a source of variable voltage-variable frequency that supplies the synchronous machine during the starting process. The SFC is basically composed of a rectifier bridge that converts the input from AC to DC and an inverter bridge that generates the variable frequency voltage from the DC stage. The inverter can be configured as a voltage source inverter or a current source inverter. In the application under consideration a current source is generally preferred. For this type of circuit a relatively large inductor is provided at the DC interface to provide the current source characteristics. Figure 4.4 shows the basic configuration of the static frequency converter.

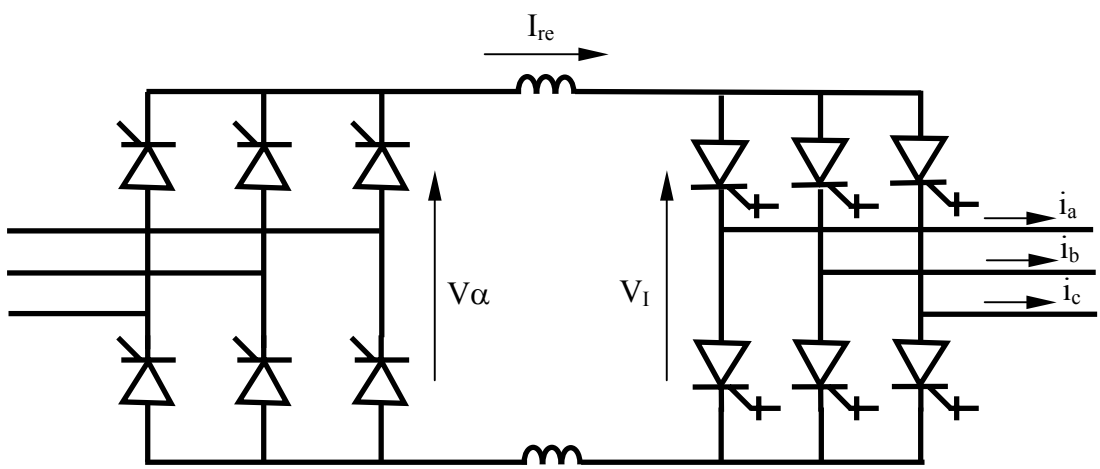

Figure 4.4 Circuit model of the static frequency converter

In the application being studied the rectifier is realized by regular thyristors while the inverter is made of gate turn-off controlled semiconductors (GTO), which can be forced to stop conduction from the control circuit. If the GTOs are forced to interrupt the current, large overvoltages can be generated creating harmful conditions over the connected equipment.

As the SFC is used to fed the synchronous machine while working as a motor, the input side refers to the network side and the output side is the machine side. Theoretical SFC waveforms on the output side can be observed in Figure 4.5. The waveform is a square wave where each thyristor conducts for 120 degrees and remain blocked the rest of the period. Also shown in the Figure 4.5 are the pulses necessary to produce those waveforms. The current waveforms produced by the SFC converter can be analyzed through Fourier decomposition. Using the Fourier series with an appropriate time reference, the currents in the three phases of the synchronous machine stator windings can be generally written as:

$$
\begin{aligned}
i_a &= \frac{2\sqrt{3}}{\pi} I_{re}\left(\cos\omega_e t - \frac{1}{5}\cdot\cos 5\omega_e t + \frac{1}{7}\cdot\cos 7\omega_e t + \cdots\right) \\
i_b &= \frac{2\sqrt{3}}{\pi} I_{re}\left(\cos\left(\omega_e t - \frac{2\pi}{3}\right) - \frac{1}{5}\cdot\cos\left(5\omega_e t + \frac{2\pi}{3}\right) + \frac{1}{7}\cdot\cos\left(7\omega_e t - \frac{2\pi}{3}\right) + \cdots\right) \qquad (4\text{-}6) \\
i_c &= \frac{2\sqrt{3}}{\pi} I_{re}\left(\cos\left(\omega_e t + \frac{2\pi}{3}\right) - \frac{1}{5}\cdot\cos\left(5\omega_e t - \frac{2\pi}{3}\right) + \frac{1}{7}\cdot\cos\left(7\omega_e t + \frac{2\pi}{3}\right) + \cdots\right)
\end{aligned}
$$

Where i_a, i_b, and i_c, are the machine line currents, I_{re} is the current at the DC interface of the SFC, and ω_e is the synchronous speed. If for the purpose of the analysis the harmonic components are neglected, the fundamental component of the currents are expressed as

$$
\begin{aligned}
i_a &= \frac{2\sqrt{3}}{\pi}\cdot I_{re}\cos\omega_e t \\
i_b &= \frac{2\sqrt{3}}{\pi}\cdot I_{re}\cos\left(\omega_e t - \frac{2\pi}{3}\right) \qquad (4\text{-}7) \\
i_c &= \frac{2\sqrt{3}}{\pi}\cdot I_{re}\cos\left(\omega_e t + \frac{2\pi}{3}\right)
\end{aligned}
$$

These currents can be converted to a rotating reference frame by using the Park's transformation. This transformation is used to convert the variables in a static frame to a synchronous rotating reference frame. According to [28] the transformation can be expressed in the matrix T (not normalized) given by the following formula,

$$T = \frac{2}{3} \cdot \begin{bmatrix} \cos\theta & \cos\left(\theta - \frac{2\pi}{3}\right) & \cos\left(\theta + \frac{2\pi}{3}\right) \\ \sin\theta & \sin\left(\theta - \frac{2\pi}{3}\right) & \sin\left(\theta + \frac{2\pi}{3}\right) \\ \frac{1}{2} & \frac{1}{2} & \frac{1}{2} \end{bmatrix} \tag{4-8}$$

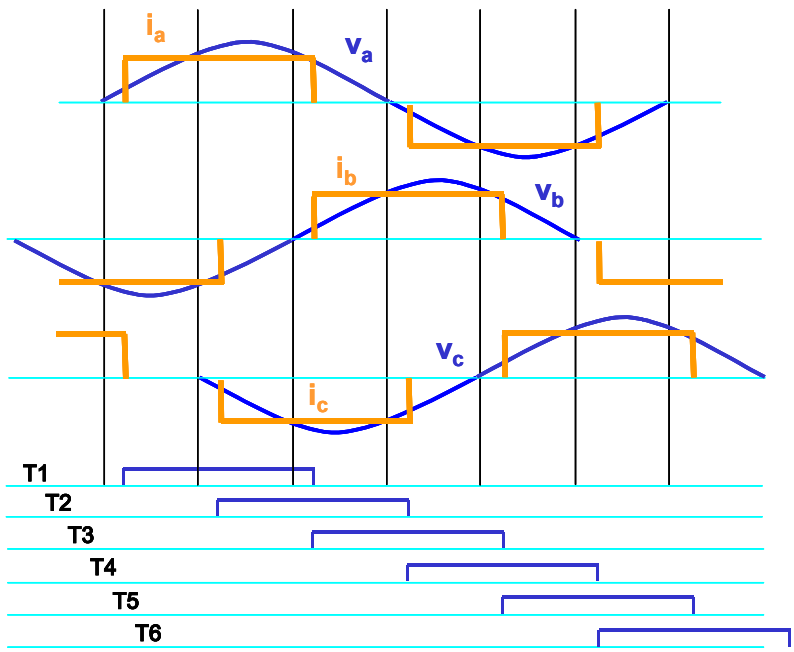

Figure 4.5 Voltage and current waveforms of SFC on the AC output side

The currents in the synchronous reference frame are obtained by:

$$i_{dqo} = T \cdot i_{abc}{}^{T}$$

Where i_{abc} and i_{dqo} are the vectors:

$$i_{abc} = \begin{bmatrix} i_a \\ i_b \\ i_c \end{bmatrix} \qquad i_{dqo} = \begin{bmatrix} i_d \\ i_q \\ i_o \end{bmatrix}$$

Applying the transformation to the first order component of the currents, equation (2-8) we obtain,

$$i_d = 0$$

$$i_q = \frac{3\sqrt{2}}{\pi} \cdot I_{re}$$

$$i_o = 0$$

In a balanced system the i_o magnitudes are zero; therefore, in the following paragraphs the magnitudes in the o reference axe wont be considered anymore. The currents in dqo reference can also be expressed as the product of a "switching function" and the rectifier current.

$$i_d = g_d \cdot I_{re}$$

$$i_q = g_q \cdot I_{re}$$

Where g_d and g_q are parameters representing the switching functions in the d and q axis.

The relation between the voltage and current in the DC side of the converter and the AC side can be obtained from the energy conservation principle calculating the power at the DC and the AC output side by,

$$V_I \, I_{re} = V_{ds} \, i_{ds} + V_{qs} \, i_{qs}$$

Where V_I represents the voltage at the DC interface; V_{ds} and V_{qs} are the voltages at the converter output in dqo coordinates, which are the same as the applied to the synchronous machine, and i_{ds} and i_{qs} are the currents at the converter output which are the same as the machine input. From this last equation the relation between the voltages at both sides of the inverter can be obtained,

$$V_I = V_{ds} \, g_{ds} + V_{qs} \, g_{qs}$$

Moreover, the voltage in the DC loop is then given by

$$V_\alpha = R_F \, I_{re} + L_F \, \dot{I}_{re} + \left(V_{ds} \, g_{ds} + V_{qs} \, g_{qs}\right) \qquad (4\text{-}9)$$

Where R_F and L_F are the resistance and inductance of the DC inductor.

Figure 4.6 represents the diagram of the equivalent circuit of the system: DC loop and inverter of the SFC, and synchronous machine. The rectifier bridge is represented as the equivalent voltage source of value V_α connected to the inverter bridge and the synchronous machine. The inverter is represented as a set of variables sources that controls the currents and voltages in the d and q circuits.

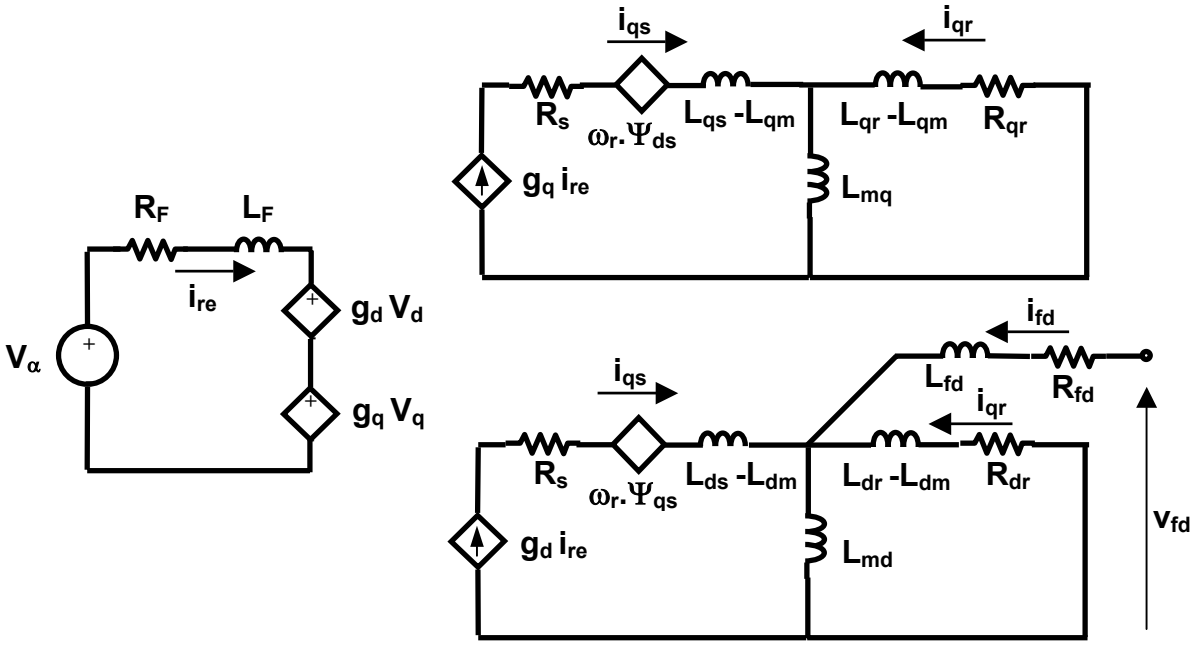

Figure 4.6 Circuit model of the inverter side of the static frequency converter and the synchronous machine

4.3.2 Parameters of the computer model of the SFC

The SFC is composed of a rectifier and a current source inverter linked by two 17 mH inductors that provide the current source mode. At both the rectifier and inverter side the converter is fully modeled by a six-pulse thyristor bridge and a GTO inverter bridge respectively. Each thyristor is modeled as a controlled resistance that changes from a large to a small value when the conduction process starts (Figure 4.7 and Table 4.3). Snubber circuits can play a significant roll during the commutation transients; therefore, these circuits are included in the model, as well as surge arresters at both AC sides of the SFC.

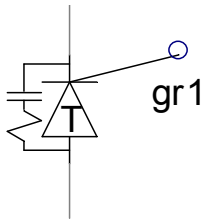

Figure 4.7 Thyristor and snubber circuit

Table 4.3 Main parameters for the thyristor model. The snubber circuit parameters were taken from a previous study

Thyristor On resistance [Ω]	0.01
Thyristor Off resistance [Ω]	1.0e6
Forward voltage drop [V]	1.0
Forward/reverse withstand volt[V]	1.0e5
Snubber resistance [Ω]	9200
Snubber capacitance [uF]	0.002

4.4 GSU Transformer

The generation step up (GSU) transformer plays a major role in this study. This transformer is not only relevant for the electric disturbance propagation phenomenon, but it has also suffered some failures in recent times becoming the object of major concern. Therefore, special carefulness is necessary in the transformer modeling. However, due to the frequency range under analysis, it is not necessary to study the electromagnetic phenomenon propagation inside the transformer windings. An appropriate terminal model is accurate enough for the purpose of this study. A comprehensive description of different transformer terminal models for computer transient studies can be found in [35], and for harmonic studies in [36], [37].

The simulations were done using three single-phase transformer models properly connected. The constructive characteristic of the transformer, with three isolated tanks where each phase core and windings lie, justifies the single-phase modeling. This modeling does not introduce an error and greatly simplifies the analysis because no inter-phase mutual coupling of any type needs to be considered. The PSCAD/EMTDC program provides built-in subroutines for the simulation of transformer models [38]. However, these subroutines are built over several assumptions and model considerations that need to be checked.

The transformer models provided in EMTDC—the study employed TSAT21—are 60 Hz models. The TSAT21 supports magnetic saturation, losses and the most relevant phenomena around the fundamental frequency. Core saturation, which can play an important role if ferro-resonances are developed, is modeled as a variable current source connected in parallel with the winding wound closest to the core. The current value is controlled by the

voltage over the connected winding and the transformer magnetic characteristic. In addition, the magnetizing current and no-load losses are represented in a simplified way by the resistance R_0. Although being complete at 60Hz, the model is not appropriate above 3 kHz. At this frequency the winding distributed capacitances must be considered. This is especially true when the voltage transfer between windings plays an important role in the analysis, as can be the case of this study. Therefore, the surge capacitances Cs_1, Cs_2 and Cs_{12}, which are not originally provided in the EMTDC routine, are added in the model producing the result of Figure 4.8.

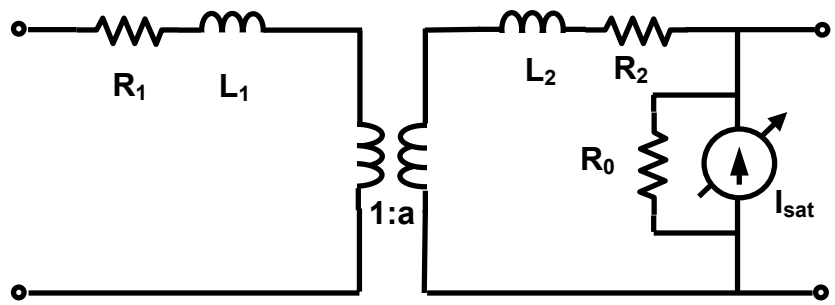

Figure 4.8 Single-phase transformer model

The transformer test data provide information for calculation of the parameters at 60 Hz. Standard values from the literature were used for the surge capacitances. The values for the transformer employed in the study are shown in Table 4.4. Although based on all the previous considerations, the model for simulation in PSCAD requires a different input format. Table 4.5 shows the main data of the transformer in the format required by the program.

Table 4.4 Transformer equivalent circuit parameters

Branch	**L [mH]**	**R[Ω]**	**C[nF]**
Primary LV	22	3.82 e-3	0.5
Secondary HV	1030	0.4	5.0
Magnetizing	-	6416	-
Inter-winding	-	-	0.3

Table 4.5 Transformer configuration data for EMTDC simulation

Main parameters	
Rated Power [MVA]	100
Short circuit reactance [pu]	0.1645
Magnetizing current [%]	0.066
No-load losses [pu]	4.24e-4
Ideal transformer modeling (#)	Yes
Saturation parameters	
Air core reactance Xair [pu]	27.06
Inrush decay time constant [sec] (*)	0.5
Knee voltage [pu]	1.085
Time to release flux clipping [sec] (°)	0.1
Saturation placed on winding	1

(#) Magnetizing current provided by only the saturation branch.
(*) Depends also on the network, realistic value
(°) Simulation parameter, for starting simulation purpose

Attention is given in this study to the possible presence of saturation phenomena. The transformer magnetizing curve provides the data for the saturation calculation. Instead of using all the data of the magnetizing curve, EMTDC simulates the saturation characteristic based on the most relevant saturation values. The calculation of these saturation values, taken from [38], is described as follows. The flux in the magnetic core, Φ_R, is calculated by the expression,

$$\Phi_R = \int v(t)\,dt$$

Considering a sine voltage,

$$v(t) = V_{\max} \sin \omega t$$

and replacing values in the flux expression results,

$$\Phi_R = 61.89 \sin \omega t$$

The air core reactance is calculated by the ratio of flux $\Delta\Phi_M$ and current ΔI_M of two points of the magnetizing curve while in saturation by the following expression;

$$X_{AIR} = \frac{\Delta\Phi_M}{\Delta I_M}\frac{\omega}{Z_b}$$

replacing with the transformer values, the air core reactance and air core inductance are calculated as,

$X_{AIR} = 27.06$ pu

$L_{AIR} = 195.4$ mH

Other important parameter is the knee point (X_{KNEE}) that gives the relation between the point at which the magnetizing curve intersects the flux ax and the rated flux. This value is given by the expression,

$$X_{KNEE} = \frac{\Phi_{Max} - L_{AIR}\ I_{Max}}{\Phi_R}$$

where Φ_{Max} and I_{Max} correspond to the extreme point of the characteristic and Φ_R is the peak value of the rated flux. Replacing in the formula, the value calculated for X_{KNEE} is,

$X_{KNEE} = 1.085$

which is inside the standard limits of $1.0 < X_{KNEE} < 1.2$. All these calculated values produce the simplified magnetizing curve shown in Figure 4.9.

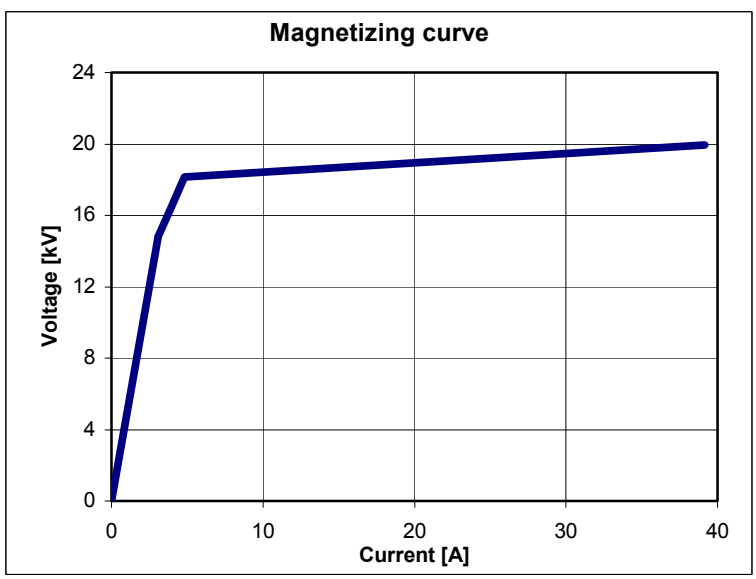

Figure 4.9 Simplified magnetizing curve

4.5 Transmission Cable

A distributed parameters line model with frequency dependent parameters is used for modeling the 345 kV cable. The election of the model is based on the simulation time step and the transient phenomena under analysis. The distributed parameter model is widely described in the literature [3], [38] With the use of the forward and backward propagation waves (F and B) and the surge impedance (z_o) the relation between voltages (V) and currents (I) at one of the line ends k can be expressed as,

$$F_k(\omega) = V_k(\omega) + z_o(\omega) \cdot i_k(\omega)$$

$$B_k(\omega) = V_k(\omega) - z_o(\omega) \cdot i_k(\omega)$$

which are similar for the other end of the line. These equations can be represented in the equivalent circuit of the line shown in Figure 4.10. The relation between both line ends is given by the equations:

$$B_k(\omega) = A(\omega) \cdot F_m(\omega)$$

$$B_m(\omega) = A(\omega) \cdot F_k(\omega)$$

Where

$$A(\omega) = e^{-\gamma(\omega)L}$$

is known as the propagation constant composed by the attenuation and phase constant. And L is the length of the line.

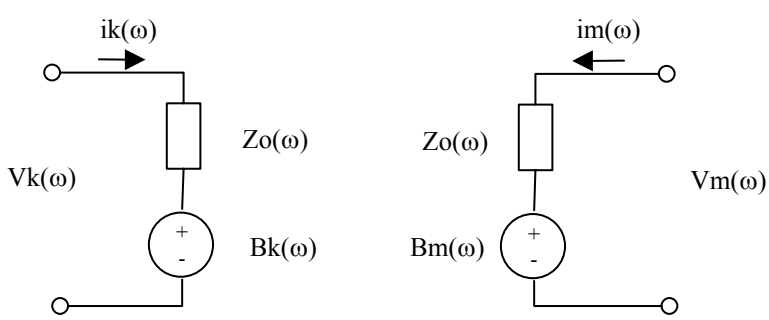

Figure 4.10 Equivalent circuit of the frequency dependent line model

The product in the frequency domain relating the forward and backward waves implies a convolution in the time domain that is solved in the computer by numerical

algorithms. For the calculation of that convolution the matrix A(ω) is numerically approximated by a curve fitting technique. EMTDC calculates the cable parameters based on the cable constructional characteristics, and the same curve fitting routine for A(ω), to calculate the surge impedance $z_o(\omega)$ at different frequencies. The range of frequency where the cable model is approximated is selected between 1 Hz and 1 MHz, which comprises the range of 5 Hz-20 kHz of the complete system model. Figure 4.11 shows the surge impedance as a function of the frequency.

The representation of three-phase transmission systems requires taking into consideration the different propagation modes that appear when more than one conductor exists. It is possible to simplify the analysis by decomposing the propagation phenomena in the different modes as each mode can be treated as a single transmission line. A transformation matrix relates the modal and circuit voltages and currents. That transformation is described by the equations:

$$\lfloor V_{ph} \rfloor = [T_e] \cdot [V_{\mathrm{mod}e}]$$

$$\lfloor I_{ph} \rfloor = [T_i] \cdot [I_{\mathrm{mod}e}]$$

$$[T_e]^T = [T_i]^{-1}$$

Where:

$$\lfloor V_{ph} \rfloor, \lfloor I_{ph} \rfloor = \textit{line phase voltages and currents}$$

$$[V_{\mathrm{mod}e}], [I_{\mathrm{mod}e}] = \mathrm{mod}\,e \textit{ voltages and currents}$$

$$[T_e], [T_i] = \textit{transformation matrix for voltages and currents}$$

An eigenvalue technique is used for the calculation of the matrices Te and Ti.

Harmonic studies require the use of a three-phase model due to the possibilities of interaction between phases. Therefore, a complete three-phase model of the whole system was developed for this study including three-phase representation of all the components. Nevertheless, in cable modeling the inclusion of the three phases ad more complexity due to the several propagation modes that appear when a multi-conductor system is considered. Besides, according to the cable data all the cable sheaths are directly grounded, this fact gives certain independence to the phenomenon of propagation in each phase. So, under this condition of electromagnetic isolation, a simplification of the cable model and the use of

three parallel single-phase cables is acceptable. The two cable models were implemented for this project and the closeness of the results totally supports the introduction of the single-phase simplification.

The value of the surge impedance calculated by EMTDC, Z_0 = 38.21 Ω, fully coincides with the value used in the previous parts of this study. Please refer to Appendix A for the cable physical data, parameters for calculation and solved constants.

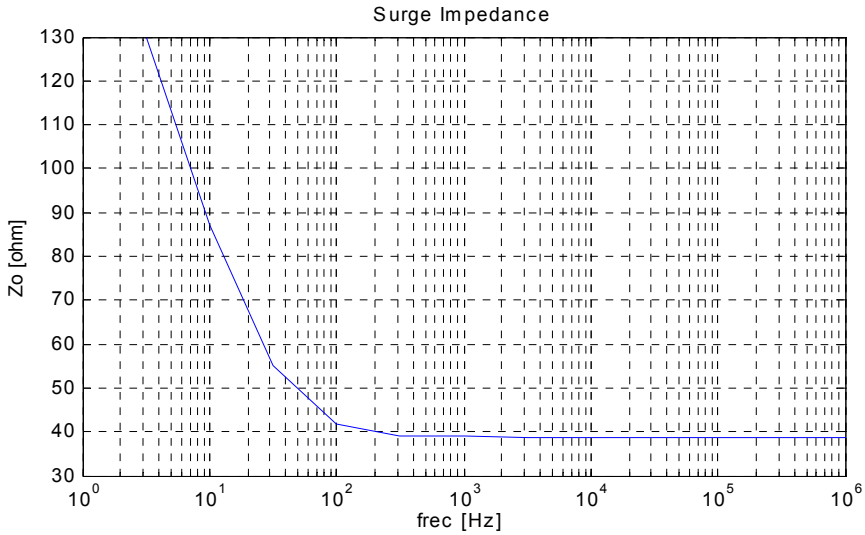

Figure 4.11 Frequency dependence of the cable surge impedance

5 Control Strategy of the Static Frequency Converter

The representation of the synchronous machine in the dqo coordinates can be used to calculate the electromagnetic torque in the motor, which is given by the following equation:

$$T_e = \frac{3}{2}\frac{p}{2}\left(\psi_{ds}\, i_{qs} - \psi_{qs}\, i_{ds}\right) \tag{5-1}$$

The meaning of each one of the variable notations appearing in this equation and the next ones has already been given in chapter three. Following [28], [39], and replacing in this last expression with the flux equations (4-4), the torque expression becomes,

$$T_e = \frac{3}{2}\frac{p}{2}\left(\left(L_{ds}\, i_{ds} + L_{md}\, i'_{fd} + L_{md}\, i'_{dr}\right)i_{qs} - \left(L_{qs}\, i_{qs} + L_{mq}\, i'_{qr}\right)i_{ds}\right) \tag{5-2}$$

Considering only the first order harmonic component of the stator currents, the current i_{ds} is null, then the torque expression can be simplified to:

$$T_e = \frac{3}{2}\frac{p}{2} L_{md}\left(i'_{fd} + i'_{dr}\right) i_{qs} \tag{5-3}$$

From this expression it is possible to see that the torque can be controlled by regulating the current i_{qs}. Therefore, controlling the current supplied by the inverter is possible to control the electric torque in the machine.

The control strategy of the SFC converter used for synchronous machine starting is divided in two stages as described in [40], [41]. The first one requires forced commutation until 8-10% (32-40 rpm) of the machine rated speed, 400 rpm. The second stage uses natural commutation supported by the voltage induced in the machine windings. During the first stage, the voltage applied to the machine is relatively low; therefore, the voltage magnitude on the high voltage side of the transformer will be also low. However, if large voltage distortion is produced during the forced commutation creating large spikes, harmful effects could appear over the transformer windings. In the second stage, while using natural commutation, the machine control strategy keeps a constant flux level in the magnetic circuit. The acceleration process increases the operation frequency. Therefore, the voltage level is increased in the same proportion, because the relationship

V/f = constant,

must be satisfied due to the constant value of the flux. The worst condition, from the point of view of the stresses over the equipment insulation is, at least in principle, achieved when the motor reaches its rated voltage and speed. Figure 5.1 shows the speed evolution of the synchronous machine during the start up process. The forced commutation stage last for only 10% of all the time required for starting the motor as a pump.

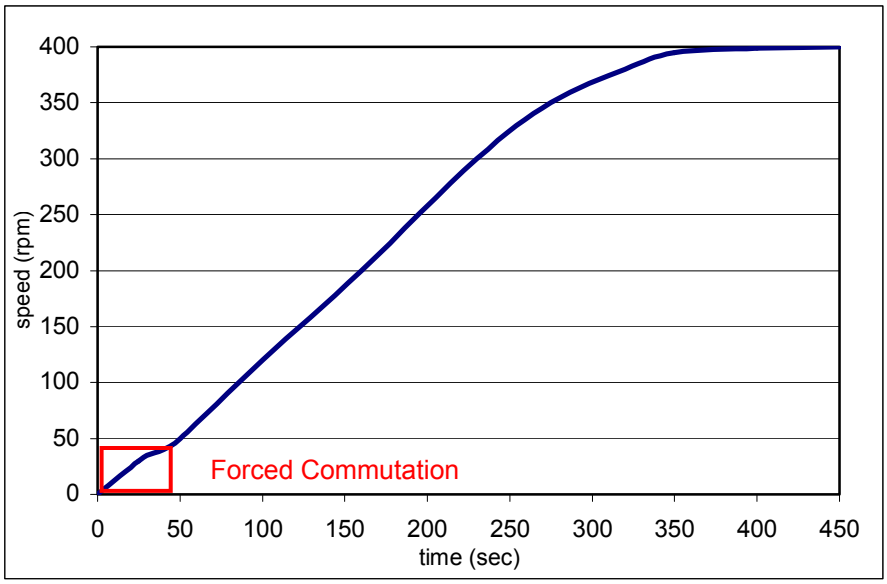

Figure 5.1 Curve of the speed evolution for the SFC starting of a synchronous machine in the facility under study [39]

The block diagram of Figure 5.2 shows the general composition of the SFC and its control system according to [39]. The inverter control is self-control commutated; therefore, the control algorithm is based in the rotor position and speed. While the inverter SCRs are fired according to the position of the machine in order to follow the speed of the motor, the rectifier controls the magnitude of the current injected to the machine [42]. The rectifier control is composed by two control-closed loops, an internal current control loop and an external speed control loop. The speed control loop also calculates and takes into consideration the torque control strategy generating the current control signal that is fed to the current controller. The speed reference signal is generated according to the desired evolution and is limited by the mechanical characteristics of the system. A sensor connected to the machine shaft provides the speed measurement signal that is compared with the desired

value closing the control loop. According to the torque control strategy the corresponding current value is generated, which is also properly limited according to the system constraints. Finally, the current control loop produces the firing angle for the thyristors in the rectifier. A phase locked loop acts over the controllers synchronizing the pulses with the network voltage. In this way, the rectifier provides the proper value of current according to the desired speed and torque, and the inverter takes care of feeding the motor with that current at the right rotor position in order to reach the desired speed evolution.

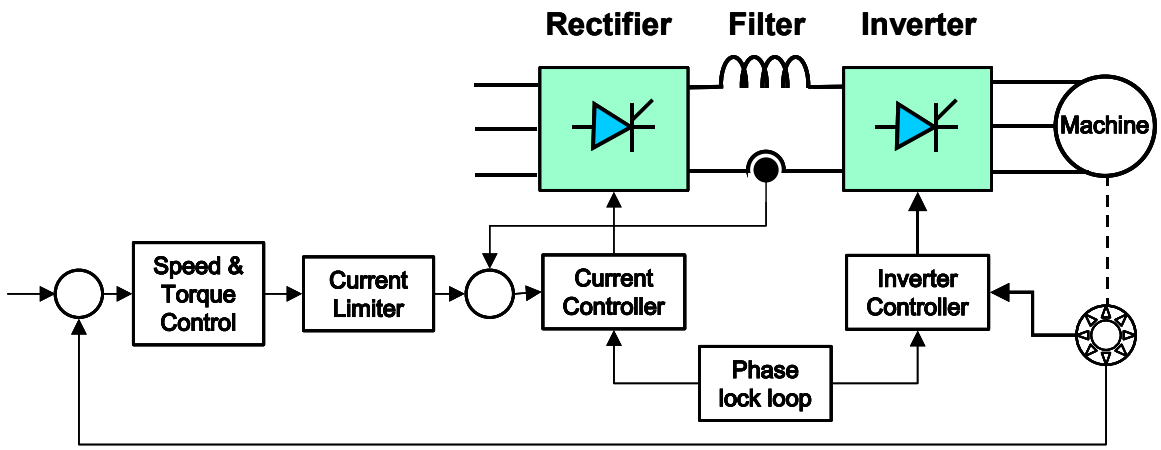

Figure 5.2 Circuit model of the static frequency converter

5.1 Inverter Control

As it was explained in the previous section, the phase angle for firing the thyristors in the inverter is based in the self-commutation strategy. This strategy is based in measuring the time delay the semiconductor is inversely polarized and the control maintains the inverse polarization time interval at a safe value. If the angle of inverse polarization is kept constant then the synchronous machine behaves as brush less dc motor. This behavior is very convenient from the point of view of the dynamic characteristics that the system presents being also quite simple to control.

The principle of the self-commutation process is described in [28], [42]. A typical thyristor voltage commutation evolution is shown in the Figure 5.3. The angle μ is measured

from the power circuit while γ is generally estimated, then according to the desired firing angle and rotor position, the firing pulses are produced. The firing angle will control the angle that the armature reaction will have, relatively to the main field flux. In the case of the application under analysis the armature reaction value will be relatively low as the current is considerably smaller than the machine rated current. Therefore, the main flux in the machine magnetic circuit is maintained constant by keeping constant the field produced by the excitation winding, which means that the excitation regime is approximately constant during the starting process.

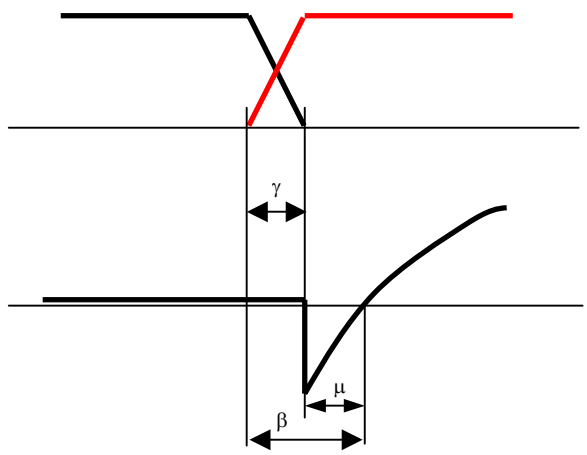

Figure 5.3 Commutation process of a semiconductor in the SFC inverter

The Figure 5.4 shows the phasor diagram of the machine voltage, current and fluxes. Where V and I are the line currents at the inverter output; Ψ_f, Ψ_a and Ψ_s are the main, armature reaction, and air gap fluxes, respectively. The angle between the main field flux and the armature reaction ϕ' is the thyristor firing angle because Ψ_s is directly related with the rotor angle; and Ψ_a is created by the armature currents produced by the inverter. From the figure, it is possible to establish the relation,

$$\phi' = 180^o - \alpha$$

As α can be calculated as,

$$\alpha = 90^o - v - \phi$$

It is valid that,

$$\phi' = v + 90^o + \phi$$

The power factor angle ϕ between V and I can be approximated as,

$$\phi \cong \beta = \gamma + \mu$$

where γ and μ are the indicated in Figure 5.3. Then the thyristor firing angle can be calculated as,

$$\phi' = v + 90^o + \gamma + \mu$$

For the calculation of ϕ', regular practices take measurement of the angle μ while estimate v and γ [28].

Figure 5.5 shows the block diagram of the rectifier control circuit as it was implemented for this study. The angle μ was measured by the configuration proposed in [43] and proper values for v and γ where estimated after some simulations.

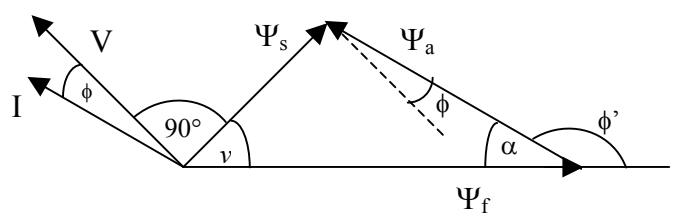

Figure 5.4 Phasor diagram of the synchronous machine voltages and fluxes

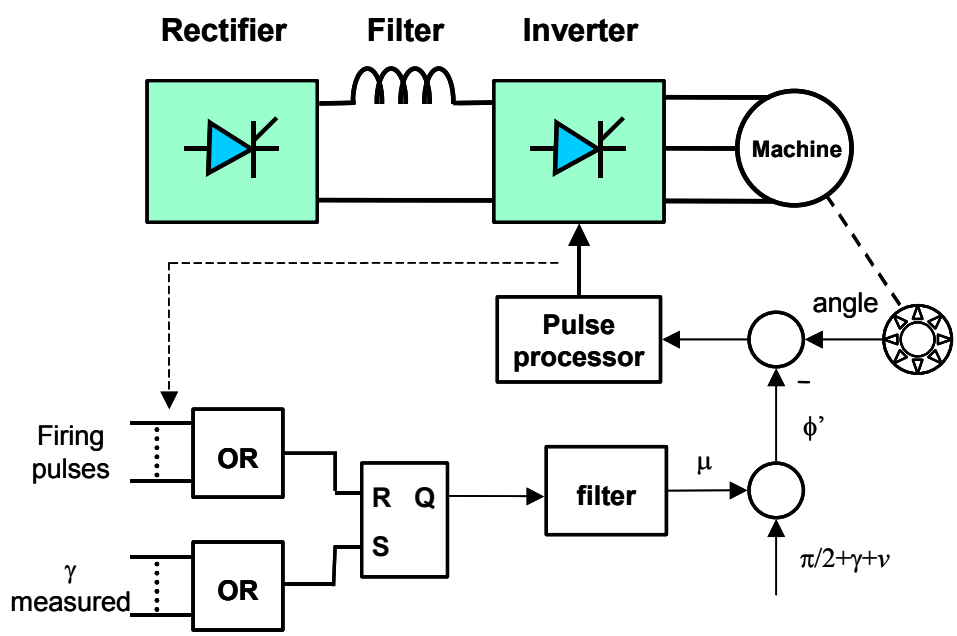

Figure 5.5 Block diagram of the inverter control circuit

5.2 Rectifier Control

The rectifier provides the necessary current in the DC interface of the SFC. That desired value of current is computed by the rectifier control loop that is composed by two control loops. The inner loop is the current controller, which is basically a controller that calculates the thyristor firing angle according to the reference and actual value of current. The outer control loop is the speed controller that generates the current reference value from the desired speed evolution and according to the torque control strategy. This configuration of the controller is widely used in different applications of machine control [44]. In the application considered in this study, it is usually desired to have a constant torque control during the self-commutated stage, from 10% to 100% of the rated speed. In this way the acceleration is kept constant and the speed increases uniformly. The torque control is maintained constant by keeping the DC current constant and therefore the corresponding AC current in the machine phases constant. According to equation (3-3) the torque depends on the stator current value and the field current. Because the field flux is desired to be constant, and the armature reaction can be considered very low, the flux is approximately constant if the field current is constant. Figure 5.6 shows the block diagram of the rectifier control as it was implemented for this study.

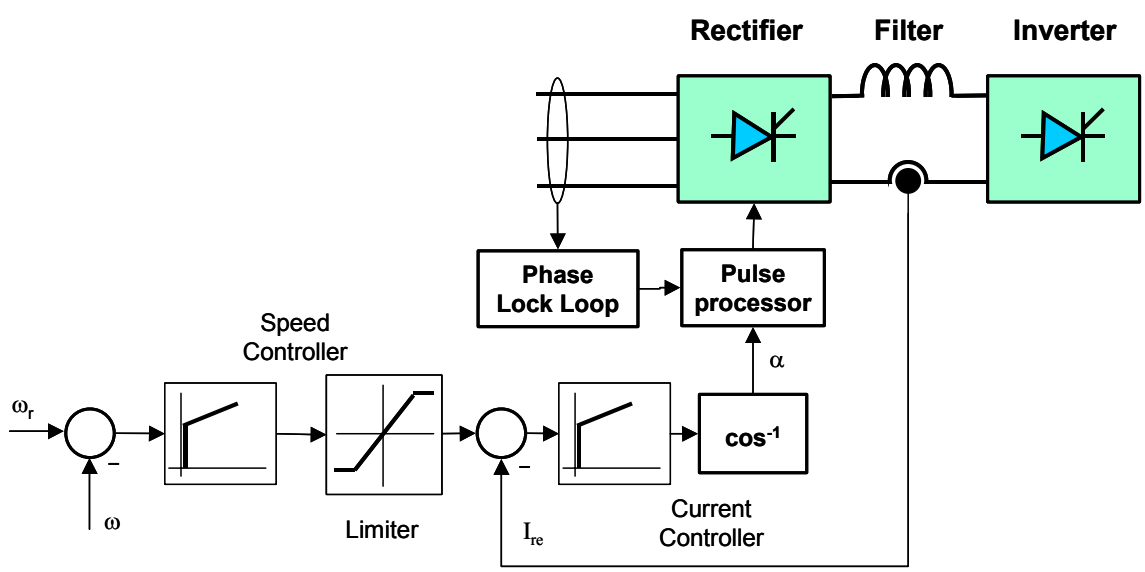

Figure 5.6 Block diagram of the control system of the SFC rectifier

In Figure 5.6 ω and ω_r represent the measured and reference current value respectively; I_{re} is the DC measured current and α the firing angle computed by the controller. The pulse processor generates the pulses for the thyristor firing with the signal received from the controller and synchronize them with the line voltages by making use of a phase locked loop. The controllers provided in each one of the loops are of the proportional integral (PI) type.

5.3 Forced Commutation Stage

During the first stage of the starting process, the voltage generated by the synchronous machine is not enough to force the commutation of the thyristors in the inverter [1]. Therefore, a mechanism to force the commutation must be developed in order to transfer the current form one of the branches of the inverter bridge to another. In the SFC, the commutation mechanism simply consists of changing the branch under conduction while the DC current has been reduced to zero. The DC current cancellation is achieved by changing the operation mode of the bridge from rectifier to inverter. In a thyristor bridge, the direction of the power flow is related with the firing angle; the relation between the firing angle and the voltage at both sides of the bridge is given by,

$$V_{dc} = \frac{3}{\pi} V_{LL} \cos\alpha_f$$

Where V_{dc} is the voltage in the DC side, V_{LL} is the line-line voltage in the AC side, and α_f is the firing angle. If the firing angle is greater than 90 degrees the bridge load flow is from the DC side to the AC side acting as an inverter. The firing angle is then changed in order to revert the voltage on the DC interface and cancel the DC current [45].

When the current is zero, the SCR in the previously conducting branch of the inverter is turned off, then a new SCR in another branch is fired and the rectifier is re-started. The operation of this commutation mechanism is allowed by the large difference between the operating frequencies of both parts of the converter. Figure 5.7 shows the firing sequence of the inverter bridge, and the theoretic waveforms of the currents in the SFC output while in the forced commutation stage. In the middle of each conduction period the current is

interrupted by a time interval long enough to assure that the previously conducting thyristor in the inverter will not be re-ignited when the rectifier is re-started.

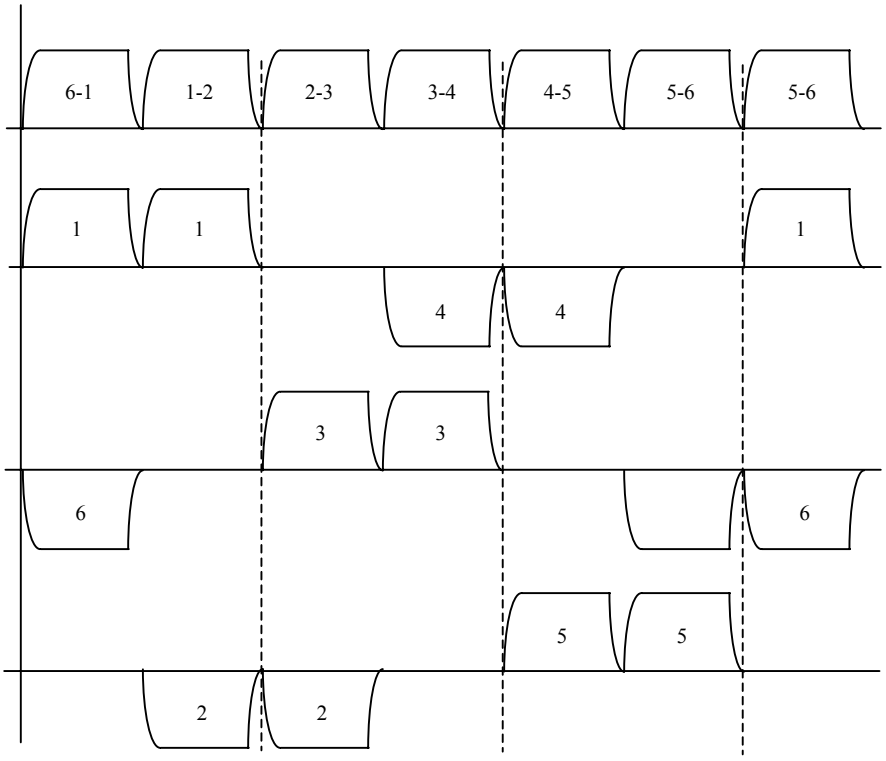

Figure 5.7 Three-phase current waveforms and forced commutation sequence in the inverter bridge

6 Operation Conditions

The main purpose of the study is to analyze the effects of the SFC operation over the HV equipment. The SFC is employed during the start up process of the synchronous machine in the pump mode. At this stage, although it is not operatively necessary, the high voltage transformer remains connected to the SFC and the starting machine. A simplified schematic of the system configuration during the SFC operation is shown in Figure 6.1. And a complete diagram of the system under analysis can be observed in Appendix A. The voltage seen at the low voltage side of the transformer, as well as its distortion content, is then transferred to the high voltage side, which is connected to the high voltage transmission cable. The goal at this point is to determine the electric stresses over the subsystem composed by the SFC, synchronous machine, transformer, and high voltage cable. This subsystem operates on a wide range of frequencies and voltage levels. Therefore, it is important to determine the operation conditions that produce the largest stresses over the equipment.

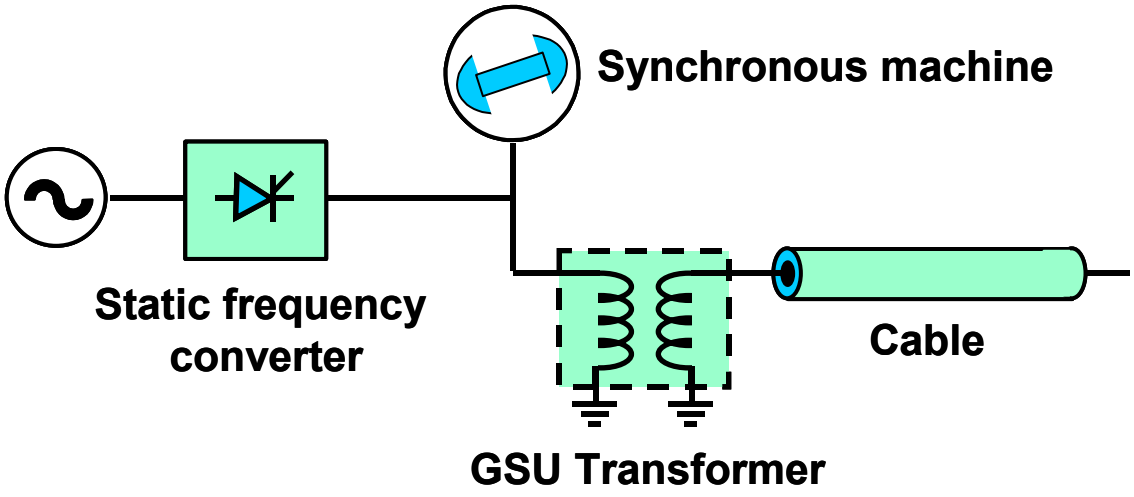

Figure 6.1 Schematic of the SFC starting system

As it was explained in section chapter five the rated voltage is applied to the machine when running at rated speed. Before that operation condition the fundamental voltage is

smaller. Therefore, for same operating mode of the SFC it is expected that other operation conditions at lower speed/ lower voltage will create less harm over the equipment. The first step was then to simulate the system operation at its rated values –that is, with the SFC supplying rated voltage and frequency. This rated parameters are shown in Table 6.1 It was also check that other operation conditions at reduced speed or reduced load do not create harmful voltages or currents on the GSU transformer.

During the forced commutation stage, the operation of the SFC is different than the natural commutation operation as it was described in 5.3. Therefore, in spite the voltage at the forced commutation mode is too low due to the very slow speed, it is necessary to check the proper operation of the SFC at that stage and the absence of dangerous conditions on the HV equipment. On the contingency operation aspect it is worth noting that there are not too many possible contingencies due to the simplicity of the starting system\ as seen in Figure 6.1. The simulation of some contingencies can like HV cable disconnection or loss of neutral connection can help to understand the role of the different system components on the behavior of the whole system.

Table 6.1 SFC parameters at the rated operating condition

Voltage [KV]	16500
SFC current [A]	1050
Power at motor [MW]	12
Field speed [rad/sec]	377

7 Harmonic Analysis of the System

There are different methods to analyze the harmonic propagation in an electric network; a compendium of them can be found in [9]. The methods for harmonic analysis can be generally classified in frequency domain and time domain methods. Frequency domain methods include frequency scan, harmonic penetration and harmonic load flow. On the other side, the time domain analysis methods are based in the calculation of the time evolution of the system magnitudes that generally is done by simulation of the operation. This chapter is dedicated to the frequency domain analysis while the next one to the time domain analysis of the system under study.

7.1 Frequency Domain Methodologies for Harmonic Analysis

Frequency domain methodologies base the analysis in the matrix admittance representation of the network under study. That representation of the network can be single or multi phase based according to the type of study and the degree of precision required. For a generic network like the one in figure 7.1, the admittance matrix is obtained from the models of each of the components in the network and is,

$$\begin{bmatrix} I_1 \\ I_2 \\ \vdots \\ I_N \end{bmatrix} = \begin{bmatrix} y_{11} & y_{12} & \cdots & y_{1N} \\ y_{21} & y_{22} & & y_{2N} \\ \vdots & & & \vdots \\ y_{N1} & y_{N2} & \cdots & y_{NN} \end{bmatrix} \begin{bmatrix} V_1 \\ V_2 \\ \vdots \\ V_N \end{bmatrix} \tag{7-1}$$

Where $I_{j,\ j=1,\ldots N}$ are the mutual currents in the network nodes, $V_{j,\ j=1,\ldots N}$ are the voltage at the network nodes, y_{jj} is the proper admittance of the matrix nodes, and $y_{ij,\ i\neq j}$ is the mutual impedance between two network nodes. The y_{ij} coefficients are generically calculated from;

$$y_{ij} = \left.\frac{I_i}{V_j}\right|_{I_k=0,\, k=1\cdots N,\, k\neq i}$$

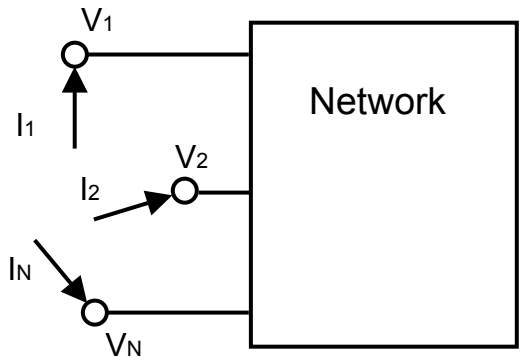

Figure 7.1 Generic electrical network

A frequency scan provides the response of the system to electric voltage or current at different frequencies. Because of its simplicity and usefulness, a frequency scan is usually the first step of every harmonic study and is also very suitable for transient studies [9]. The scan provides a first picture of the system behavior for a wide frequency range, allowing detection of possible problems that otherwise would be difficult to cover with time domain simulations at different system conditions. The scan study is done from one of the points in the network called the driving point. From this point a variable frequency current (or voltage) is injected into the network, the voltage (or current) response is measured at the same point or another point of interest and the result is usually given as a frequency-impedance plot. The range of variation of the source frequency depends on the type of study being developed. The injected current will generate a set of network voltages according to the admittance equation

$$\tilde{I}(h) = [Y(h)]\tilde{V}(h) \qquad (7\text{-}2)$$

Where Y(h) is a network admittance matrix, whose parameters must be valid over the whole range of study; $\tilde{I}$ the array of network currents when one current is injected and $\tilde{V}$ the set of voltages generated by the current injection. For a unitary current, the voltage value coincides with the impedance seen from the driving point.

It is also possible to do a frequency scan by feeding the network with a voltage source and calculating (or measuring) all the other voltage values in the network. In this case the relation obtained is called the voltage transfer function. The election of feeding the system with a voltage or a current source depends on the purpose of the frequency scan study. For

this work, where the system behavior under the influence of a generating harmonic current source is investigated, the current injection type of scan is more appropriate.

Other type of frequency domain harmonic study is called the harmonic penetration study [8]. This study is based in the same modeling of the network used by the frequency scan, equation (7-1). Differently from that method, the penetration study places harmonic current sources at all the places where non-linear components introduce harmonic distortion in the system at the same time. The non-linearities in the system have then been replaced by the source harmonic injections; the topology is now linear allowing to apply the superposition principle. The result of the study is a collection of the voltages (magnitudes and phases of the different harmonic components) at all the network nodes. This study is more complete than the frequency scan and is very popular in harmonic studies because it allows for multiple non-linear loads to be present in the system, It also allows for consideration of the influence of the fundamental voltage value on the generation of harmonics at the different components. Nevertheless, this method has some limitations that can be overcome with the employment of the harmonic load flow.

The most complete frequency domain type of study is the harmonic power flow, which combines the current source methodology discussed in the previous paragraph with the conventional power flow algorithms. The harmonic power flow technique is described in detail in [46]; here we will present only a brief description of it. There are basically two different ways of doing an harmonic power flow;

1- One technique is based on a standard power flow and the current source representation of the loads. The voltage resulting from the power flow is automatically used to adjust the harmonic currents injected by the different loads.
2- The other technique is based on a complete representation of the different loads where the harmonic current injected at each node is a complex function of the voltages and several other parameters generically expressed as;

$$\begin{bmatrix} I_1 \\ \vdots \\ I_N \end{bmatrix} = \begin{bmatrix} f(V_1 ... V_N, C_1 ... C_M \\ \vdots \\ f(V_1 ... V_N, C_1 ... C_M \end{bmatrix} \qquad (7\text{-}3)$$

where the parameters C_i represent the dependence of the load with parameters such as the motor speed –in case of a drive, etc. This technique is much more complex and complete and give the most accurate results.

In this study a combination of both frequency and time domain analysis were employed. The frequency scan was used to seek for preliminary results and provide some orientation for the study. Otherwise, the time domain simulation was widely used to study not only the effects of the harmonic components existing in the system but also other phenomena such as the magnitude of commutation transients and notches generated by the SFC operation.

7.2 Frequency Scan of the System Components

As previously stated the subsystem SFC, generator, transformer, and cable is an object of major attention. Therefore, several frequency scans were carried out to get the frequency behavior at these critical circuit elements. EMTDC provides an easy way to perform frequency scan with a variable frequency current source that can be placed in the driving point of interest. Because the goal was to obtain the frequency response over a wide range covering the harmonic and transient spectrum, we made the scan in two ranges for a better visualization. One range covers up to 200 kHz and the other only up to 5 kHz. Figure 7.3.1 shows the circuit disposition for the scan of the transmission cable.

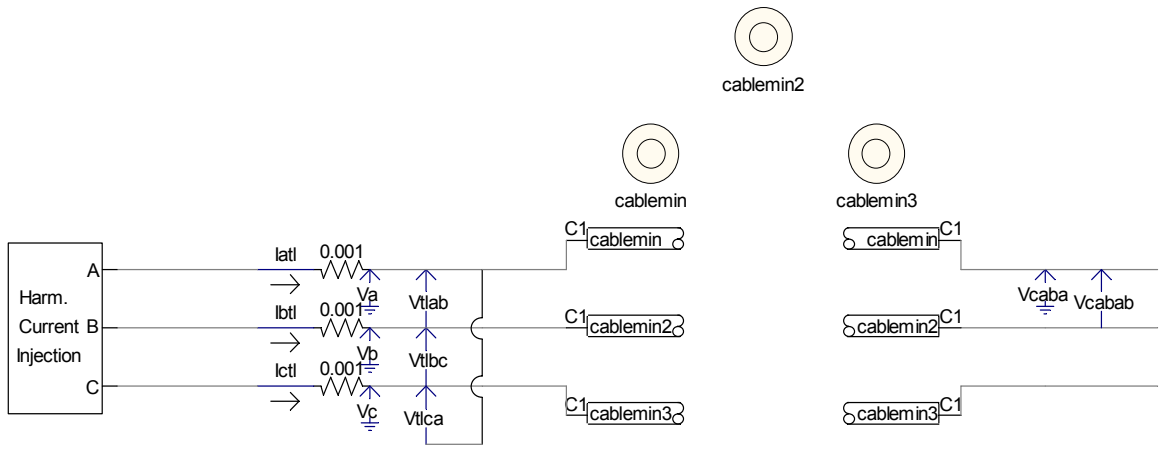

Figure 7.2 Circuit for cable frequency scan showing the variable frequency source, cable and different meters

7.2.1 Cable Frequency Scan

The cable is considered an open circuit on the side of the high voltage network for all the simulations carried out in this study because this is the actual operating condition when the machine is started. Therefore, only the cable is connected to the GSU transformer high voltage side. The first frequency scan was done only for the cable; the parameters for the scan ranges are shown in Table 7.1, and the results in Figure 7.3 and Figure 7.4. While no particularities are observed in the low frequency case, the high frequency scan reports the lowest series and parallel resonances at approximately 82 kHz and 167 kHz, respectively.

Table 7.1 Range and parameters of low and high frequency scan

Scan	Range [Hz]	f step [Hz]	t step [usec]	Resonance
High freq	500-200 k	500	0.1	82 k – 167k
Low freq	5-5000	5	10	-

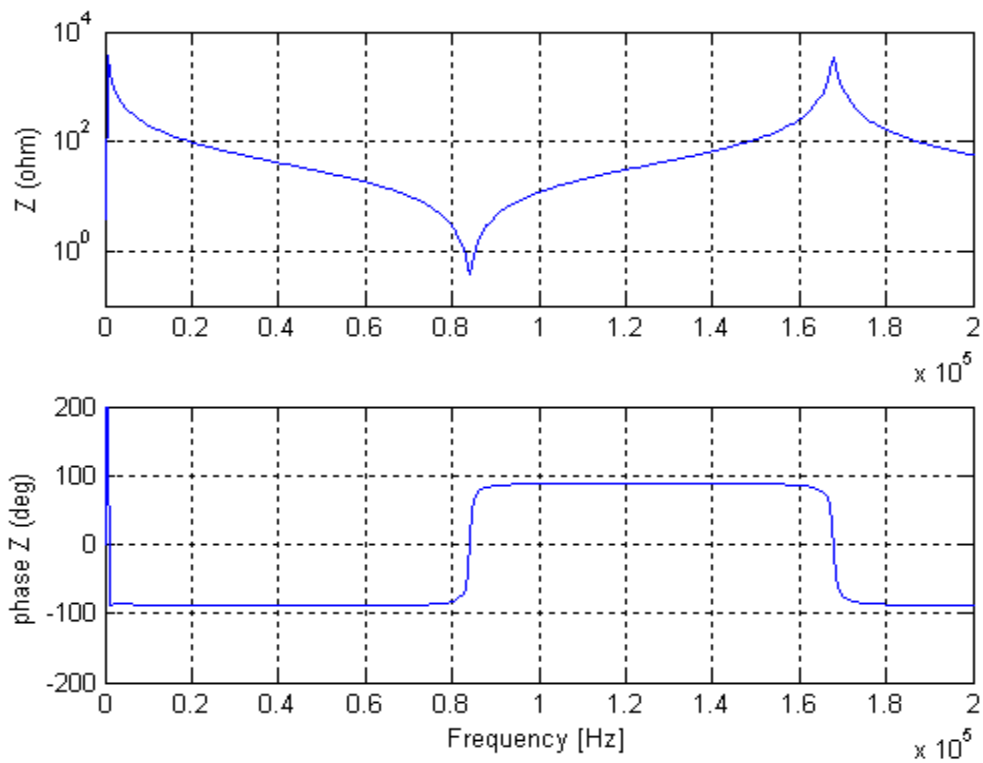

Figure 7.3 Result of the frequency scan for the cable model. Although our main interest and model validity is on the 0-20 kHz range, the scan covers up to 200 kHz. It is observed a series resonant frequency of the EMTDC model at 81 kHz

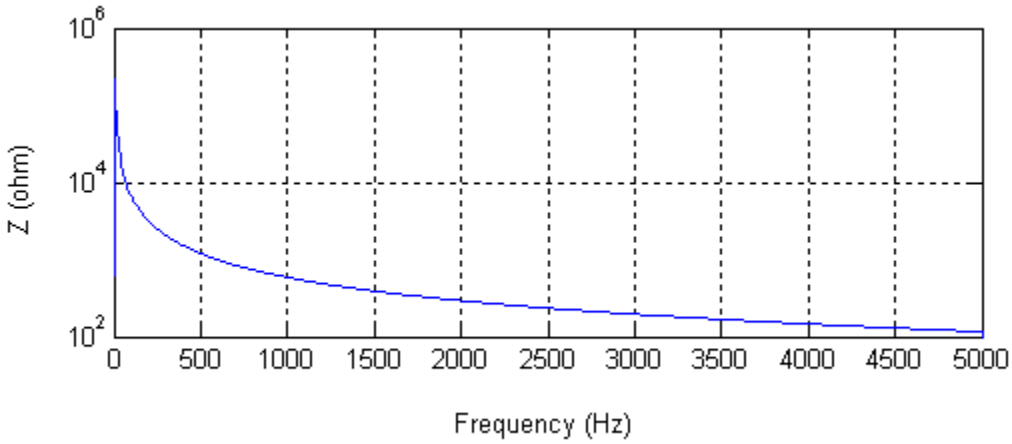

Figure 7.4 Result of the frequency scan for the cable model on the low frequency range

7.2.2 Cable and Transformer Frequency Scan

The next step of the study was to determine the frequency response of the cable and the GSU transformer. This characteristic is useful to understand the response to surges reaching the transformer. Therefore, a frequency scan with a driving point for z(ω) at the low voltage side of the GSU was performed. The scan was done on both frequency ranges of Table 2.1. Because of the transformer, the response at low frequencies is primarily inductive. When frequency increases, the surge capacitances appear, and after a resonance at around 195 kHz, the capacitance effect dominates the frequency response. Note that because 195 kHz is above the frequency range where this model is valid, this resonant frequency can have certain degree of uncertainty. Figure 7.5 shows the high-range scan characteristic; the low frequency plot does not present any interest and is omitted. The response at the internal nodes is not considered at this stage of the analysis. The circuit diagram is similar to the complete set cable, transformer and generator scan (without the generator branch) that is shown in Figure 7.6.

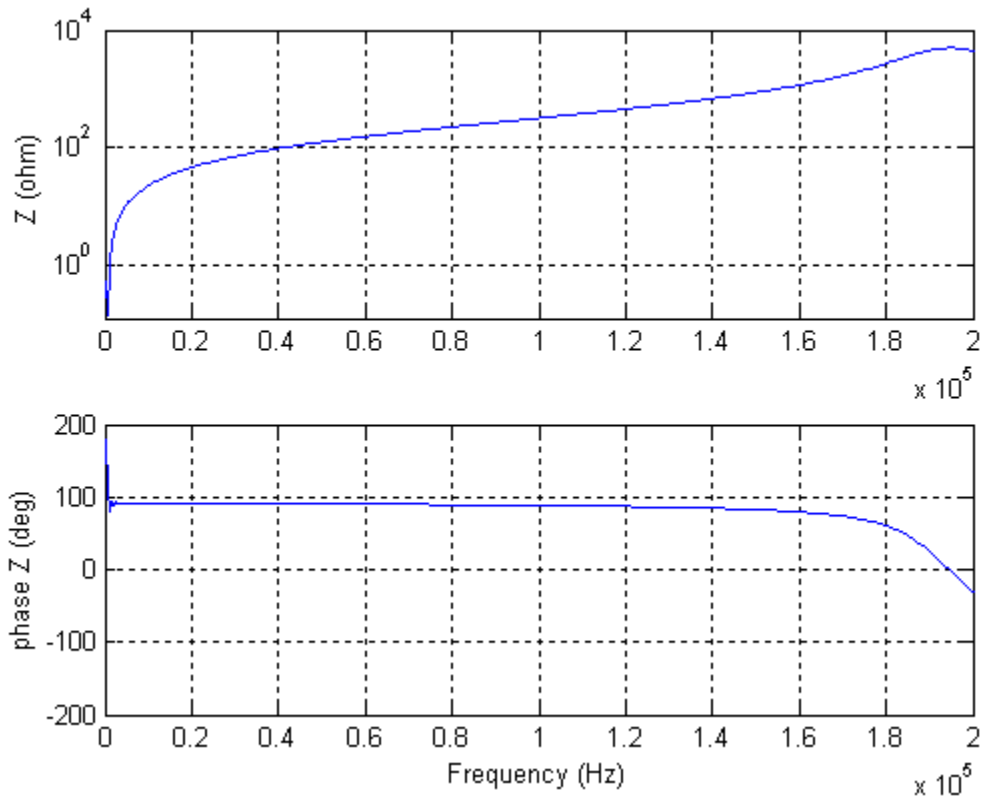

Figure 7.5 Result of the low frequency scan for the cable and transformer

7.3 Frequency Scan of the Starting System

The most interesting circuit for frequency scanning is the complete starting system composed by cable, transformer, and generator, because it provides the impedance seen by the disturbance source, which in this case is the SFC. If the generator were represented in a simplified way as an equivalent impedance plus a voltage source behind the impedance, the scan could be done by short-circuiting the voltage source and following the same procedure as above. Although the simplified modeling provides less accurate results, it is interesting to analyze the scan under this condition to provide more insight on the system harmonic behavior and the role of the synchronous machine in this behavior. A complete and more accurate model for the generator is not justified for the kind of picture of the system response for which a frequency scan is intended. The circuit used for the scan is shown in Figure 7.6 and the impedance seen from the SFC output node in Figure 7.7. This figure shows a clear

parallel resonance around 820Hz (13th harmonic) and some other resonant frequencies around 1250Hz (21st harmonic).

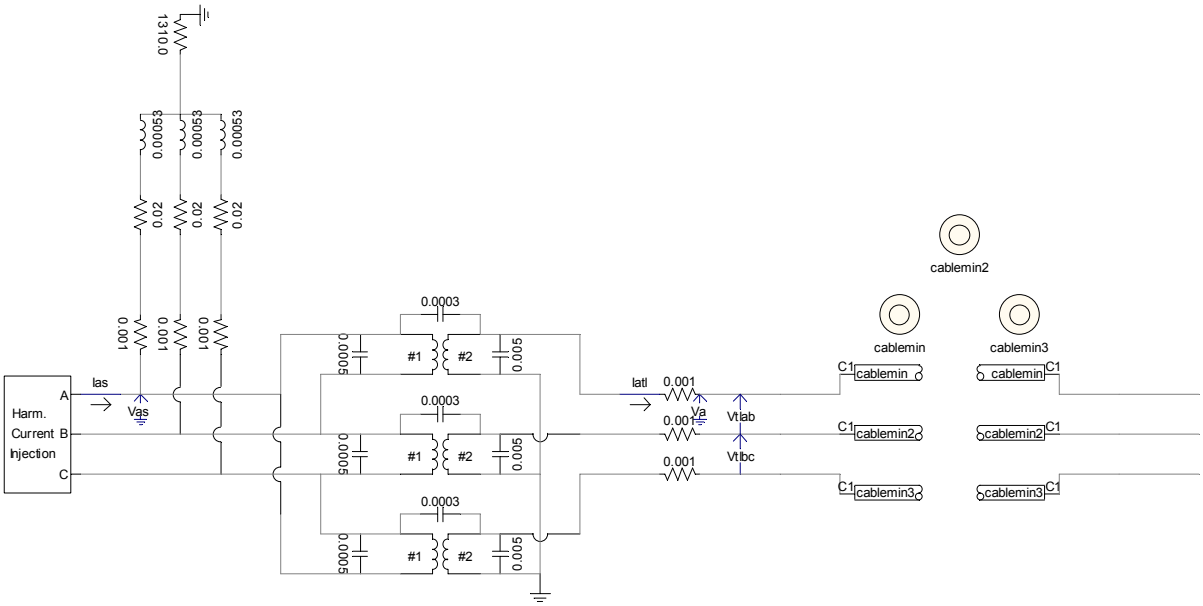

Figure 7.6 Frequency scan circuit for the cable, transformer and generator group

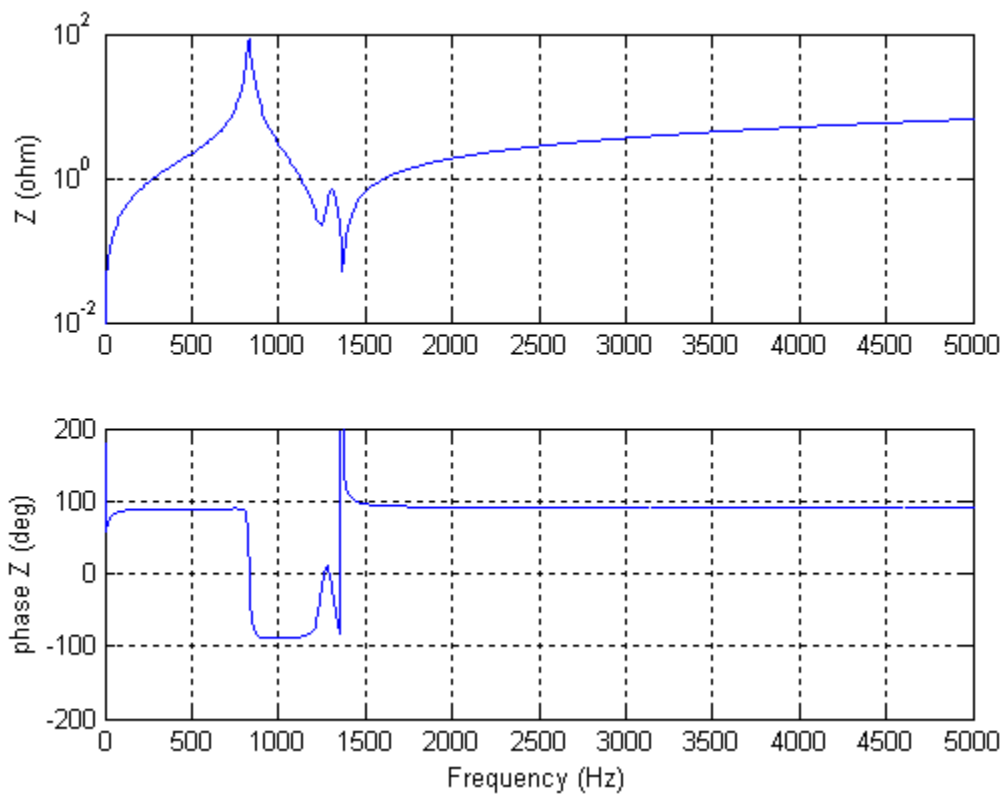

Figure 7.7 Frequency response of the cable, generator and transformer group

7.4 Analysis of Frequency Scan Results

Several resonances are observed in the impedance characteristics obtained from the frequency scans. The cable presents a resonant frequency at 82 kHz which is consistent with other studies done over this same cable [16]. The scan with the simplified model of the generator shows resonant frequencies at some frequency values that can possibly amplify harmonic components existing in the circuit. Because of some differences that exist between the simplified model and the actual generator, it is necessary to investigate how much of these possible resonances appear in the real case. The time domain simulation in the following chapter provides more insight on this subject.

The frequency scan at several driving points was done to get a first picture of the system response at different frequencies. A time domain simulation based on the operating conditions described in chapter six followed the scan study. Based on this basic information, some other cases were simulated in order to get a better understanding of how the system behaves. Finally, the results are analyzed on both different aspects: harmonics and transients generated by the thyristor commutation.

8 Time Domain Simulation

Time domain methods for the analysis of electric systems are generally more accurate than other frequency domain techniques such as power flow; on the other side, they are more complex to implement [46]. Some special conditions existing in the power system cannot be represented accurately by the power flow technique requiring the use of time domain simulation. These conditions can be summarized as:

1- The distortion produced by the devices can vary according to the conditions under which they are working. And this fact cannot be properly described by an equation like (7-3).
2- Interactions between different harmonic orders cannot be represented by time invariant models as the ones used for harmonic power flow.
3- When power electronic conversion is used, the presence of distortion in the system magnitudes can influence on the control of the gating signals.

Moreover, the time domain simulation allows the simultaneous existence of all the electric phenomena existing in the actual system operation like the transients produced by the switching of the power electronic devices that compose the energy converters.

In addition to a proper modeling of the different systems components, as developed in chapter four, some other consideration should be made in order to obtain accurate results from a time domain simulation of the system behavior. These considerations include the proper calculation of the initialization process and magnitude of the different variables. Some physical phenomena as the magnetic flux in electrical machines may take a relatively long time to reach its steady state regime. The loops associated to the control schemes of the power electronic converters can require special initialization procedures. The extinction of the transient phenomena related to the initialization process must be verified before using the data for the analysis.

In this work the harmonic phenomena and the commutation transient are, at least preliminarily, studied from the same models according to the modeling considerations previously explained. The simulation parameters (time step, etc.) are different according to the type of investigation. The complete system was modeled in EMTDC/PSCAD according

to the guidelines and conditions described in chapter four and the complete circuit diagram is shown in Appendix A. The base case is the SFC operating at its rated conditions. In addition, some other conditions were studied and the waveforms obtained for those cases are included when considered useful for the analysis.

8.1 Rated Operating Conditions (Base case)

The analysis of the electric magnitudes and their harmonic content at different points of the system allow analyzing the stress levels and effects over the equipment. In addition, with the analysis it is possible to infer the action each component has in the behavior of the complete system and its electrical magnitudes. The data in this section is presented in a way intended to help the analysis. First the voltages at different nodes are analyzed and then the currents and some other magnitudes if relevant. The waveforms are presented in a sequence starting at the far end of the cable and going through the different components until the supplying voltage source at the MV auxiliary bus of the station. Each waveform plot shows a two-cycle waveform plus the harmonic spectrum of that waveform. On the harmonic charts, the relative content is related to the fundamental component, which implies that the fundamental percentage is always one hundred. The names of the signals refer to the names in the circuit diagram in Appendix A. In this chapter only a reduced set of waveforms are included for each simulation case. A complete set of waveforms for the different tested cases can be seen at the Appendix B.

Figure 4.1 shows the voltage at the transformer HV side. It is observed the important level of 13th harmonic and a relatively high total harmonic distortion. The harmonic content does not considerably increase the maximum voltage value; a crest factor of 1.64 implies only a 15% of increment over the maximum voltage under sine wave conditions. The waveforms of the voltage at both sides of the transformer and at the cable end are completely similar; therefore, only one is presented here. Table 8.1 shows a comparison between the harmonic content in the voltage waveforms before and after the transformer. It is possible to see a reduction in the harmonic content at the transformer low voltage side. This fact suggests the idea that the cable plays an important role in generating the harmonic generation and the abnormal level of 13th harmonic.

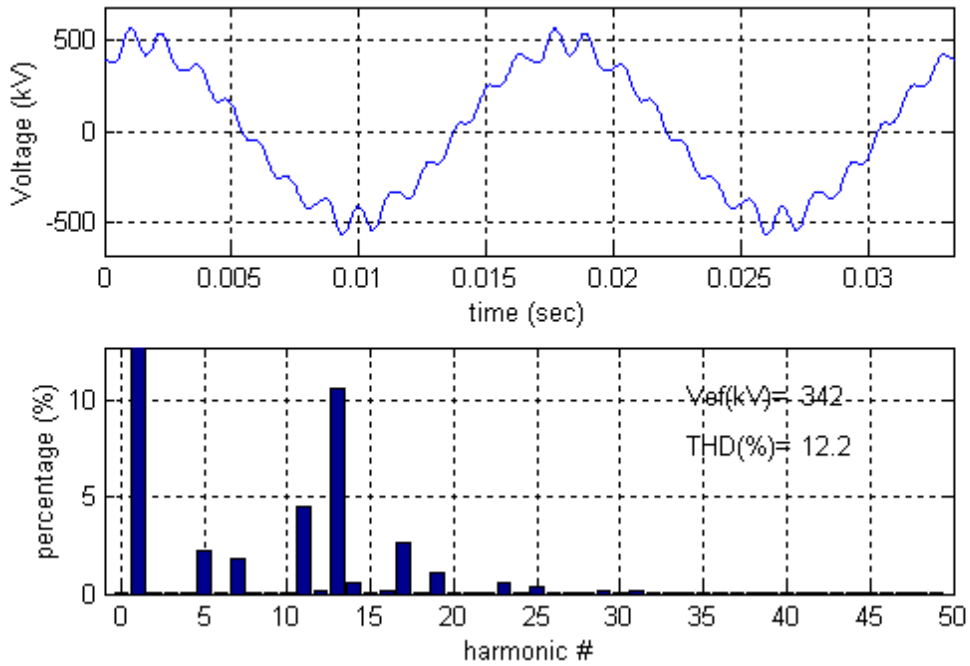

Figure 8.1 Vtab Line –line voltage at the transformer HV terminal. As the cable is not loaded it is very close to the voltage at the cable open-end

Table 8.1 Harmonic characterization of the voltage at the cable end, and at the GSU low and high voltage side

Network point	THD [%]	13th [%]	CF [%]
V cable	12.2	11.0	1.64
V transf HV	12.2	11.0	1.64
V transf LV	8.2	6.9	1.51

The voltage waveforms before and after the SFC are shown in Figure 8.2 and 8.3 respectively. The voltage at the output shows a disproportionate amount of the 13th and 11th harmonics, which do not follow the general exponential decaying tendency of a phase-controlled converter [47].

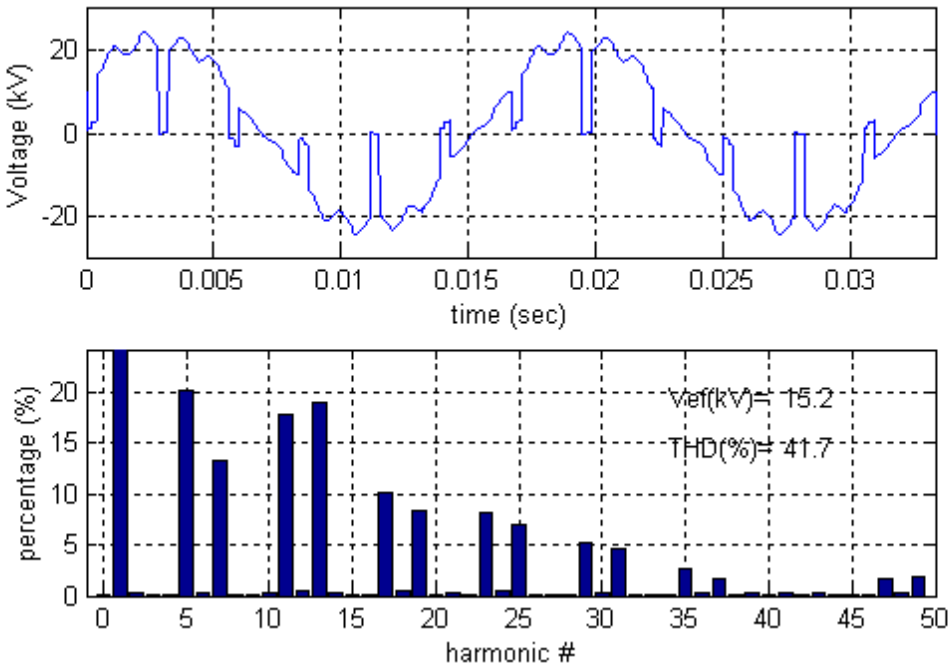

Figure 8.2 Vab Line – line voltage at the SFC converter output side, 16.5 kV

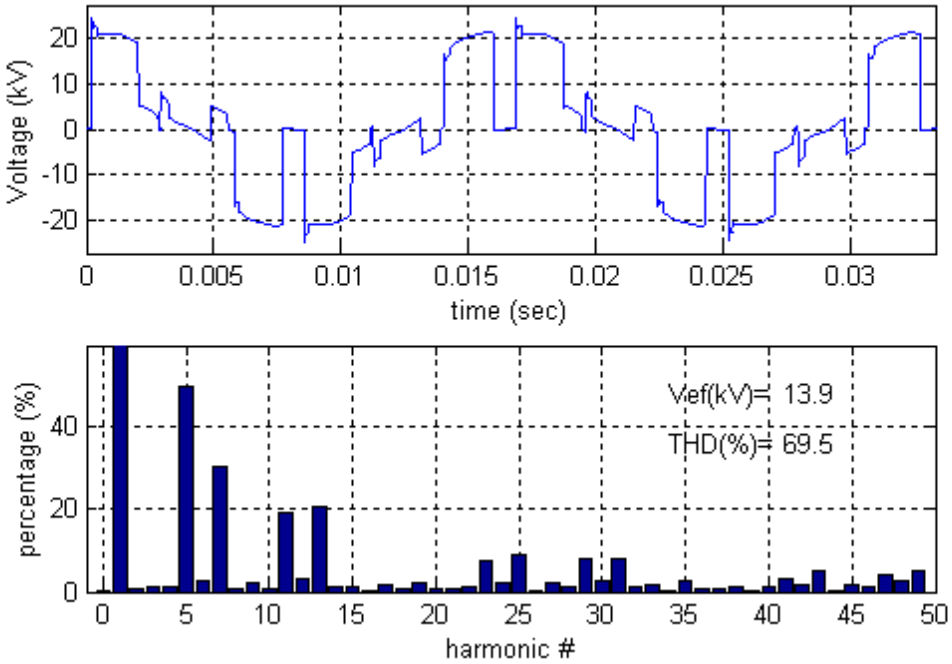

Figure 8.3 Vsab Line –line voltage at the converter input side, 16.5kV

The major difference between the Figure 8.2 and 8.3 is in the content of the 11th and 13th harmonics. These harmonic orders are generated by the interaction among the equipment connected at the SFC output, as it is suggested by the resonant frequencies found in the frequency scan. It is important to note that he presence of harmonic in the SFC input side is very important being larger than at the output. Therefore, it is possible they create problems to other equipment connected on the SFC input side. Figure 8.4 shows the line to ground voltage at the primary side of the SFC auxiliary transformer. Although the harmonic distortion has been considerable reduced, the level of disturbance is still large and can create problems in auxiliary equipment and illumination devices. In the facility object of the study problem created by harmonics over auxiliary equipment has been observed, producing failures in discharge lamps used for lighting.

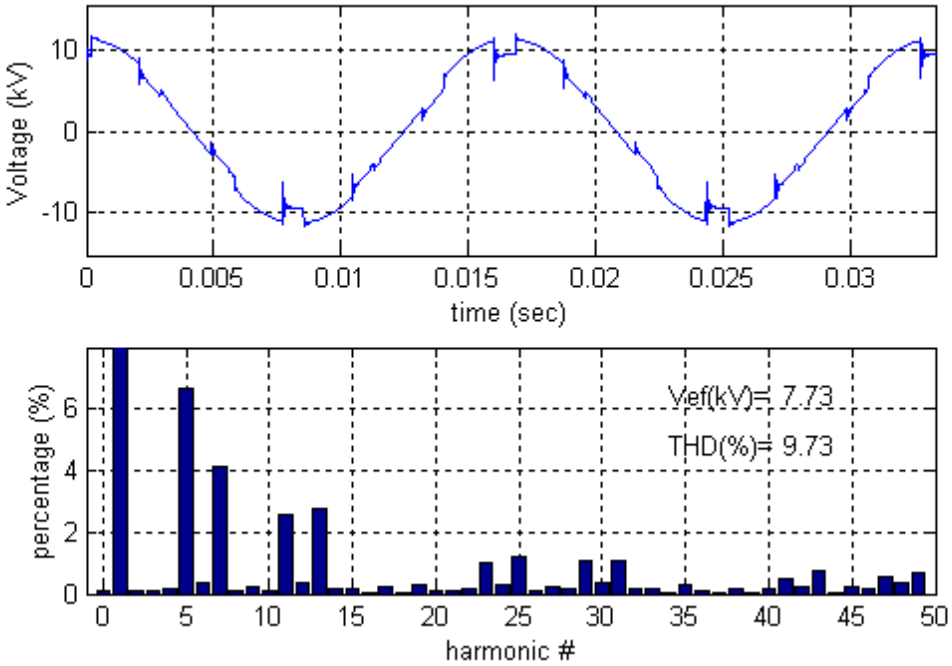

Figure 8.4 Vna Line –ground voltage at the auxiliary bus if the station, 13.8 kV.

In the following figures, the current waveforms for the base case are presented. The sequence of the figures in this case starts at the transformer LV side. Figure 8.5 shows the current at the primary winding of the GSU transformer. It is possible to see that the harmonic distortion is very large and the content of the 13th component is even larger than the

fundamental. The magnitude of the 13th order current is large considering that the transformer is unloaded. Figure 8.6 shows the current on the synchronous machine where the harmonic content is superposed to the stepped current waveform being the 5th and 13th harmonics the predominant orders.

Making a comparison of the 13th harmonic component at the transformer and synchronous machine, the content of that harmonic result:

I_{13}= 135 A at the transformer LV line current

I_{13}= 143 A at the synchronous machine input

which are very close values. This fact shows that the 13th harmonic component circulates in the path between the synchronous machine, GSU transformer and cable; and that the SFC introduces only a small portion. The waveform of the transformer line current at the LV side can be observed in Appendix B and is very similar to the one presented in Figure 8.5 with the expected difference in the third order components due to cancellation by the line-line addition effect. Figure 8.7 shows the line current at the SFC output with the typical waveform and harmonic content of a current source inverter.

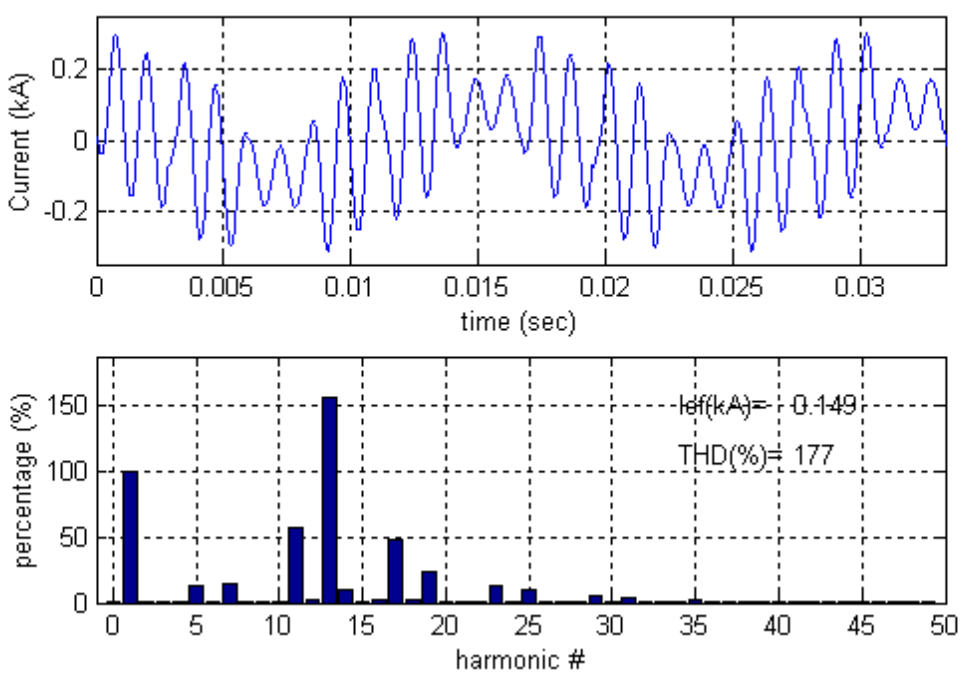

Figure 8.5 Iatr Phase current at the LV winding of the main transformer, in the delta winding

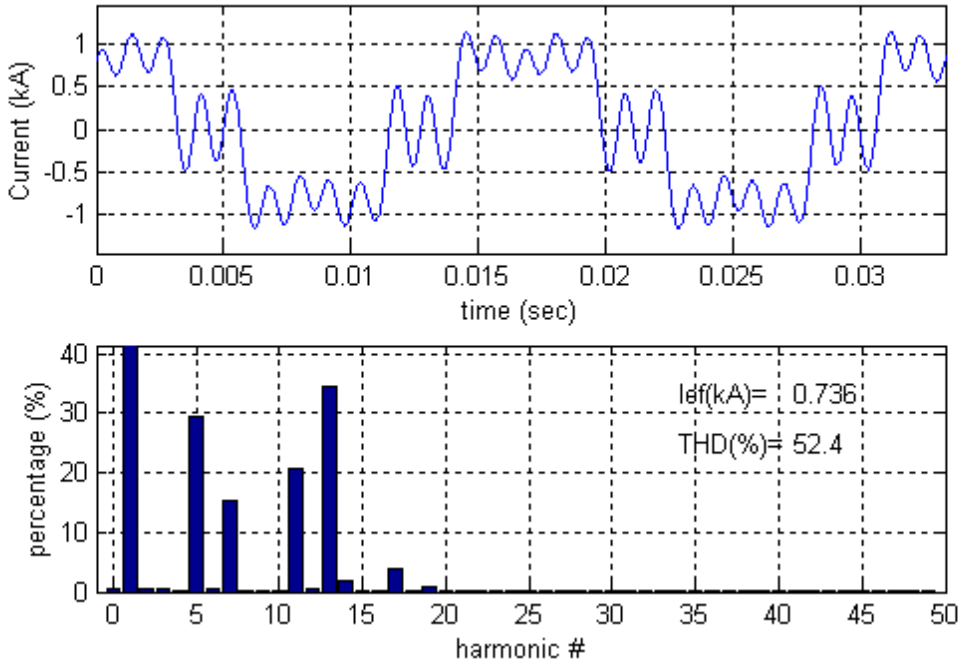

Figure 8.6 Iag Synchronous machine input current

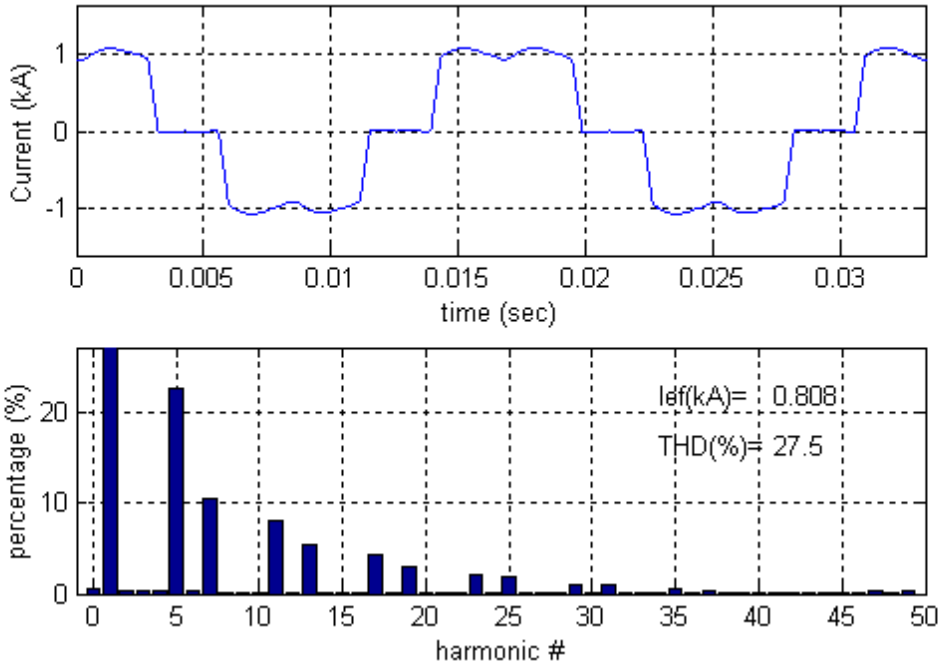

Figure 8.7 Iato SFC output current. There is no major difference with Isa_2, the input current of the SFC

The addition of the currents in the delta-wye windings of the auxiliary transformer makes the current in the primary side of the transformer to have the waveform shown in Figure 8.8. The harmonic content has no significant change, but the difference in the phase angle of the components produces a different waveform.

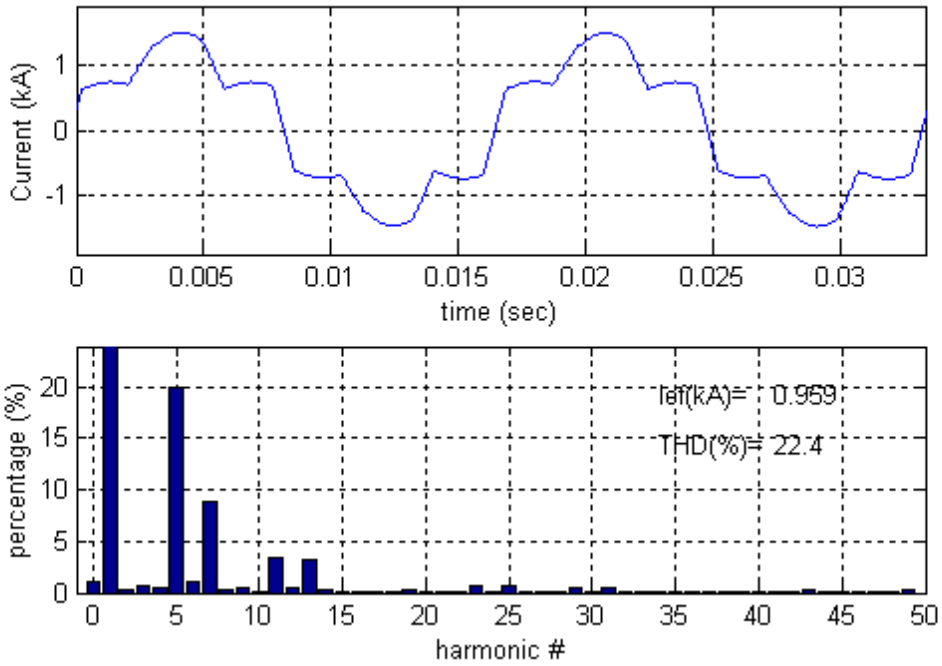

Figure 8.8 Isa SFC input current at the primary side of the auxiliary transformer, 13.8kV

Summarizing the analysis of the voltage and current waveforms for the rated operation conditions it is possible to reach the following conclusions. The voltage waveform and harmonic content are according to what can be expected for the type of phase-controlled rectifier and converter in use, except for the level of the thirteenth harmonic [47]. The magnitude of that harmonic is considerably larger than what can be expected, especially in the transformer HV side and the cable terminals. This fact indicates the HV cable as the amplifier of that harmonic order. Nevertheless, the effect is produced by interactions between all the system components. The current also presents a considerable amount of thirteenth harmonic in the GSU transformer and generator. The abnormal levels of that harmonic component in the voltages and currents are not seen at the SFC input side and the auxiliary

bus at 13.8 kV, but the total harmonic content at this points is considerably large and can have harmful consequences over the equipment connected a that level.

8.2 Other Operating Conditions at Natural Commutation

8.2.1 Effect of the load current on the circuit behavior

The system was also simulated with the machine taking less power from the SFC. Mechanical and electrical no-load losses define the minimum power the machine takes when rotating at rated speed and no mechanic load is connected to the shaft. Even though the value of these losses can be closely approximated and the respective current used for the simulations, it is important for the harmonic study to see how much of the harmonic generation changes with the current level. A simulation was carried out at approximately half of the rated power in order to observe the effect of the current value on the harmonics. This value of current is closer to the existing in the circuit when the machine is started following the acceleration characteristic previously presented. A reduced set of charts is included here for the purpose of comparison, especially when differences appear respect to the base case. More waveforms can be seen in Appendix B.

Figure 8.9 shows the voltage waveform at the GSU transformer terminals. From there it is possible to observe a reduction in the total harmonic distortion level. On the other side the spectra follows a similar pattern to the full load condition with a remarkable predominance of the 13th order harmonic. In Figure 8.10 it is possible to observe the waveform of the line-to-line voltage at the output of the SFC. The time-length of the notches in the waveform has been considerably reduced, as the time of current commutation between two inverter branches is smaller. This is fact is directly related with the current value. The total harmonic distortion is also smaller than the full current load case while the harmonic pattern is the same. The last figure corresponding to this simulation case is Figure 8.11, which shows the line current at the transformer primary side. From the analysis of the circuit magnitudes under the condition of reduced load current, it is possible to conclude that a reduction in the current lowers the harmonic perturbation in all the system. The

characteristics of the harmonic and transient phenomena are similar independently of the current regime, but the level of the harmonic distortion is reduced with the current value.

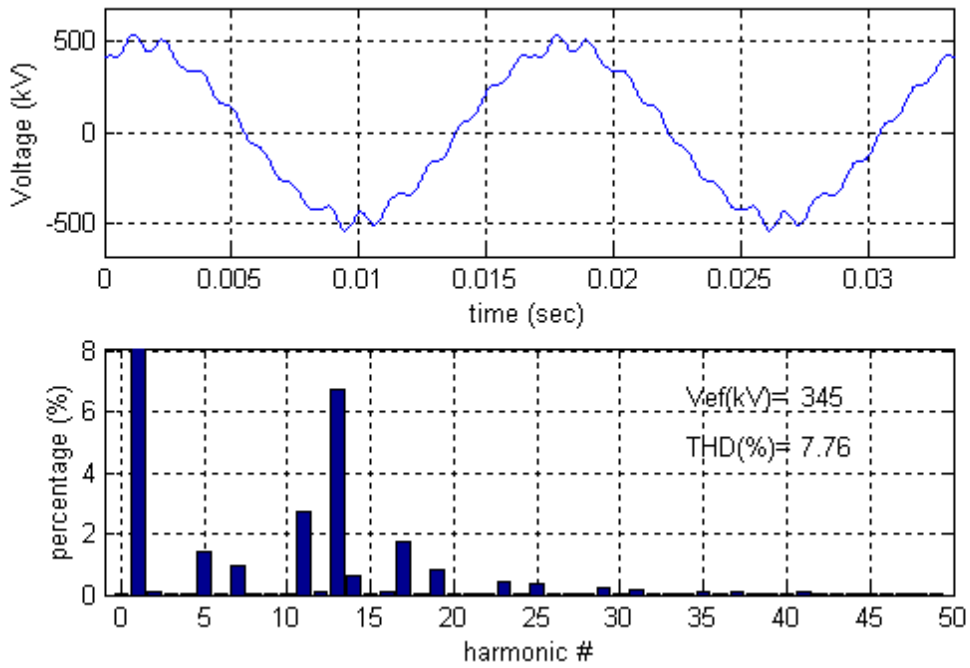

Figure 8.9 Vtab, line –line voltage at the transformer HV terminal. The harmonic content is reduced respect to the base case

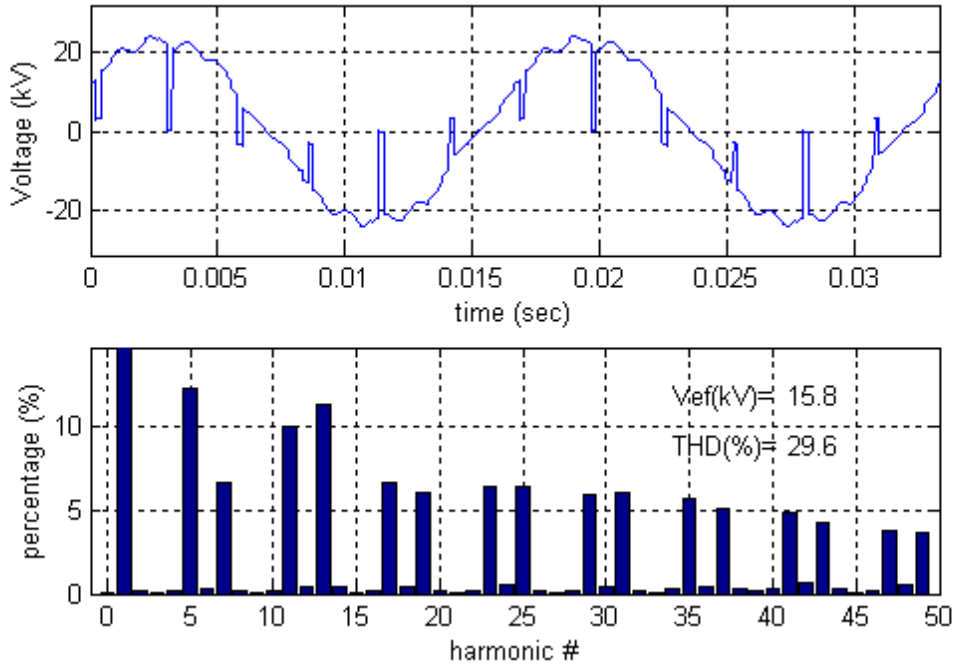

Figure 8.10 Vab, line – line voltage at the SFC output (the machine side)

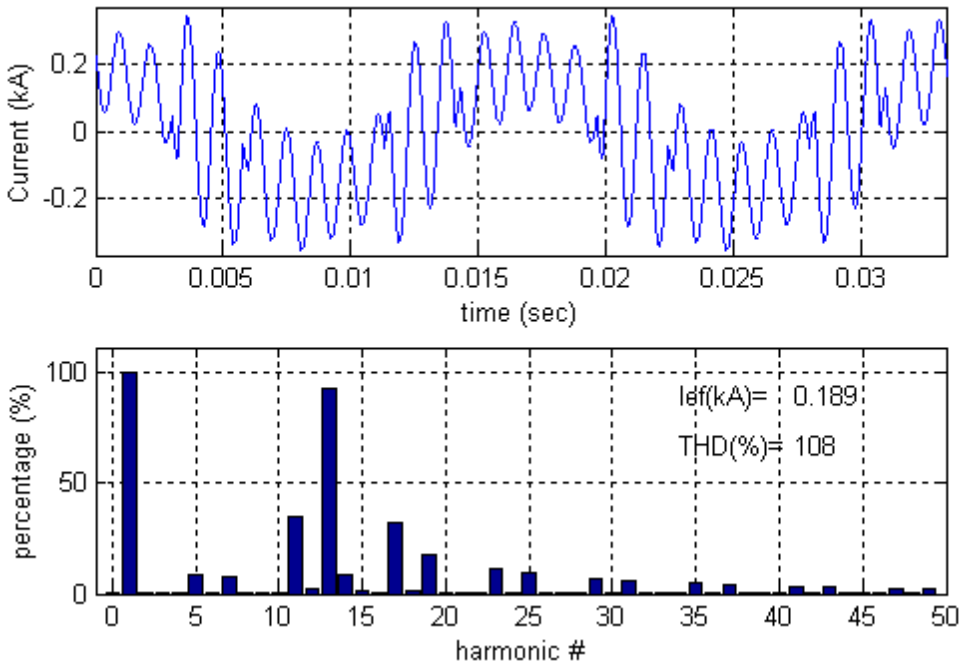

Figure 8.11 Iat, line current at the LV side of the main transformer

8.2.2 Effect of the system speed on the circuit magnitudes

The system was simulated at a reduced speed while still at natural commutation. At this point of the starting process, the counter electromagnet motive force c.e.m.f. generated by the synchronous motor is reduced according to the rule,

$$V \propto f \cdot \psi$$

Where V is the voltage at the machine terminals, f is the frequency and ψ is the airgap flux. Because the control strategy is to keep the magnetic flux constant (section 5.1) the voltage is proportional to the machine frequency and hence the rotor speed.

Figure 8.12 shows the voltage evolution in the HV side of the GSU transformer, in this case the maximum magnitude is reduced to almost half of the rated voltage while the harmonic orders present in the spectra vary according to the value of the fundamental frequency. In the frequency scan, the resonant frequency was found at approximately 820 Hz. If the fundamental frequency is 30Hz, the related harmonic is,

$$n = \frac{820}{30} = 27.33$$

The 27th harmonic is a triplen order harmonic and therefore is canceled on the line magnitudes. The following closest harmonics is the 29th, which has a considerable value as is observed in the spectra; also the 25th harmonic is considerable increased. It is possible to observe how the effect of the parallel resonance shifts the harmonic spectra according to the system frequency.

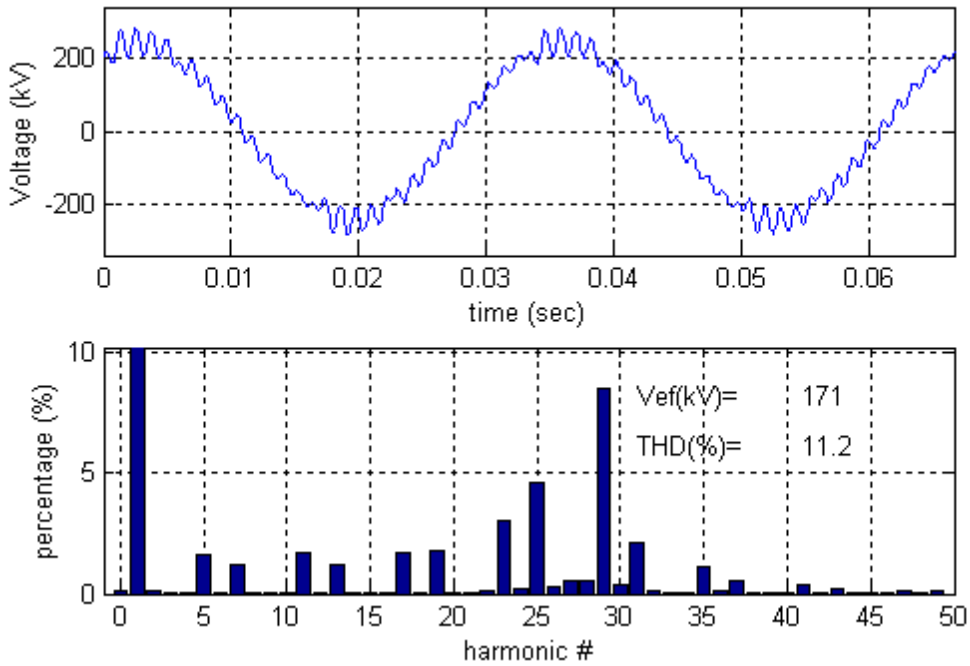

Figure 8.12 Vtab Line to line voltage at the high voltage side of the GSU transformer

Figure 8.13 shows the line-to-line voltage at the output of the SFC, which has a shape close to the rated speed case, but with different harmonic spectra. It is observed an abnormal reduction in the 29th harmonic in this case; this fact can be originated by a canceling effect generated by the voltage drop produced by the 29th harmonic current circulating between the generator and the transformer. The change in the spectra is also valid for the transformer LV winding current as it is shown in Figure 8.14 being the largest component at half of the rated speed the 29th harmonic order. The harmonic distortion is increased respect to the base case due to a reduced value of the fundamental component because the system voltage is reduced. On the other side, because the voltage harmonic components are not reduced in the same proportion, a large harmonic flux value exists in the GSU transformer. This harmonic flux

will originate large harmonic magnetizing currents at those orders that are observed in Figure 8.14.

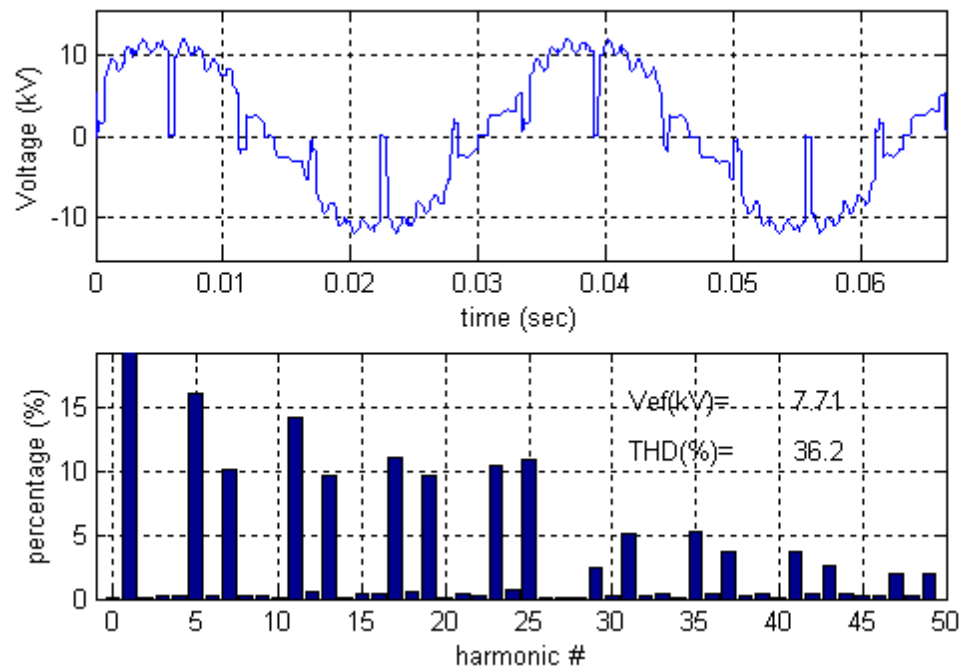

Figure 8.13 Vtab Line to line voltage at the high voltage side of the GSU transformer

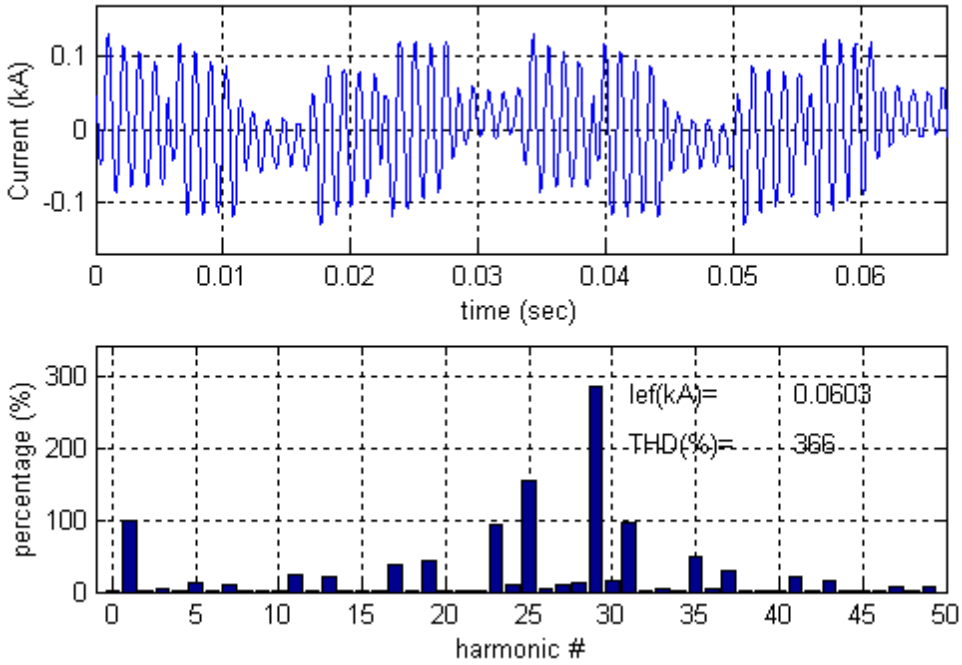

Figure 8.14 Iatr Current at the transformer LV winding

The SFC input and output currents are shown in Figure 8.19. Each of the currents has the frequency of the system connected to each side of the SFC, which are 60 Hz and 30 Hz. The harmonic spectra and total distortion is similar at both sides of the converter. Moreover, the presence of components induced by the circuit resonance at the SFC is small as was previously discussed in section 8.1.

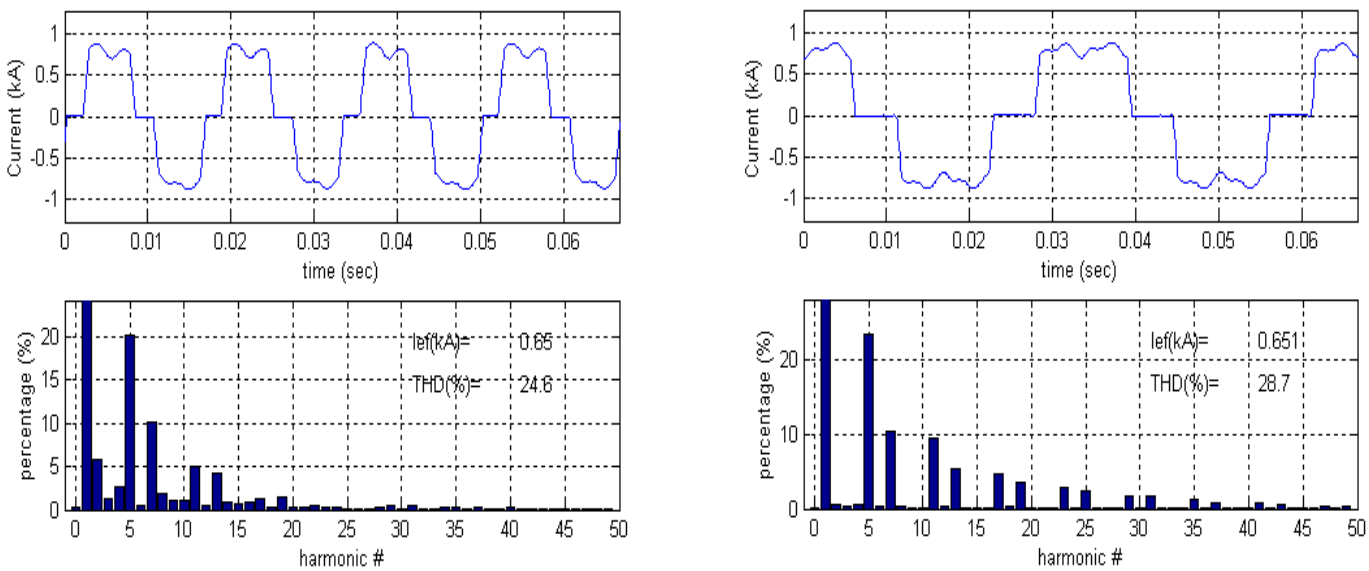

Figure 8.15 SFC currents (a) at the SFC input the frequency is 60Hz (b) at the SFC output, f=30Hz

8.2.3 Effect of the transmission cable on the circuit behavior

Other interesting condition for the analysis of the system behavior and the interaction between the different components is obtained by disconnecting the cable form the HV side of the GSU transformer. Although this condition is not possible from the point of view of the operation, it helps to understand the behavior of the equipment under normal operating conditions. Figure 8.16 shows the voltage waveform at the HV side of the GSU transformer and its harmonic content. Comparing this result with the previous waveforms at the same point, it is possible to note a completely different harmonic spectrum. In Figure 8.17 the current at the LV winding of the GSU transformer shows an important presence of higher

order harmonics superposed to the magnetizing current. In Figure 8.18 it can be observed that the thirteenth harmonic component has almost completely disappeared in the current at the synchronous machine. This current is almost the same as the current in the SFC output as the magnetizing current in the transformer is small.

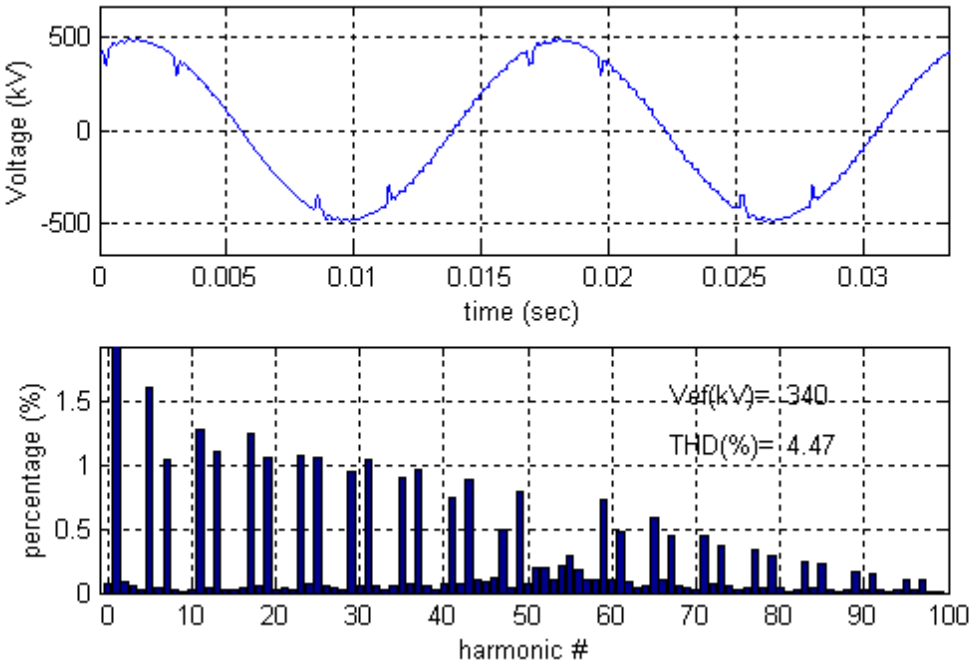

Figure 8.16 Vtab Line –line voltage at the transformer HV terminal

From the analysis of this operation condition, with no cable connected, it is possible to observe that the abnormal increment in the thirteenth harmonic disappears. On the other side, higher harmonic orders around the sixtieth component exist in the system but its value is small. These high order harmonics are also present when the cable is connected but its presence is hidden by the relatively large value of the harmonic distortion existing in the system. The magnitude and level of this distortion at relatively high harmonic level is related with the values of the surges capacitances of the transformer. Because the capacitance values were estimated during the transformer modeling, some differences with the actual values are possible, but in any case its relevance is very small.

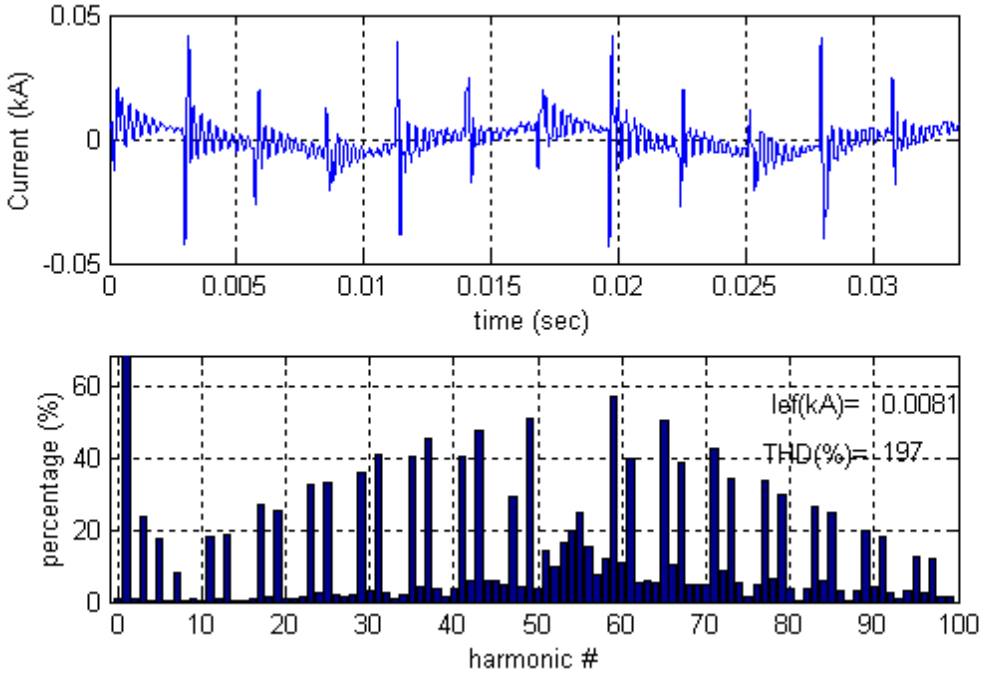

Figure 8.17 Iatr Current at the LV winding of the main transformer, inside the triangle connection

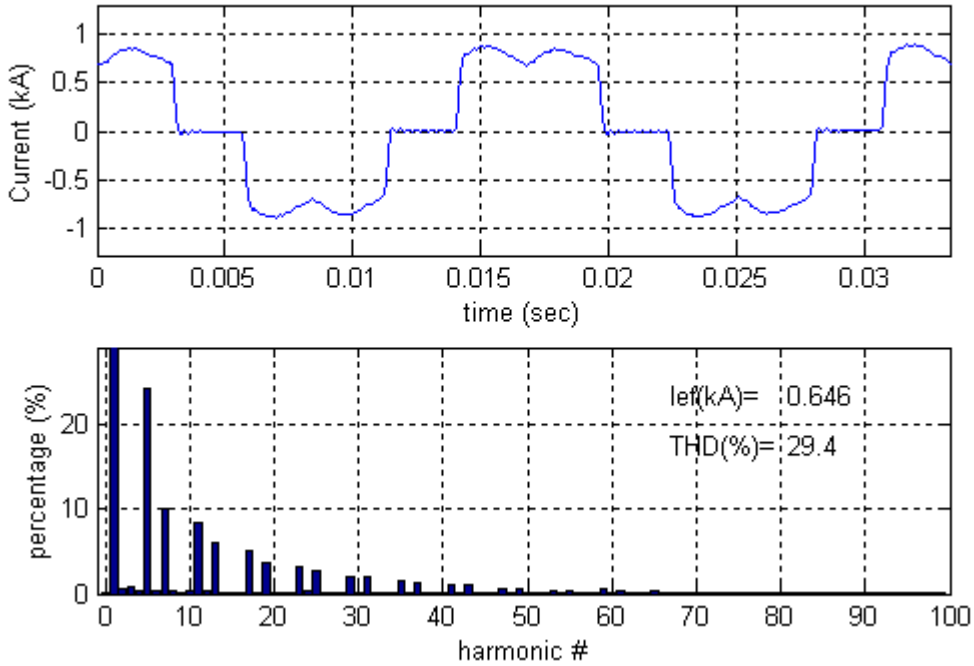

Figure 8.18 Iag current taken by the synchronous machine

8.3 Operation at Forced Commutation

It was explained in section five that the control process of the SFC is composed by a forced commutation stage from start up to 8~10 % of the rated speed and a natural commutation stage from there up to rated speed. At forced commutation, the c.e.m.f is very low according to the low speed of the rotating field. On the other side, the switching of the SCRs both at the rectifier and inverter bridge requires more complexity due to the forced commutation process. Therefore, the machine work was simulated at the forced commutation stage to verify proper conditions and the absence of dangerous spikes that can affect the GSU transformer or other connected equipment. As it was explained in chapter five, the forced commutation process requires the cancellation of the current in the DC interface to allow the commutation of the SCRs in the inverter. In the system under study the inverter is build with GTO devices allowing for a turn off process of the circulating current. Nevertheless, if the GTOs are forced to turn off, the overvoltage generated by the current source –inductor at the DC interface- would be very large creating hazard to the connected equipment.

Figure 8.19 shows the current at the DC interface during forced commutation. The period of the "rectified" current is related to the speed of the synchronous motor. In the case of the Figure 8.19 the waveform corresponds to a frequency of 5.75 Hz. Due to the working point characteristics, the input currents are not periodical as can be observed in Figure 8.20 where the current in the line input is plotted. Because of the non-periodicity of the signal, it is not possible to get its spectra by Fourier analysis.

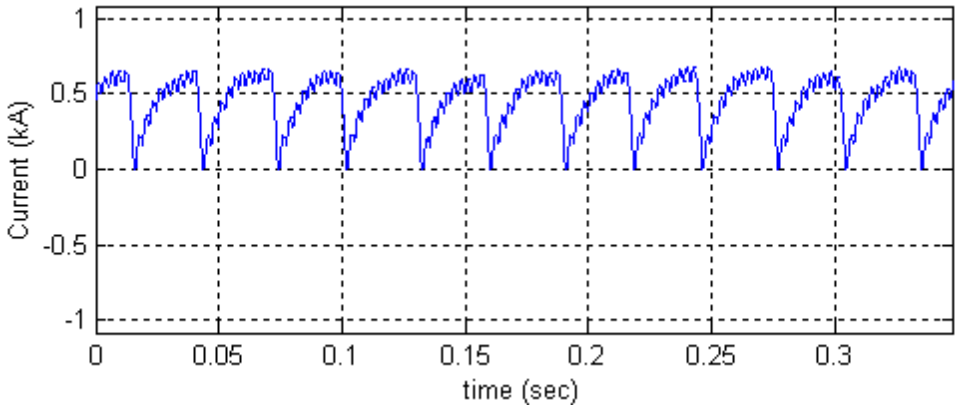

Figure 8.19 Irect Current at the DC interface between the rectifier and inverter

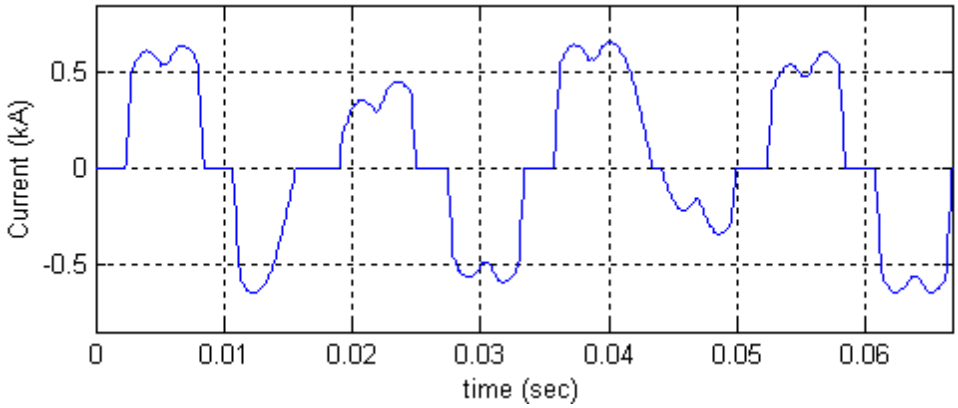

Figure 8.20 Isa2 Line current at AC three phase input of the SFC, at 16.5 KV

The voltage applied to a SCR in the inverter bridge is shown in Figure 8.21, the negative spikes correspond to the instant when the current is reduced to zero. At this instant the rectifier operation mode is switched to inverter mode, then the voltage applied to the DC loop is inverted and used to cancel the current. As it was also explained in chapter five, the instant when the voltage at the GTO is negative is used as a control parameter for the generation of the firing pulses.

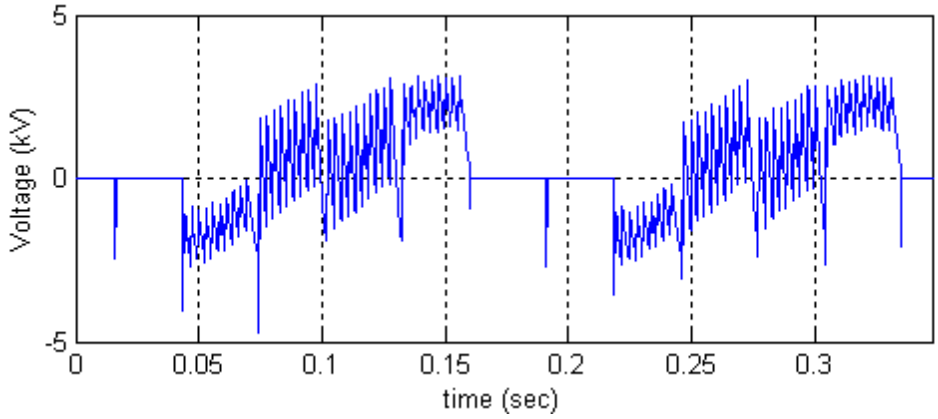

Figure 8.21 Et3 Voltage at terminals of a GTO in the inverter bridge

The main purpose of this study was to analyze the electric disturbances at the HV equipment. Figure 8.22 shows the voltage at the high voltage side of the GSU transformer. As it is possible to observe in the figure, the magnitude of the voltage is relatively low.

Moreover, the relative magnitude of the spikes has been reduced compared to the SFC output voltage due to some filtering introduced by circuit elements as reactors. The presented waveforms were obtained with the inverter operating at a frequency approximately of 5.75 Hz. Therefore, the Fourier analysis was done relative to this frequency to get some insight on the sources generating the higher frequency components. From the spectrum decomposition it can be observed that a set of components is around the 60th harmonic that corresponds to:

$$f = 5.75 \times 60 = 345 \text{ Hz}$$

This frequency is close to the switching frequency of the rectifier of 360 Hz. The other important set of components is located around the 140th component that corresponds to:

$$f = 5.75 \times 140 = 805 \text{ Hz}$$

which is close to the parallel resonant frequency of the circuit detected at 820 Hz.

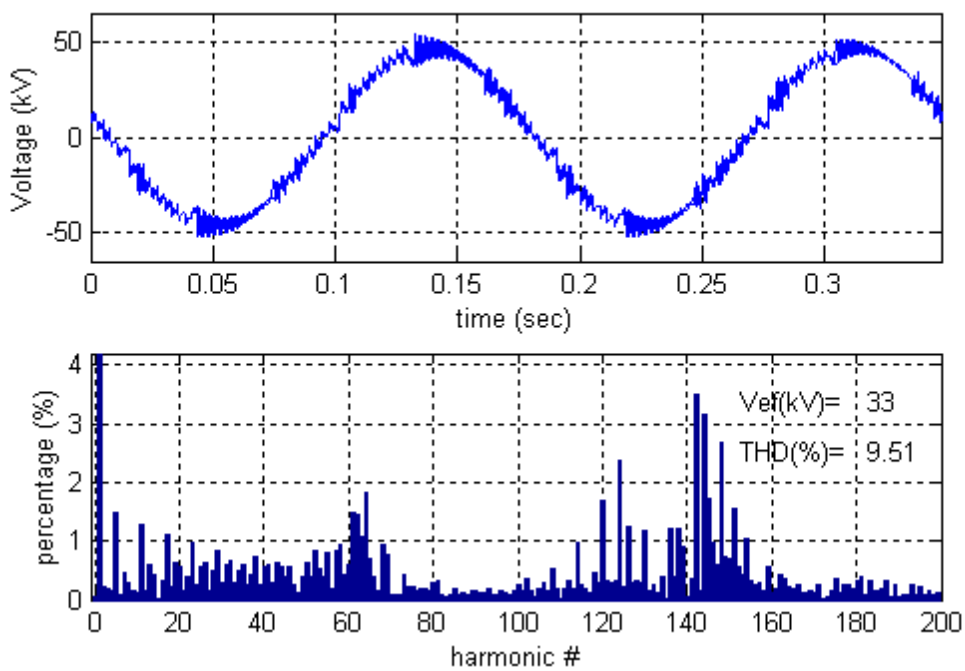

Figure 8.22 Vtab Line to line voltage at the GSU transformer HV winding

The current at he LV winding of the transformer is shown in Figure 8.23. The current spectrum has large components around 820 Hz and 345 Hz similar to the voltage spectrum. The components around 820 Hz are related with the natural resonance of the circuit and is present during all the starting process. The components around 345Hz are related with the

switching frequency of the SFC and hence change with the fundamental frequency of the current supplied by the SFC.

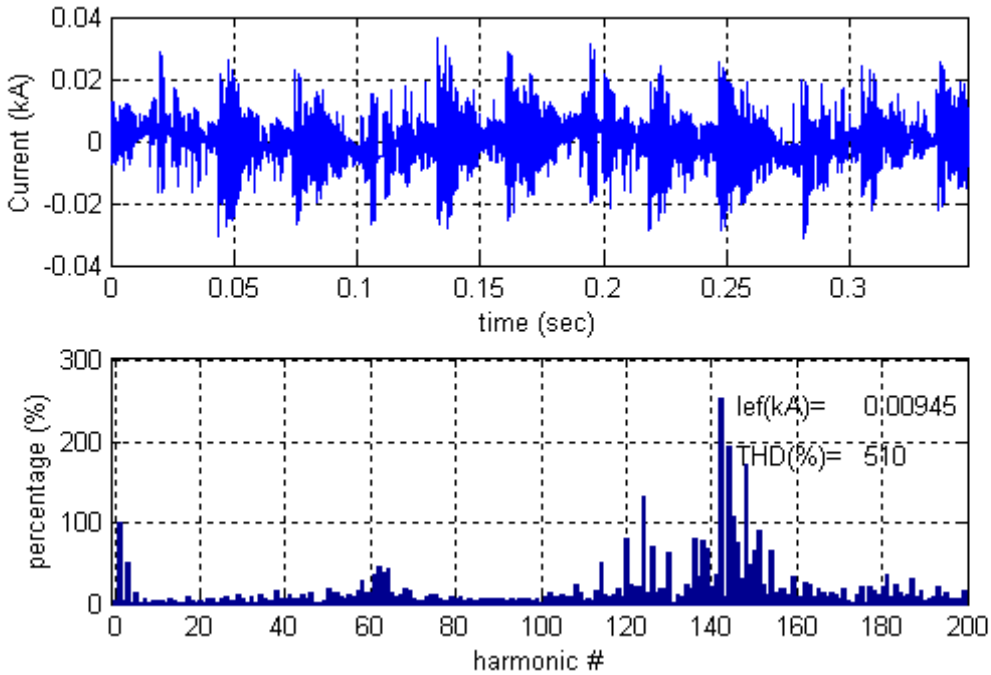

Figure 8.23 Iatr current at the LV winding of the GSU transformer

8.4 Analysis of the Commutation Transient

This section analyzes in detail the transients produced by the commutation of the SRCs during the SFC operation. A general review on how the commutation process generates transient overvoltages was done in chapter three. The waveforms presented up to this point do not show an important amount of commutation transient. This fact led us to investigate more closely the evolution of the voltage at both sides of the converter during the operation and search for possible spikes in the voltage waveforms. In addition of knowing the characteristics of the commutation phenomena, it is important to know if the mitigating devices provide the proper degree of protection to the equipment.

The characteristic frequency of the commutation transient depends on the circuit parameters and some other parameters that usually are not totally well known as the stray

capacitances and inductances. Moreover, as a matter of fact, the order of the frequencies involved is generally larger than the basic 20 kHz under what the model of the system was developed. Nevertheless, as it was explained before, when protecting devices that have the purpose of limiting the steepness of the transients are present in the circuit the frequency of the transient is diminished. A detailed and accurate study of the commutation transient phenomena would require the development of a new model of the system more appropriate for higher frequencies. However, the formulation of this model can be quite difficult and uncertain due to the difficulty in knowing some system parameters such as the stray capacitances. In order to avoid this problem and check the absence of harmful transient overvoltages on the GSU transformer terminals, the SFC operation was simulated adding stray capacitances, because they, combined with the inductances of the circuit elements, play the major role in the generation of the commutation transient [3]. The values of the stray capacitances were estimated based on literature values and practical knowledge. For the purpose of the detecting a possibly faster transient, the time step was reduced for the simulations (0.5 μsec).

The primary purpose of snubber circuits on each device is to limit the dv/dt on the SCRs to avoid non-desired triggering. Depending on the circuit configuration, the snubbers also can play a role during the commutation transient because they limit the voltage rise time over the SCR device. To investigate the effect of these RC circuits on the commutation transient the system operation was simulated without snubber circuits connected. In that condition, the waveforms obtained for the voltages were very similar, showing the low relevance of the snubber circuits in the transient overvoltages generated by the SFC. Figure 8.24 shows the line-to-line voltage at the SFC input, which is totally similar to the base case, showing small spikes generated by the commutation. On the other side, the line to ground voltage in Figure 8.25 shows some small voltage oscillations after the commutation. The value of this voltage oscillation is very small and can be observed only in places close to the SFC, as the line to ground voltage at the SFC output shown in Figure 8.26. This light voltage oscillations are mainly due to the existence of the phase to ground stray capacitances. From the comparison of several other voltages along the system it is possible to conclude that the overvoltages generated during the regular operation of the SFC are relatively small. Moreover, the perturbation created reduces quickly as we get away from the SFC by the

action of the synchronous machine and other connected equipment that damp the transient overvoltages. Therefore, the perturbations due to the commutation transients on the SFC can hardly reach the main transformer terminals. This is an interesting result because it implies that the main transformer of the station is barely affected by the commutation at the SFC. Figure 8.27 shows the phase to ground voltage at the transformer HV terminal of the GSU transformer in which no perturbation is observed. The line-to-line voltage waveform is completely similar to what it was presented before. The simulation of the machine under natural commutation conditions show waveforms that totally agree with the previous discussion. More simulation results can be seen at Appendix B.

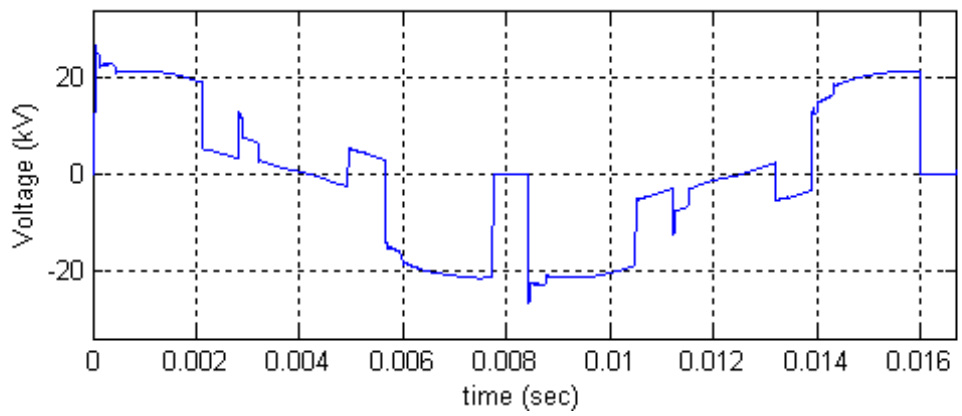

Figure 8.24 Line to line voltage at the SFC input 16.5 KV

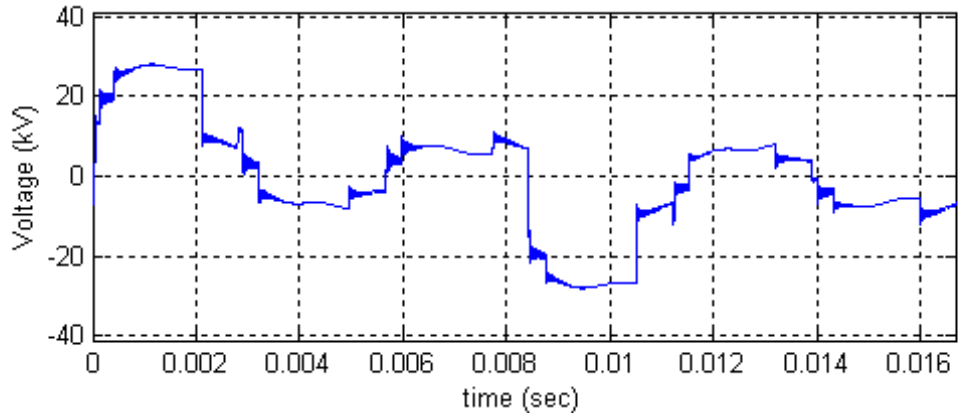

Figure 8.25 Line to ground voltage at the SFC input 16.5 KV

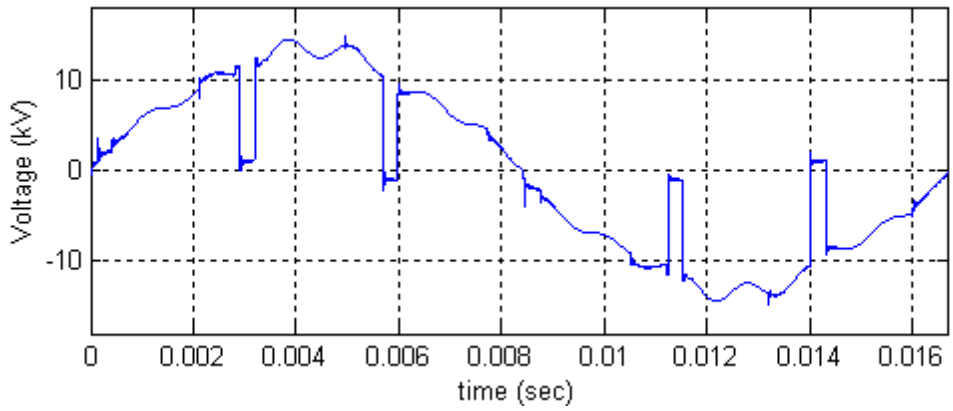

Figure 8.26 Line to ground voltage at the SFC machine side, 16.5 KV a small commutation disturbance is observed

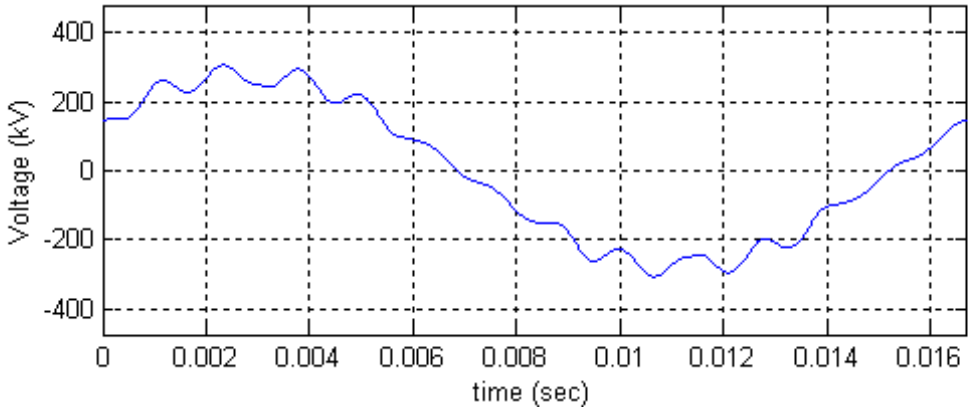

Figure 8.27 Line to ground voltage at the transformer HV side 345 KV, at rated frequency

A very important factor in the generation of overvoltage transients by a power electronics converter is the proper control and synchronization of the firing pulses. This fact is even more important when gate-turn-off (GTO) devices are employed, as in the system under study. Forced commutation of a GTO can create significant overvoltages, or the self-destruction of the device. The SFC operating sequence during forced commutation requires the current in the DC interface to be equal to zero before a new SCR in the inverter side is triggered. For reducing the DC current to zero the rectifier bridge is switched to inverter operation mode at the appropriate time. Then, the GTO previously in conduction turns off and the next one is triggered. Figure 8.28 shows the DC voltage in the inverter side during normal the forced commutation operation

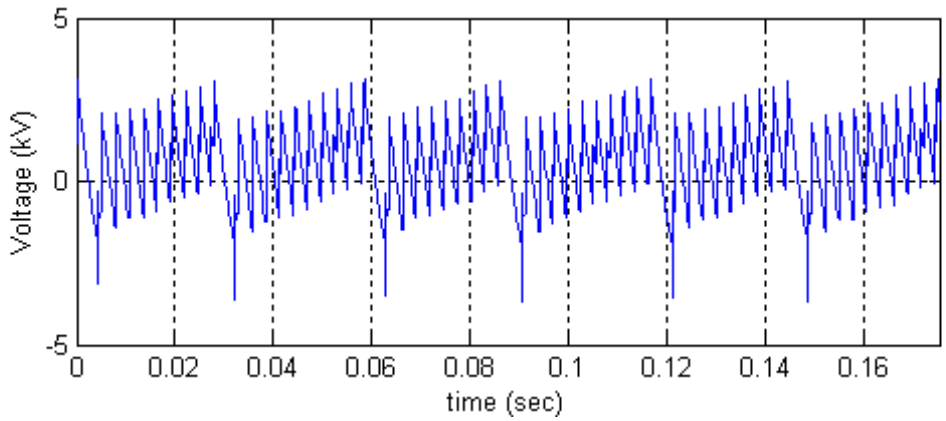

Figure 8.28 Voltage in the DC current loop during normal operation (forced), the negative spikes correspond to instants where current is cancelled

During the process of forced commutation if by any reason a GTO is turned off before the DC current is zero, an extremely large overvoltage is generated due to the sudden interruption of an inductive current. This process will probably destroy the mentioned GTO, or trigger the GTO protection mechanism. In any case, the generated overvoltage will not reach the theoretic value, but can be considerably large. For the case when large overvoltages appear in the circuit, the SFC has been provided surge arresters at the input and output for protection of the SFC itself and the connected equipment. These surge arresters must provide the appropriate level of protection against overvoltages. In order to investigate the performance of the surge arresters, the SFC operation simulating miss coordination in the triggering circuit was simulated. The line-to-line voltage for this case is shown in Figure 8.29. The large peaks in Figure 8.29 (a) correspond to the instant where the current is interrupted by the GTO turn-off. The amplitude of the peaks is limited by the surge arrester operation. Figure 8.29 (b) shows an amplification of a spike generated in the same circumstance; that peak is cut before its amplitude reaches 50 KV.

It is also important to analyze how will be the propagation of possible voltage spikes in the network and if the overvoltage generated by the SFC can reach the GSU transformer with a magnitude harmful to the insulation. As it was said before the voltage spike is damped and distorted when it travels along the system. Figure 8.30 shows the phase to ground voltage at the transformer HV terminal under the same conditions of Figure 8.29, where the absence

of large peaks is noticed. On the other side, significant voltage oscillations generated by the spikes produced during the SFC operation are observed in the waveform.

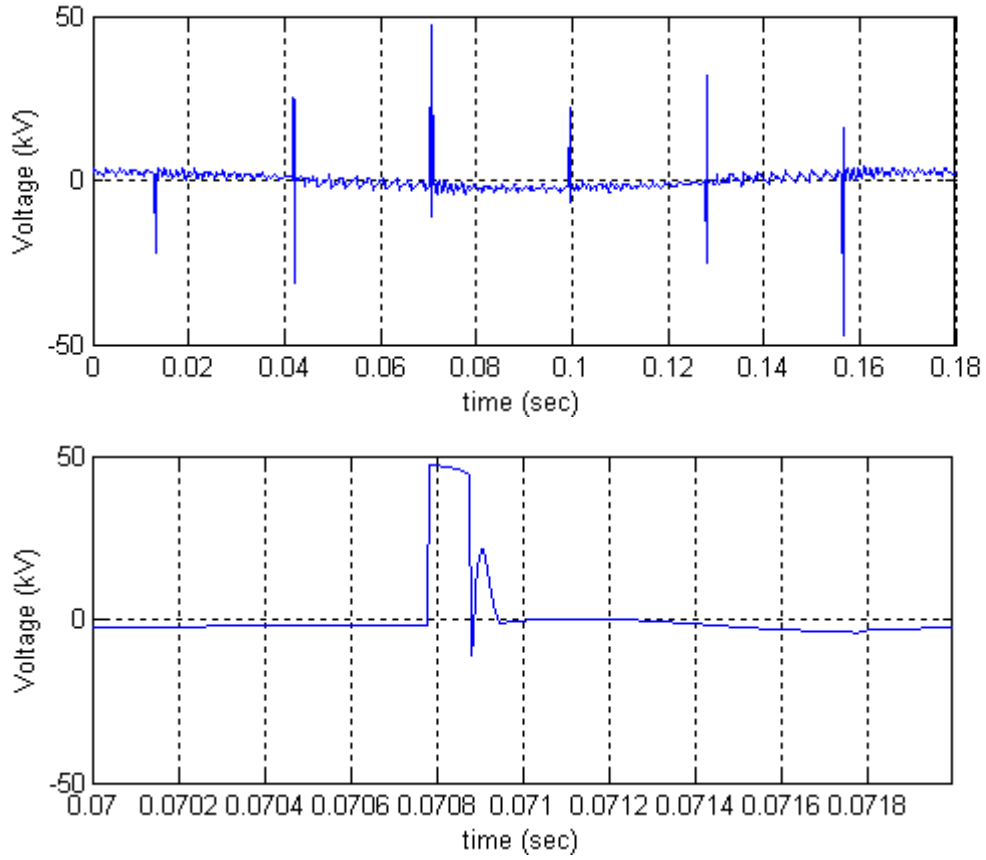

Figure 8.29 Vab voltage at the SFC machine side; (a) waveform with the spikes at current interruption (b) detail of a spike, the peak is limited by the surge arrester operation

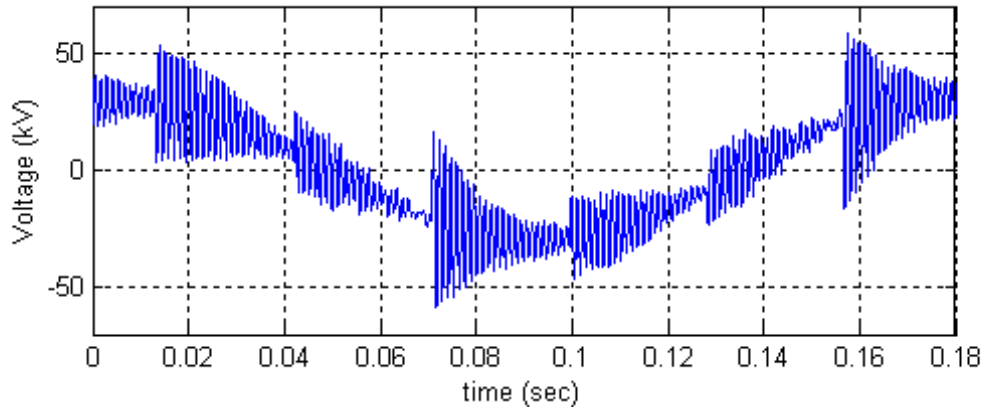

Figure 8.30 Vta phase to ground voltage at the transformer HV side, forced commutation, failure in GTO triggering

In Figure 8.30 the total magnitude of the voltage on the transformer terminals is much smaller than the rated voltage because of the low operating frequency. In any case, to analyze the possible harm of a voltage transient, not only the maximum peak but also other parameters of the wave shape must be considered as it was explained in section 3.1. For the voltage waveform on the HV side of the GSU of Figure 8.30 the relevant parameters are shown in Table 8.2, they do not represent any harm to the transformer.

Table 8.2 Characteristic parameters of the transient waveforms over the GSU HV side during forced commutation and failure in the triggering logic

Vtransf HV	Peak (kV)	Max change (kV)	Max rate (kV/μs)	Frequency (Hz)
Line-line	107.3	115	228	833
Line-ground	58.7	74	200	833

8.5 Validation of the Simulation Results

In electromagnetic studies based on computer simulations it is important to validate the results and check the realism of the conclusions derived from the calculated values. There are several items related with a study that have to be properly set in order to get results that match the reality. These items generally are:

1- the models of the different elements present in the system. In this study the component modeling was extensively discussed in chapter four,
2- the simulations must be done following the same operating procedures as the real system, when no all the operating conditions can be checked, a study to detect the cases producing the most relevant cases must be previously done
3- the software used for the simulations should be based on algorithms that provide accurate results. In the case of electromagnetic studies in power systems, different software packages are available to be used being most of them reliable and appropriately tested [48].

Once the results are obtained from the computer simulation, it is also important to compare the values against measurements in the real field. In the case of this study, the values and waveforms obtained were matched with measurements taken in the field and presented in other works [49], [50]. Although these studies were intended for different purposes, the results and waveforms they provide allow for a comparison, and they basically support the waveforms and values obtained here.

9 Analysis of the Results

The purpose of this chapter is to summarize the results obtained from the study and the simulations. As it was previously stated in chapter three, there are three major effects of power electronic system operating in a high voltage system. These three effects will be analyzed in each of the following sections.

9.1 Harmonics

The presence of harmonics in current and voltage is expected when power electronic devices are introduced in a power system because they create distortion of the voltages and currents. Phase angle controlled converters, as the one used in the SFC under study, create a harmonic spectra with values inversely decreasing with the increment of the harmonic order [47]. This fact is observed as a general tendency in the waveforms obtained from this system, but there are some exceptions as the thirteen-order harmonic that require an explanation. The generation of harmonics is not only based on the SFC converter control but also on the interaction between the different components of the system.

The operation of the SFC creates harmonics in the voltage and current that propagates along the system. As was stated at chapter three, these harmonics can excite some resonances existing in the system. This is precisely the effect that causes the increment in the thirteen harmonic. In other words, the operation of the SFC creates a thirteenth harmonic that is amplified by the resonance of the group of transformer, cable and synchronous machine. This fact was first detected during the frequency scan test and confirmed with the time domain simulations, where a more appropriate machine model for harmonic studies was used showing also a resonance close to that 13th order. Although it is possible that exist some differences in the exact value of some system parameters, the fact that certain "tuning" of the power equipment increases some harmonic components was determined. Any possible difference between the parameter used for the study and the actual value can change the frequency at where the resonance takes place, and then the order and magnitude of the harmonic. If the system parameters changes the resonances also varies. For example, in the

case of the cable disconnected from the transformer, the resonance move to a higher frequency and almost disappear, but the phenomenon is similar.

The harmonic order that is amplified by the resonant effect changes with the system frequency (machine speed). The resonant frequency at around 820 Hz corresponds to the 13th harmonic at 60 Hz, but is switched to the 25th-29th order at 30 Hz. The main conclusion regarding the harmonic presence in the system is the amplification due to resonance of some of the harmonic components created by the SFC operation.

9.2 Overheating effects

When the SFC is operating, no load is applied to the transformer; therefore, the only currents in the transformer are a reactive component due to the cable capacitance at 60 Hz, which is relatively low, plus the transformer magnetizing current. This fact and the small time that the SFC is used for the machine starting process can be enough to assure that the GSU transformer will never experience overheating due to the SFC starting process. Nevertheless, the calculation of the overheating effects by the harmonic current and voltage will be presented in the following paragraphs.

The machine-accelerating regime is variable in frequency, voltage and current over the GSU transformer. The frequency and voltage are related because the relation V/f is maintained constant; therefore, lower frequencies are linked to lower voltages, and this implies lower currents. With conservative criteria it is possible to calculate the losses under non-sine wave conditions for the rated SFC rated operation at 60Hz being the losses at different conditions smaller.

Equation (5-1) establishes that the transformer losses could be classified as load and non-load ones. In the case of the transformer under study the losses are:

P_{NL}= 127.3 kW

P_{LL}= 952.4 kW

Under non- sinusoidal conditions while the non-load losses are related to the voltage waveform, the load losses depends on the current waveform. For calculation of the losses under distorted conditions it is important to know the values of the different terms of equation (3-7). The first term is the DC losses and can be easily calculated given the value of

the winding resistance. In contrast, the separation between stray losses and eddy current losses is not as simple. For the purpose of the calculation the percentage of eddy current and stray losses was estimated based on typical values for this kind of transformers. The different components of the loss under distorted conditions can be calculated according to factors presented in chapter three. While the DC losses remain constant, the eddy current losses are corrected by the K factor of equation (3-11) and the P_{OSL} by equation (3-10). The K factor and the factor for correcting the other stray losses for the current Iatr result,

$K = 0.17$

$K_{OSL} = 7.6\ e\text{-}3$

On the other side, considering that the voltage distortion is not too big, condition (3-9) is valid; the no-load losses under non-sinusoidal conditions are calculated by equation (3-8) assigning half of them to eddy currents and half to hysteresis according to [20]. The results of these calculations are presented in Table 9.1.

Table 9.1 Transformer losses for rated conditions and under the non-sinusoidal regime of the SFC operating at rated speed

Type of loss	**Sine wave, rated V and I**	**SFC starting**
P_{NL} (kW)	127.3	128.9
P_{I2R} (kW)	723.9	0.44
P_{EC} (kW)	104.7	17.78
P_{OSL} (kW)	123.9	0.94
P_{LL}(kW)	952.4	19.16
P_{Total} (kW)	***1212.4***	***167.26***

It is seen in the table that the load losses have decreased very much due to the small current circulating in the transformer. Even though, the eddy current losses do not decrease in the same proportion as the other load losses due to the relative importance of the harmonics. The result P_{Total} shows that the total losses generated in the transformer under the operating conditions imposed by the SFC are much smaller than the losses at rated conditions.

Therefore, it is possible to conclude that the magnitude of the harmonic regime during the start process cannot cause transformer overheating. Moreover, as seen in Figure 5.1, the SFC starting process last for a very short time compared to the transformer time constants, giving less importance to any possible heating problem existing for that period of time.

9.3 Commutation Transients

The level of the transients found in the normal operation was not relevant and seems to have more effect on the auxiliary starting bus than on the GSU transformer, synchronous machine and related equipment. The presence of the generator is quite relevant sustaining the voltage at the SFC output side. Moreover the windings of the synchronous machine and some other devices present in the system like smoothing inductors filter the commutation transients. No significant overvoltages due to commutation transients were found at the GSU transformer terminals. In addition, the surge arresters and snubber circuits provide suitable protection to the high voltage equipment.

10 Conclusions

The presence of harmonics is quite significant in the system under study. Some of the harmonic components are amplified due to resonances existing between the different equipment increasing the harmonic content over the level expected for the kind of equipment employed. Nevertheless, the harmonic level is not relevant enough to create harm to any of the equipment in the facility. The maximum voltage peak increased by the harmonic content at the high voltage side of the GSU transformer does not create a voltage that can be considered dangerous. The effect of overheating due to harmonics has no impact due to the reduced values of the currents circulating during the starting period because the equipment is working unloaded. Moreover, the starting process lasts for a short period over the complete operation cycle of the different machines and equipment. Therefore, the impact over that equipment is considerably reduced.

From this study we can conclude that most probably the SFC played no significant role in the GSU transformer failures that have taken place in the past.

Appendix A

The following data was not included in the model section but is required for the study.

A.1 Synchronous Machine Data

Table A.1 Synchronous machine reactances

Reactance	**Normal (%)**	**L (H)**	**Saturated (%)**
Synchronous direct-axis Xd	112.7	2.71e-03	99.5
Transient direct-axis X'd	28	6.74e-04	26
Subtransient direct-axis X"d	21	5.06e-04	18
Subtransient quadrature-axis X"q	23	5.54e-04	23
Negative sequence X2	22	5.30e-04	20
Zero sequence X0	12	2.89e-04	

Table A.2 Synchronous machine time constants

Time constants	**(sec)**
Transient direct-axis T'd	2.4
Subtransient cc direct-axis T"d	0.052
Aperiodic	0.31

A.2 Transmission Cable Data

Due to its constructive characteristics the cable is modeled as three single-phase cables.

Line Model General Data

Name of Line: cablemin
Steady State Frequency [Hz]: 60.0
Length of Line [km]: 0.63
Number of Conductors:

Frequency Dependent (Phase) Model Options

Travel Time Interpolation:	On
Curve Fitting Starting Frequency:	5 [Hz]
Curve Fitting End Frequency:	1.0E6 [Hz]
Maximum Order of Fitting for YSurge:	20
Maximum Order of Fitting for Prop. Func.:	20
Maximum Fitting Error for YSurge:	2 [%]
Maximum Fitting Error for Prop. Func.:	2 [%]

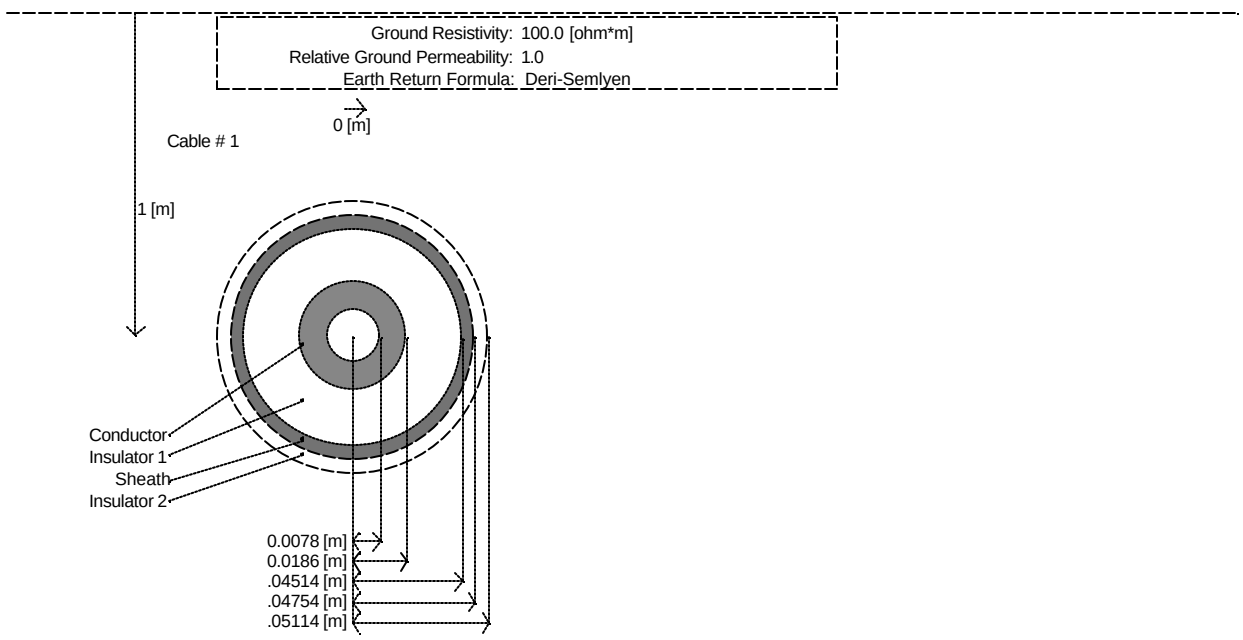

Figure A.1 Transmission Cable model

A.3 SFC Control Circuit Diagram

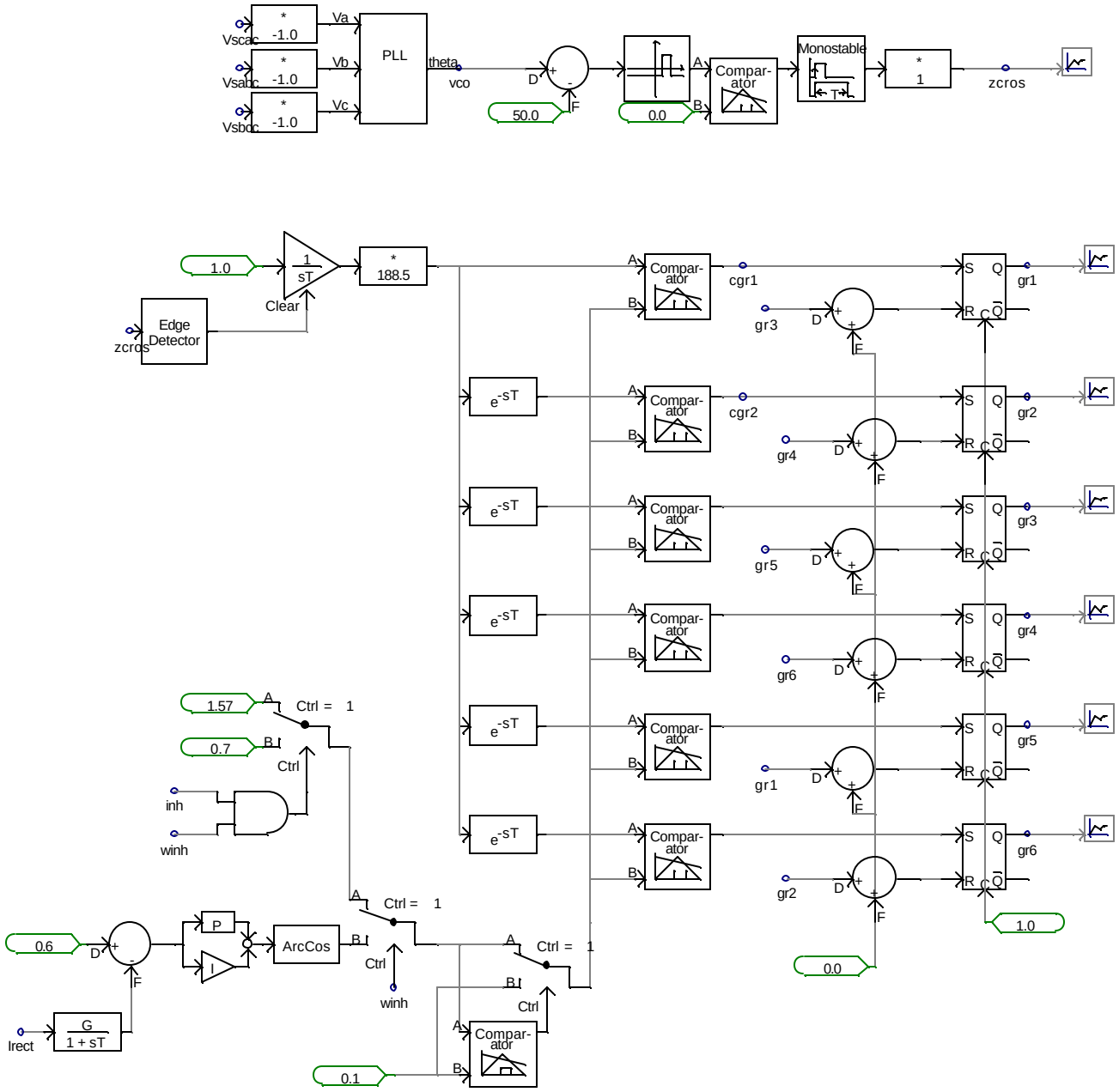

Figure A.2 SFC Control circuit: Rectifier control

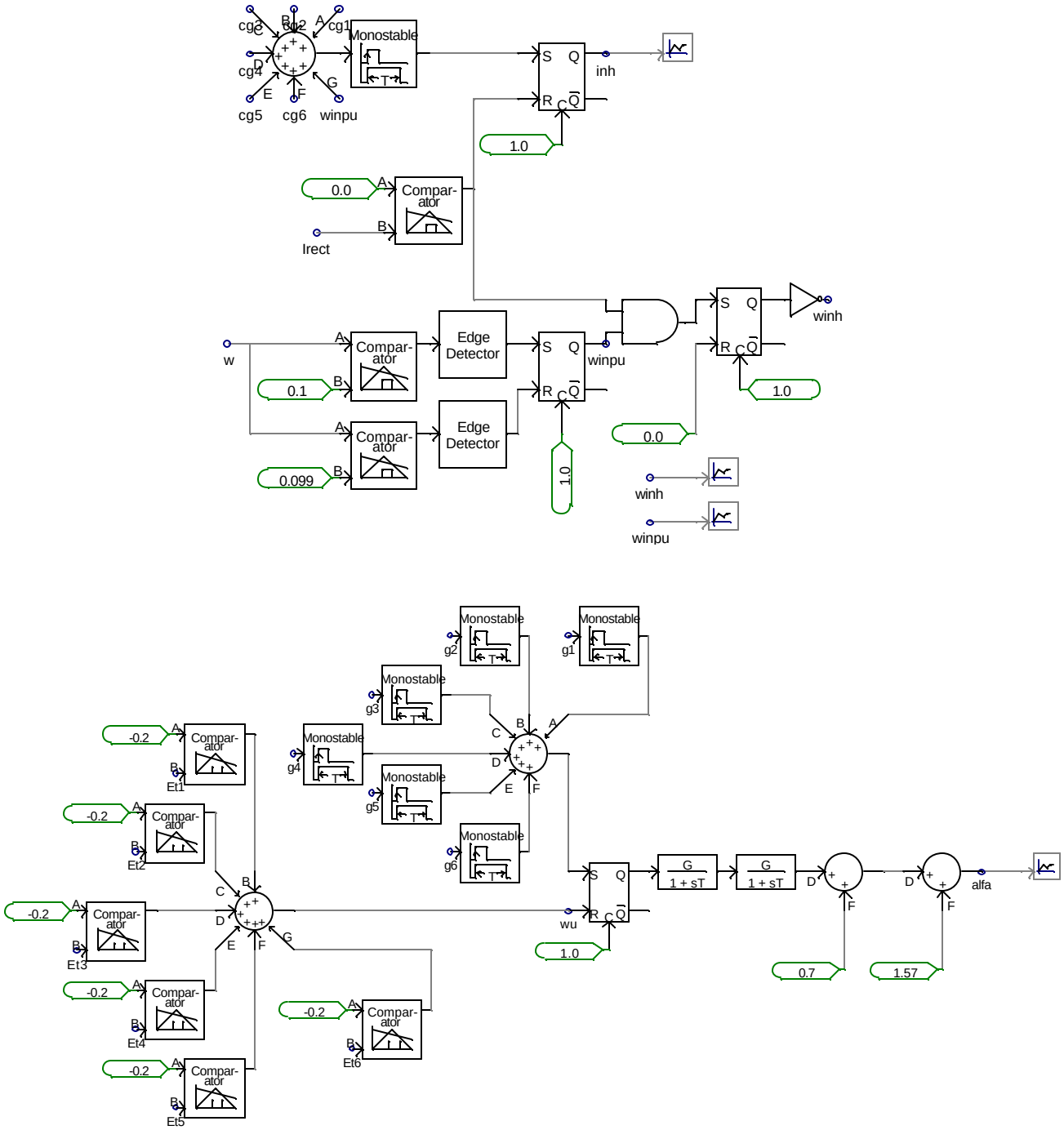

Figure A.3 SFC Control circuit: Rectifier-Inverter control circuits

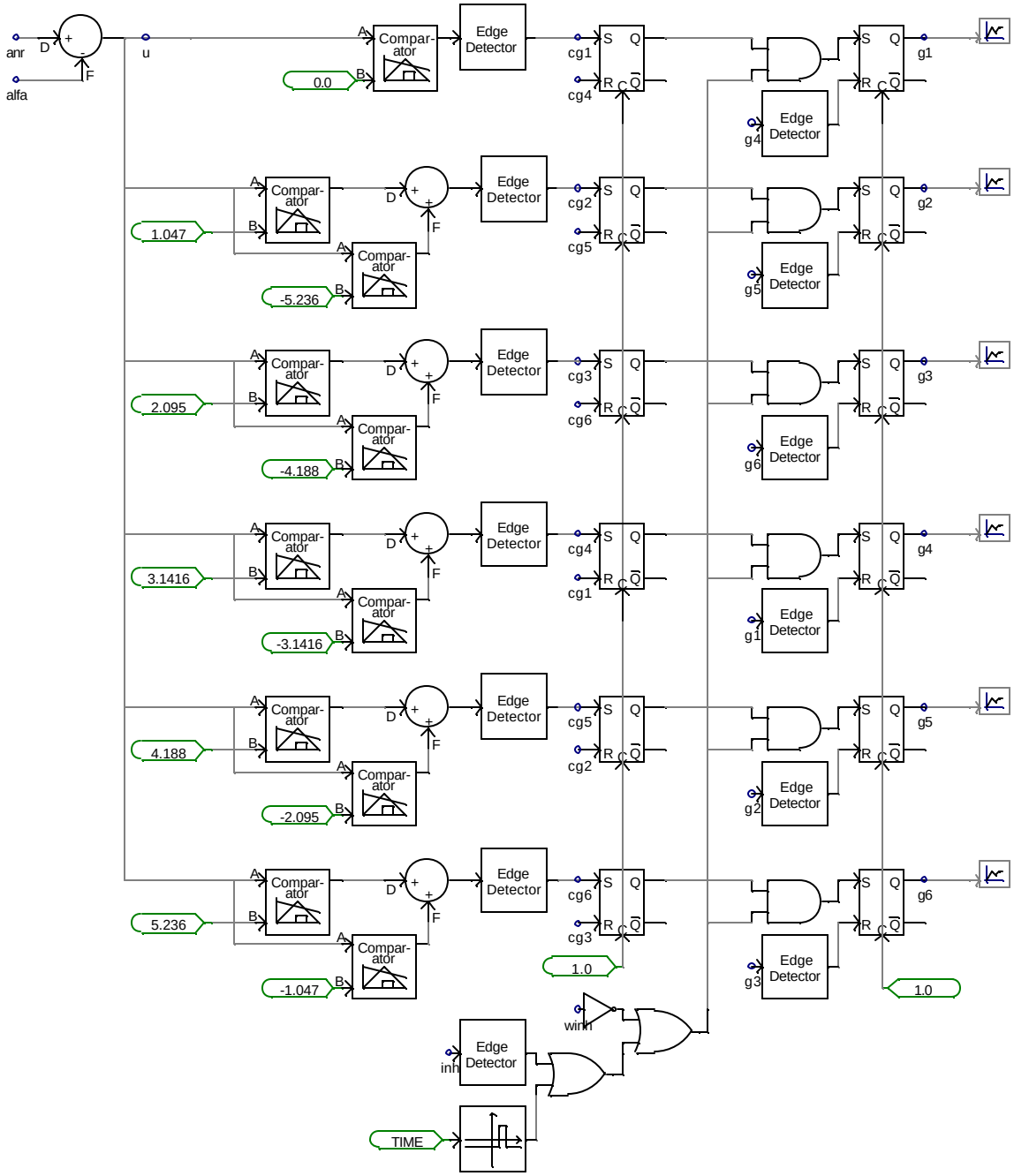

Figure A.4 SFC Control Circuit: Inverter control

A.4 SFC Power Circuit Diagram

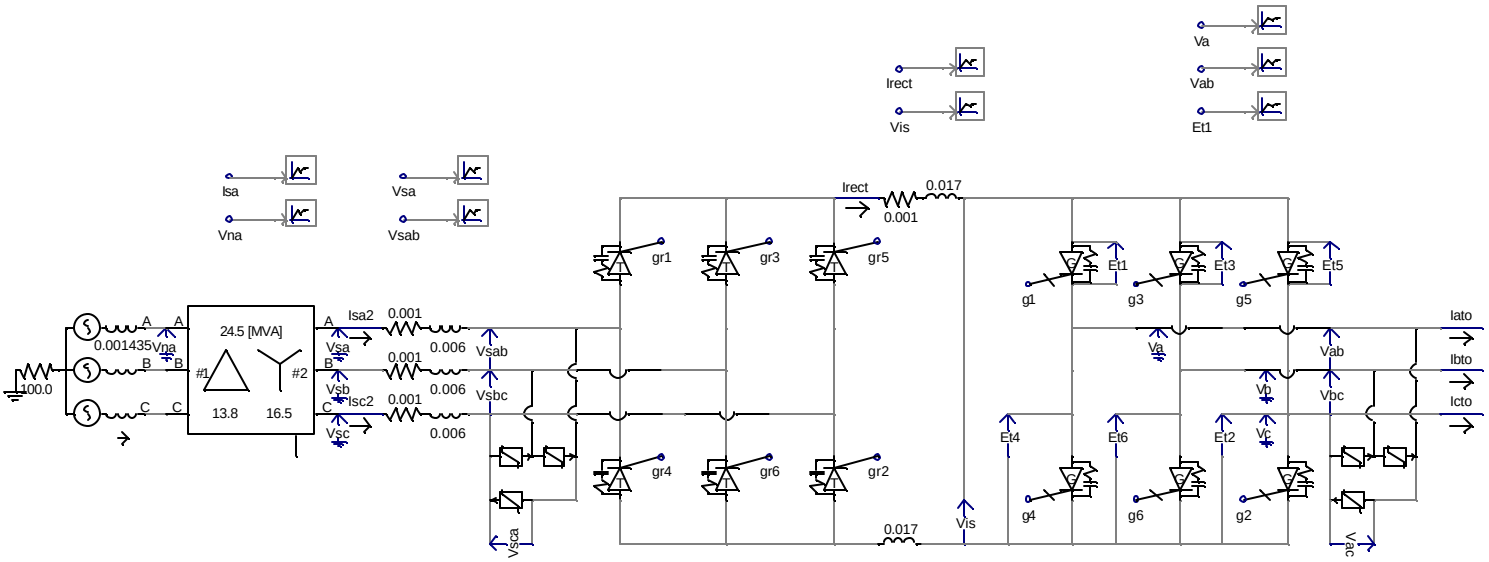

Figure A.5 SFC Power Circuit: this portion shows the SFC itself and the auxiliary source

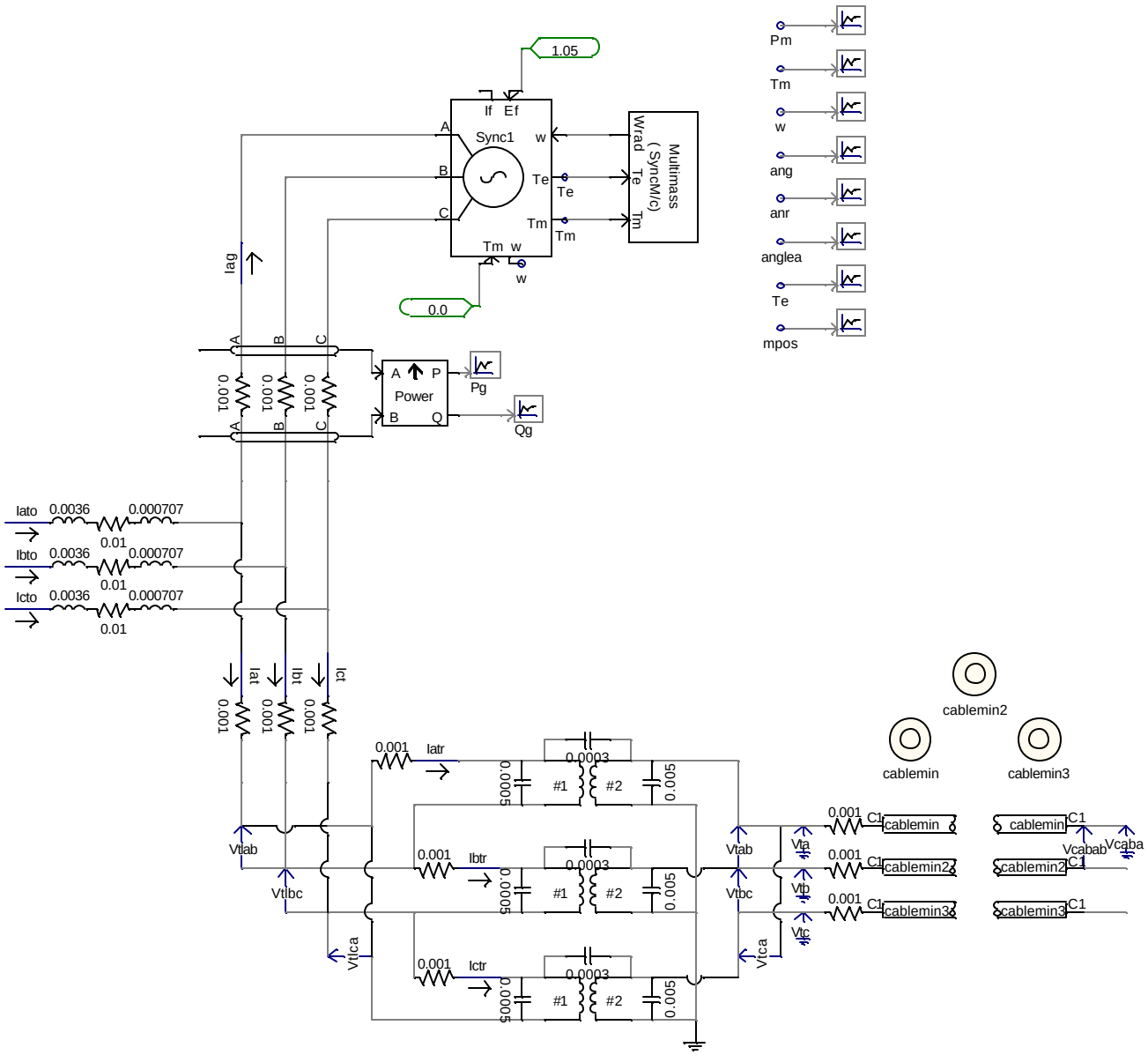

Figure A.6 SFC Power Circuit: this portion shows the synchronous machine, GSU transformer, and HV cable

Appendix B

This Appendix shows additional waveforms for the following operation cases:

1. Rated operating conditions –base case
2. Reduced load condition
3. Reduced speed condition
4. Operation without HV transmission cable
5. Forced commutation mode
6. Snubber circuit not operative
7. Snubber circuit operative: natural and forced commutation
8. Failure in the firing sequence

The way the waveforms are presented is always the same staring from the HV side of the transformer to the auxiliary bus of the station. The voltage waveforms are presented first followed by the current waveforms.

B.1 Rated operating conditions –base case

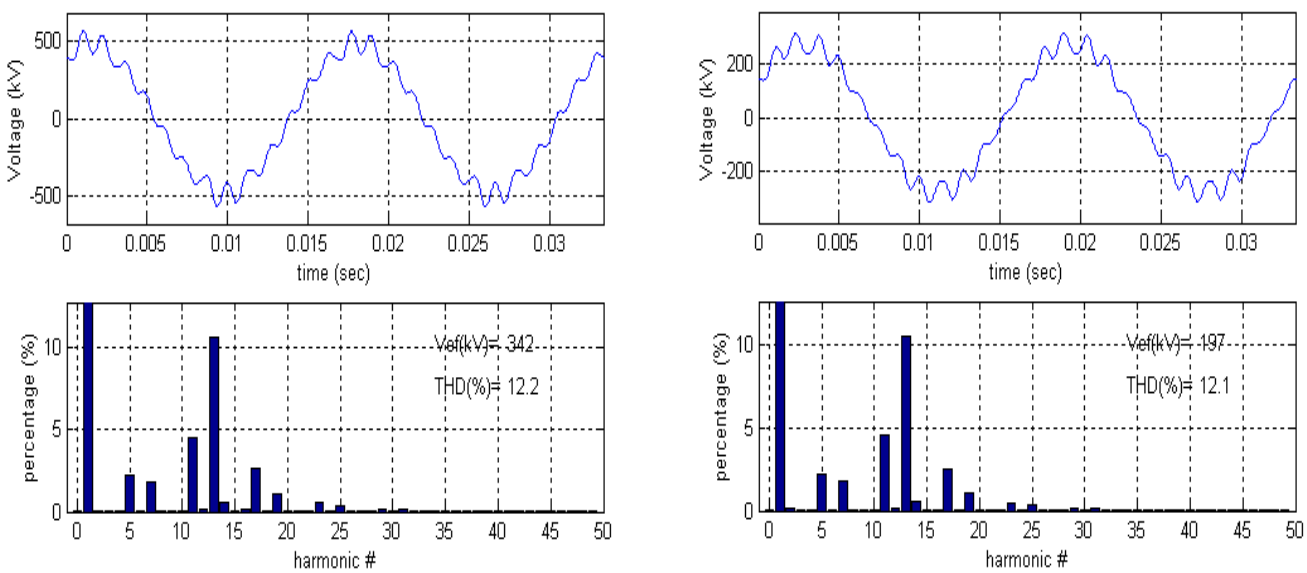

Figure B.1 Voltage waveforms at rated conditions at the transformer HV terminals (a) line-line (b) line-ground

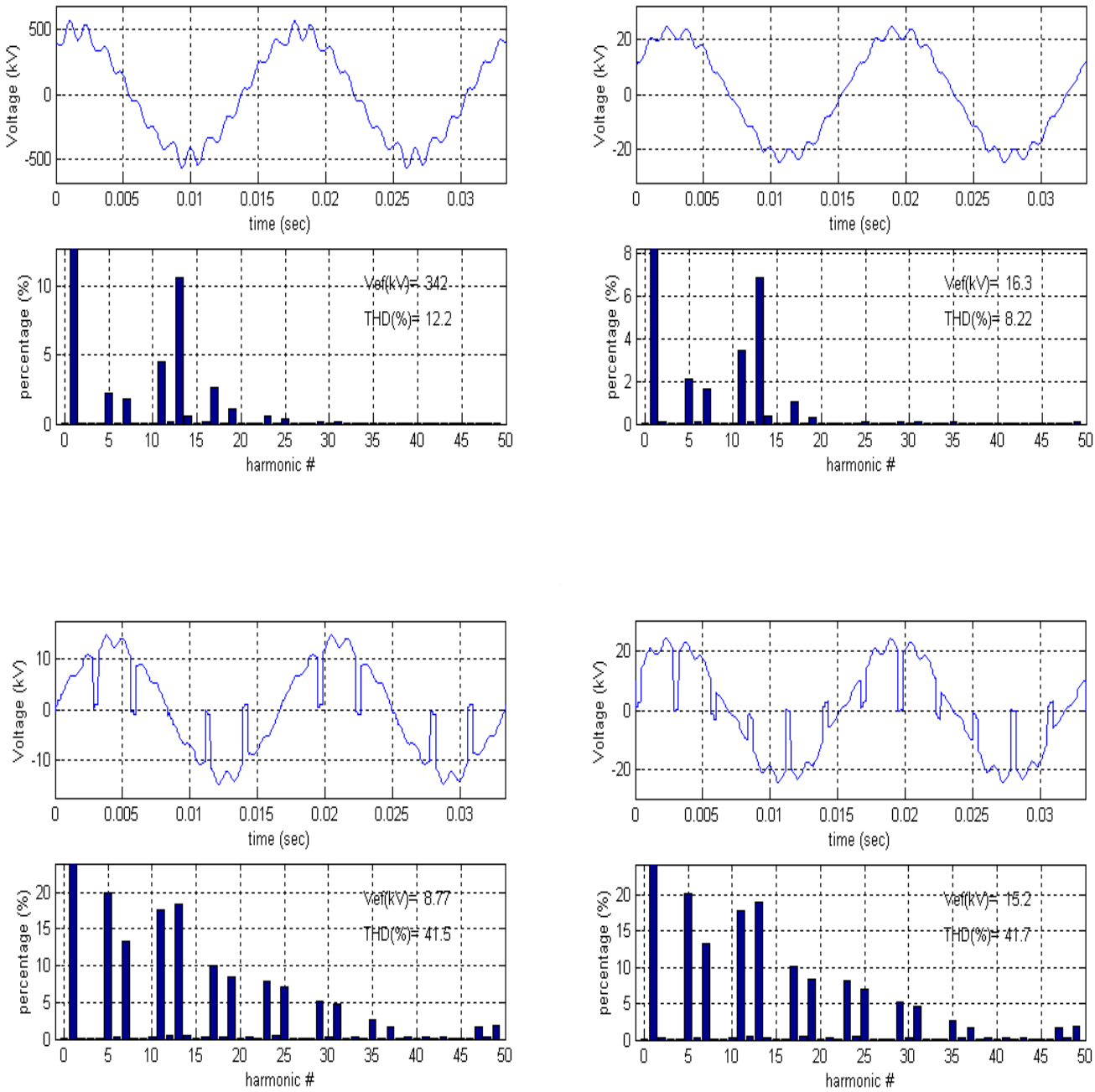

Figure B.2 Voltage waveforms at rated operating condition (a) Vcabab Line –line voltage at the cable open terminal (b) Vtlab Line –line voltage at the transformer LV terminal. The shape is the same as the HV side, but the harmonic content is smaller (c) Va Line – ground voltage at the converter output side (d) Vab Line – line voltage at the SFC converter output side

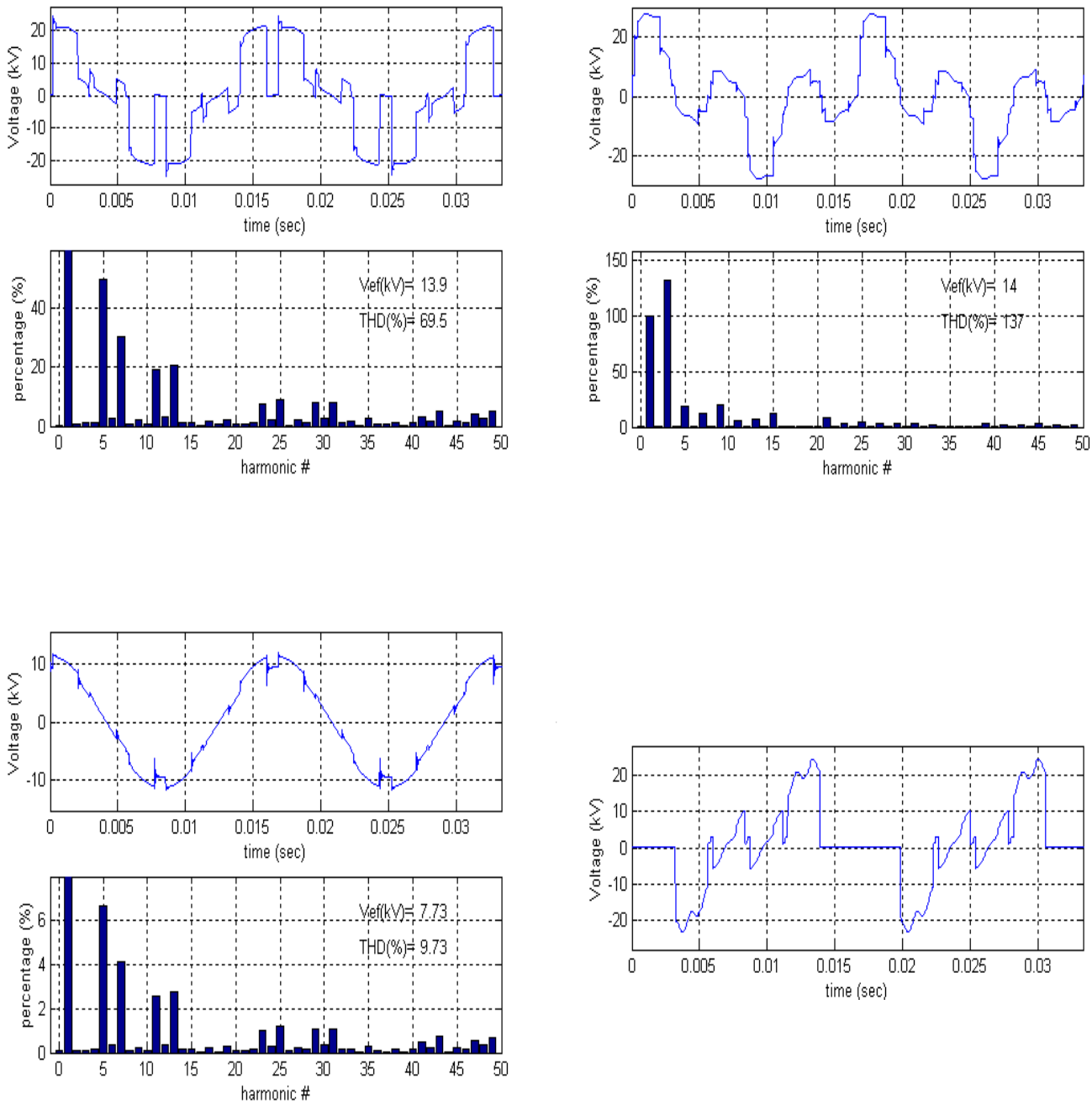

Figure B.3 Voltage waveforms at rated operating conditions (a) Vsab Line –line voltage at the converter input side, (b) Vsa Line –ground voltage at the converter input side (c) Vna Line –ground voltage at the auxiliary bus of the station, 13.8 kV (d) Et1 voltage at the terminals of a GTO inverter

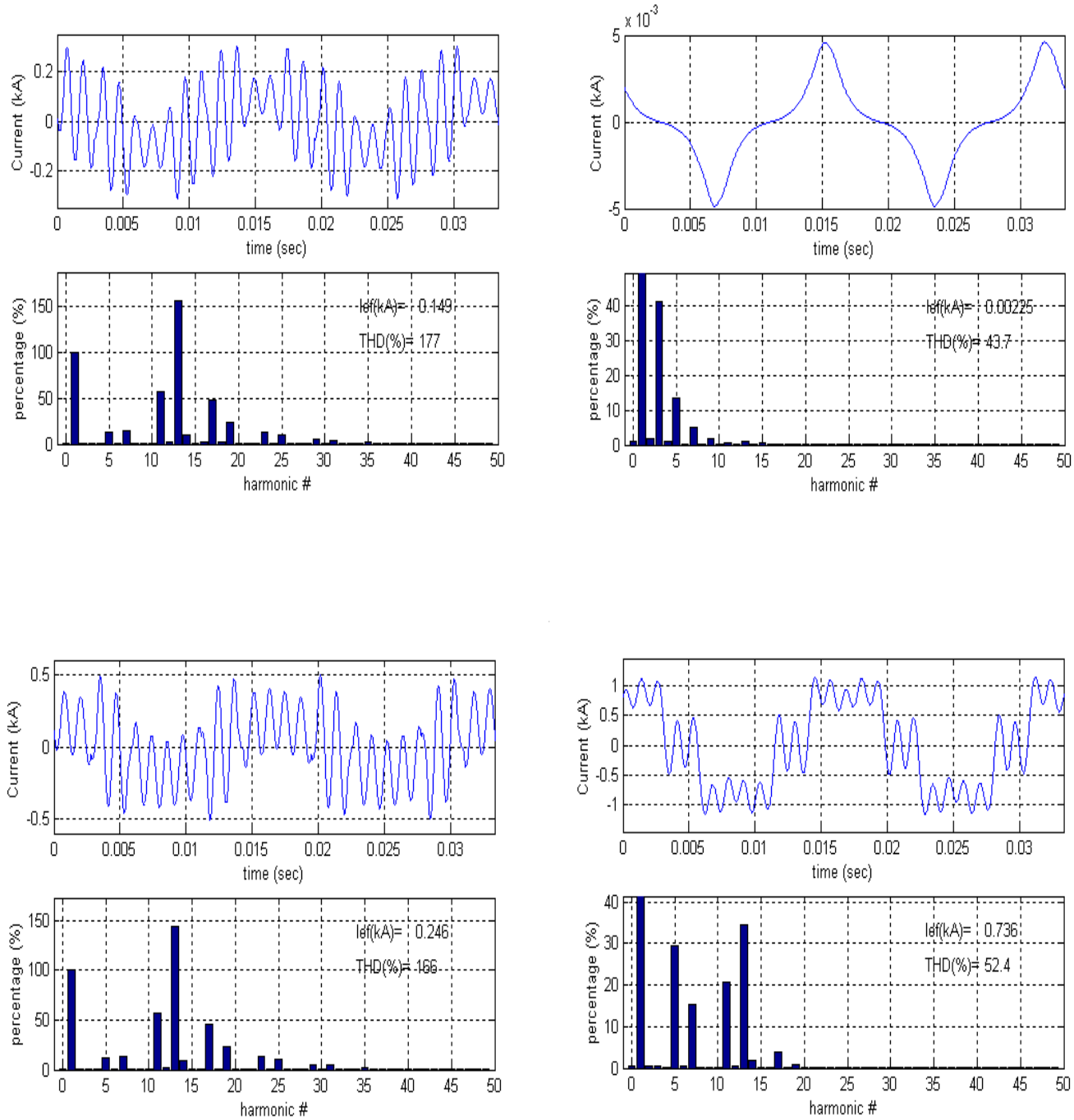

Figure B.4 Current waveforms at rated operating conditions (a) Iatr Phase current at the LV winding of the main transformer, in the delta (b) Itla Magnetizing current at the LV branch of the main transformer (c) Iat Line current at the LV side of the GSU transformer (b) Iag Synchronous machine input current

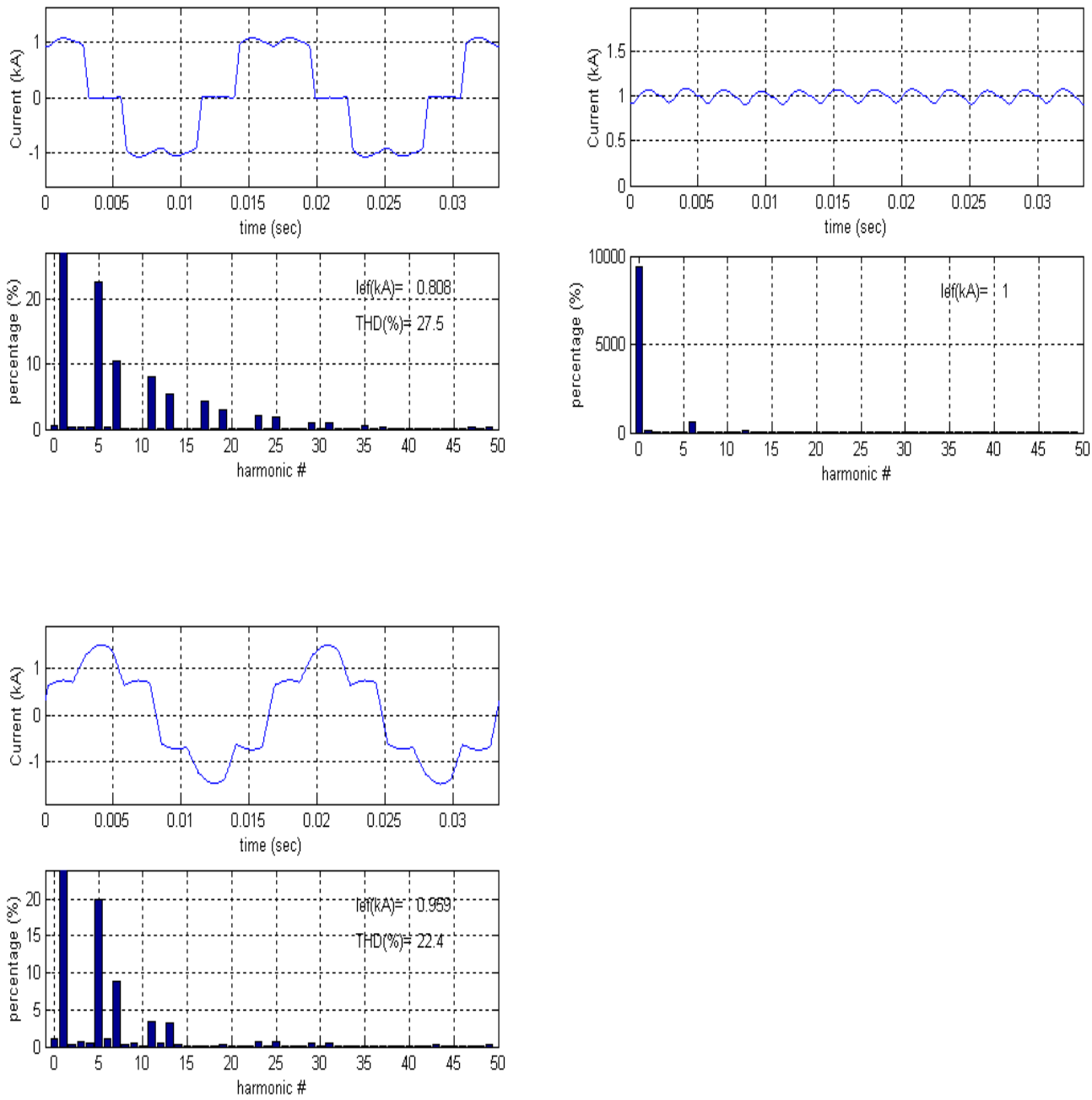

Figure B.5 Current waveforms at rated operating conditions (a) Iato SFC output current, there is no major difference with Isa_2, the input current of the SFC (b) Irect current at the DC interface of the SFC (c) Isa SFC input current at the primary side of the auxiliary transformer, 13.8kV

B.2 Reduced load condition

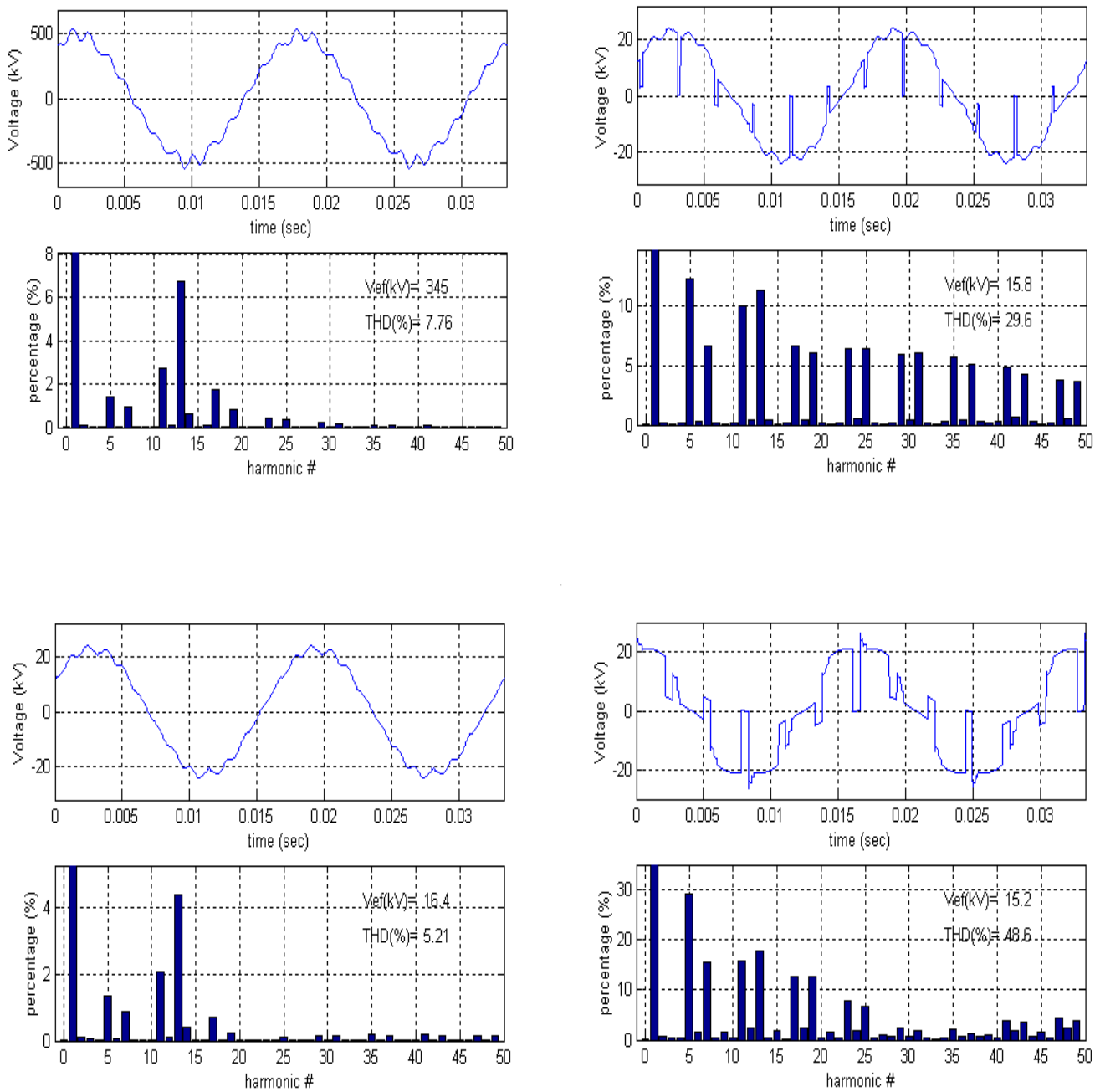

Figure B.6 Voltage waveforms for reduced load condition (a) Vtab Line –line voltage at the transformer HV terminal. The harmonic content is reduced respect to the base case (b) Vab Line – line voltage at the SFC at the machine side (c) Vtlab (d) Vsab Line – line voltage at the converter input side, 16.5kV

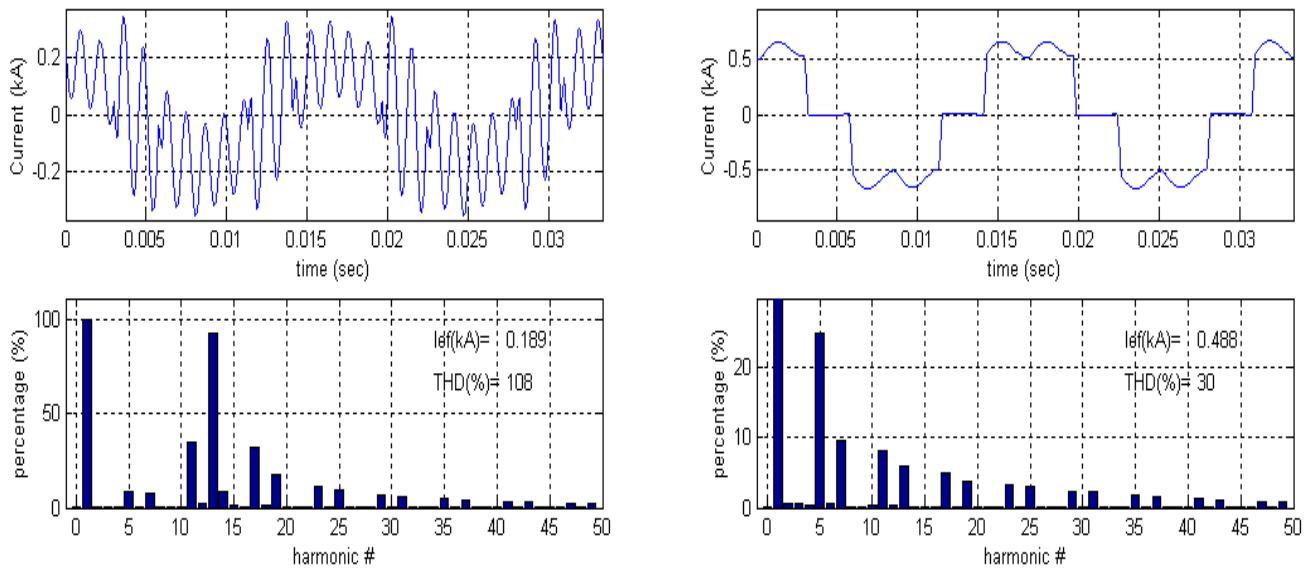

Figure B.7 Current waveforms for reduced load conditions (a) Iat Line current at the LV side of the main transformer (b) Iato the SFC output current at 16.5 kV

B.3 Reduced Speed condition, $\omega=0.5*\omega_r$

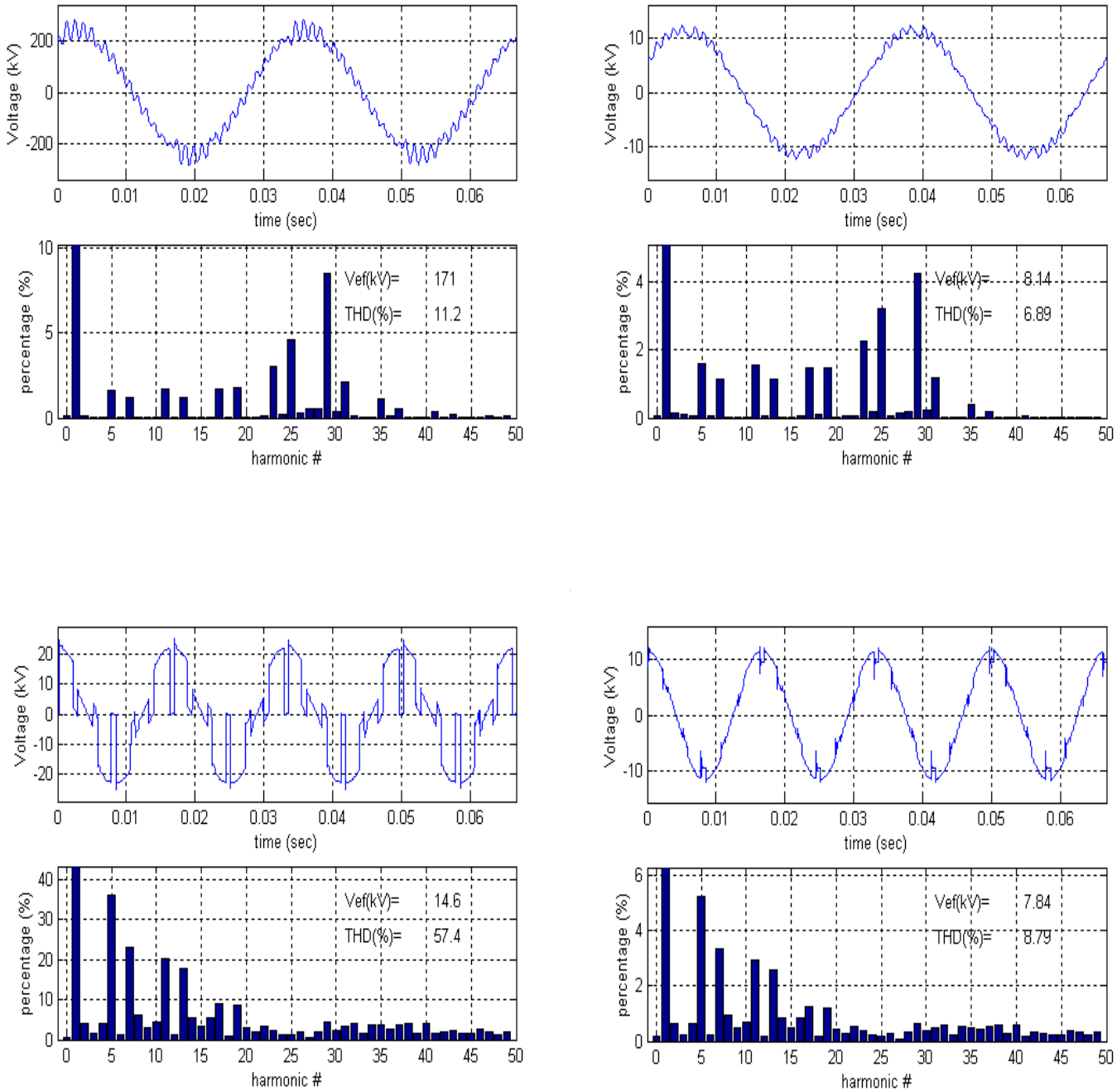

Figure B.8 Voltage waveforms at reduced speed operation (a) Vtab line-line voltage at the transformer HV terminals (b) Vtlab line-line voltage at the transformer low voltage terminals (c) Vsab line-line voltage at the SFC input (d) Vsa line-phase voltage at the SFC input

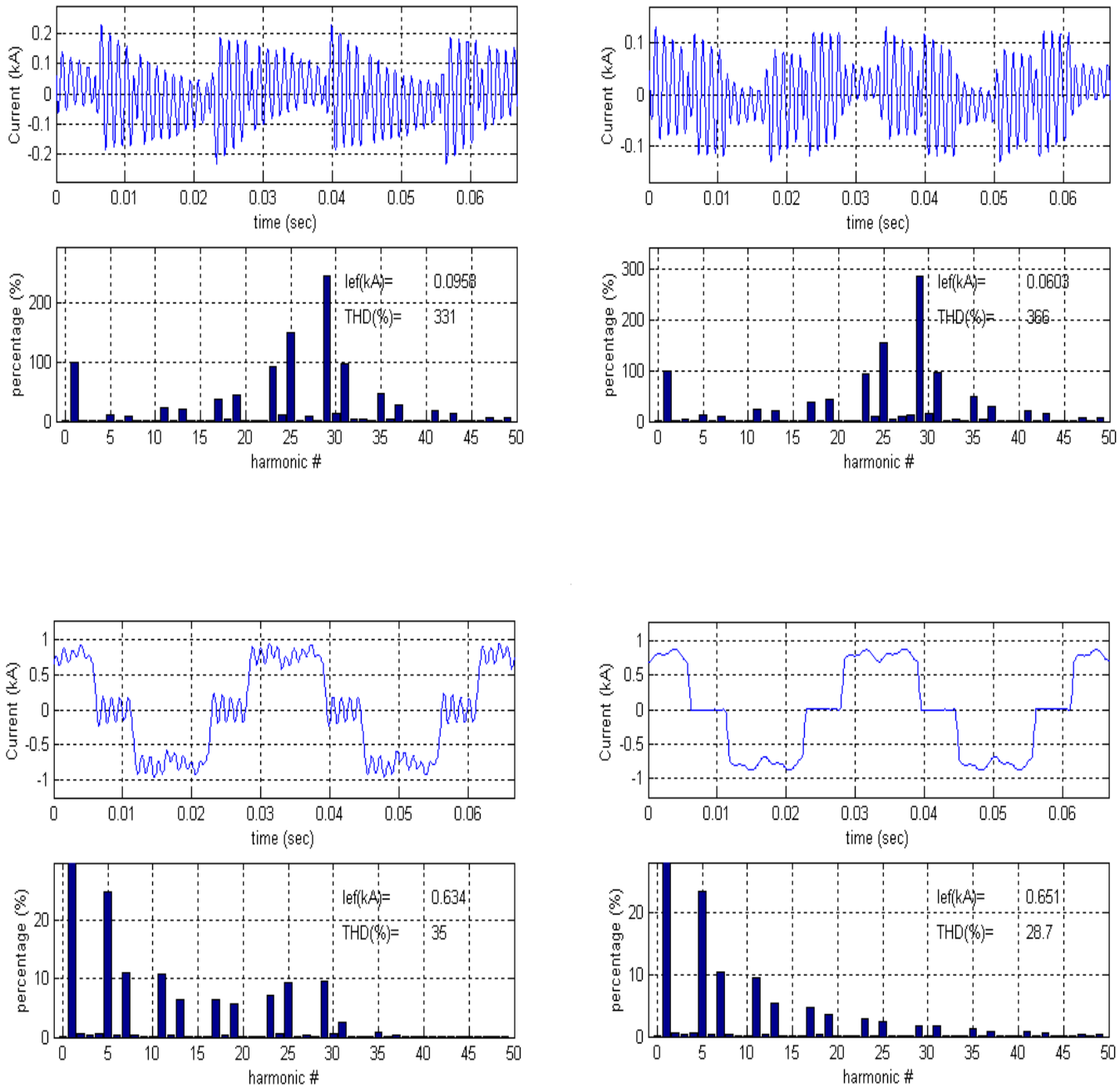

Figure B.9 Current waveforms at reduced speed operation (a) Iat line current at the transformer LV side (b) Iatr phase current at the transformer LV side (c) Iag Line current at the generator (d) Iato SFC output current

B.4 Operation without HV transmission cable

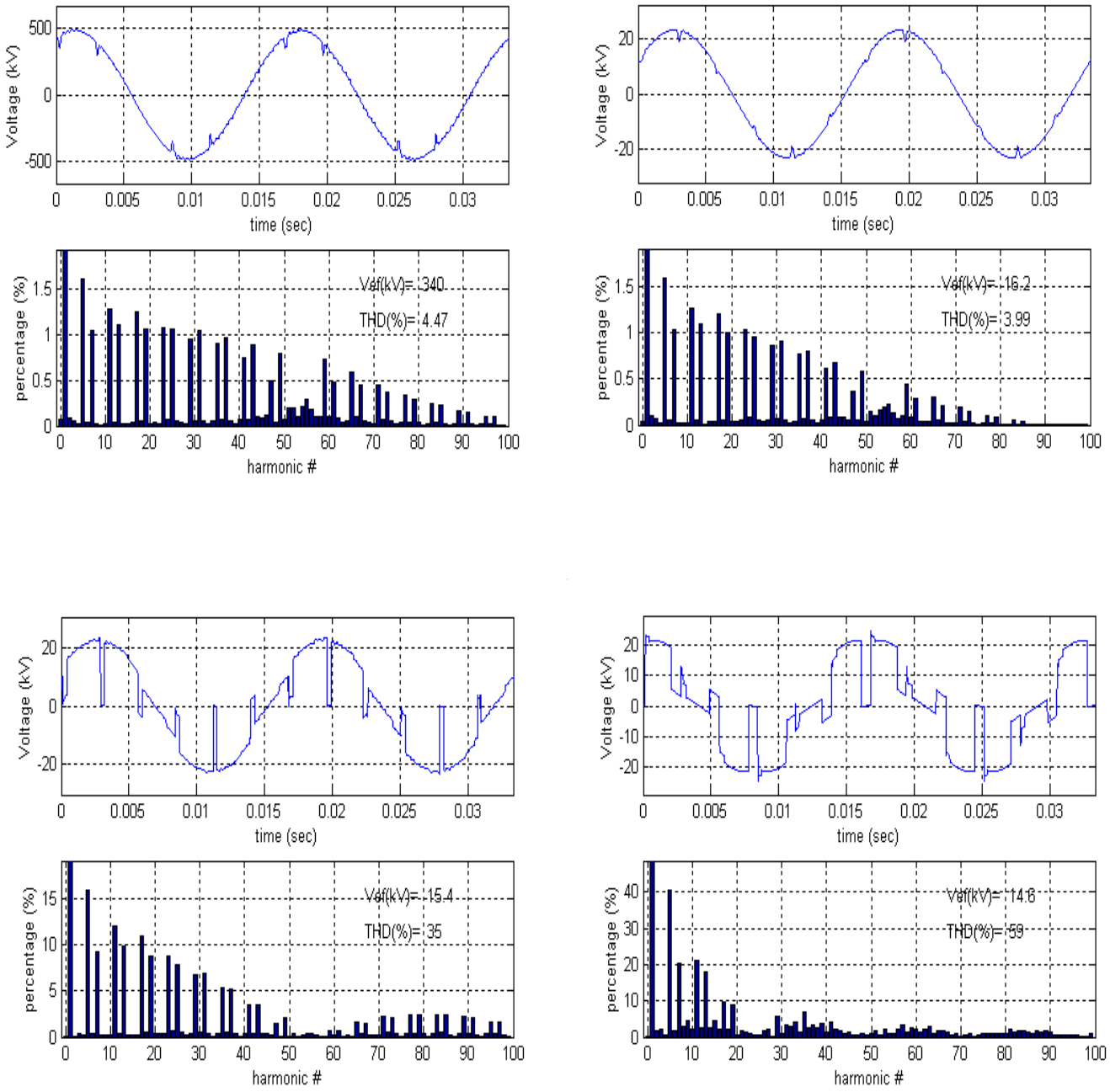

Figure B.10 Voltage waveforms for operation without HV cable (a) Vtab Line –line voltage at the transformer HV terminal (b)Vtlab Line –line voltage at the transformer LV terminal (c) Vab Line –line voltage at the SFC output (d) Vsab Line – line voltage at the SFC input side, 16.5 kV

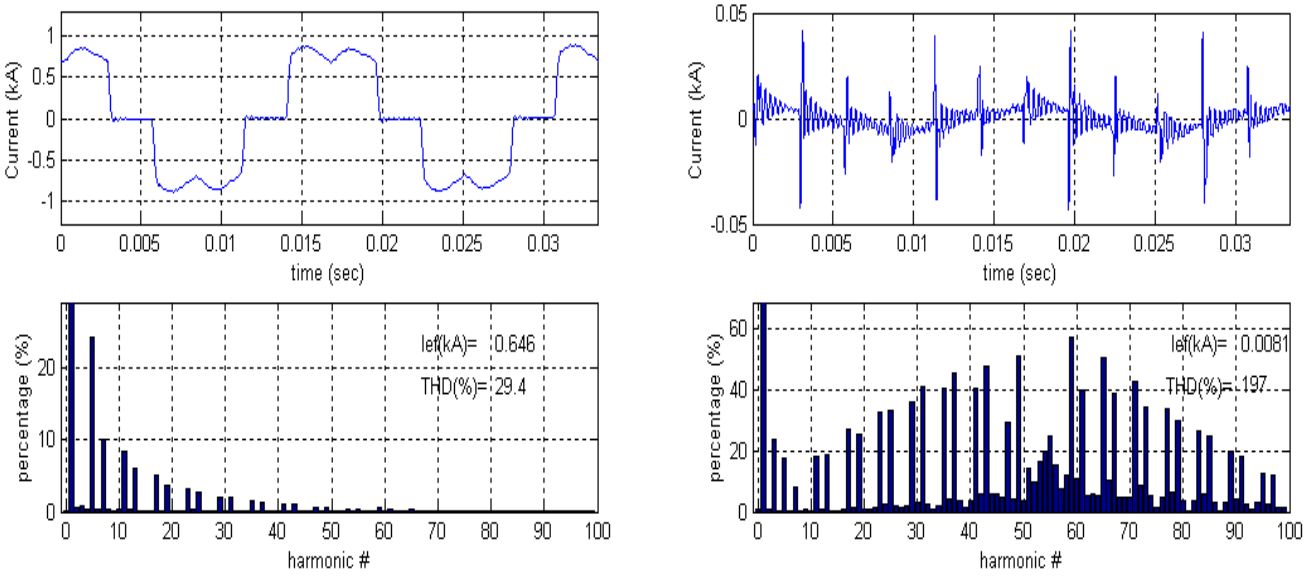

Figure B.11 Current waveforms for operation without HV cable (a) Iag current taken by the synchronous machine (b) Iatr Current at the LV winding of the main transformer, inside the triangle connection

B.5 Forced Commutation Mode

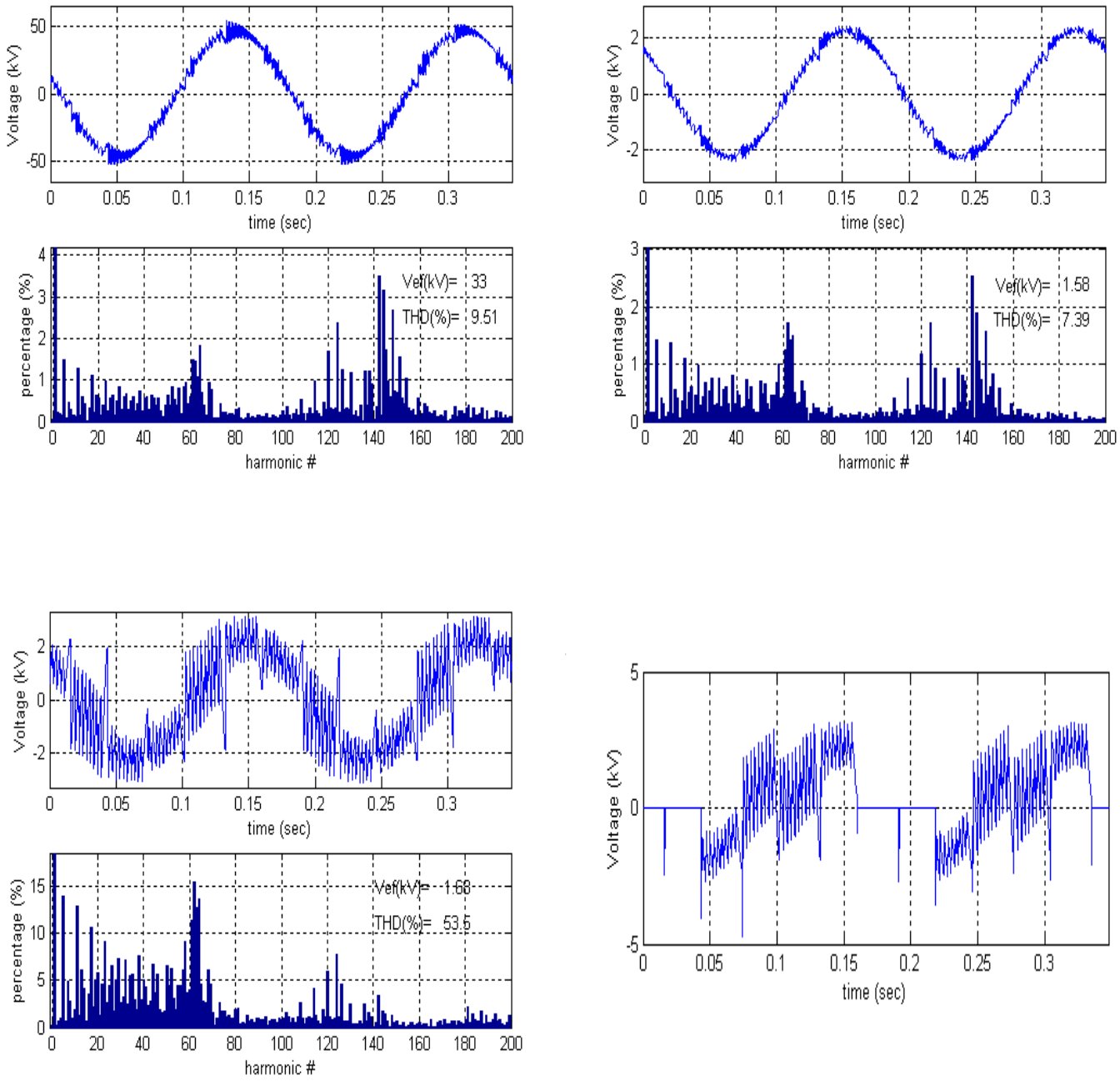

Figure B.12 Voltage waveforms at forced commutation (a) Vtab line-line voltage at the transformer HV side (b) Vtlab line-line voltage at the transformer LV side (c) Vab Line line voltage at the SFC output (d) Et3 Voltage at the terminals of an inverter GTO

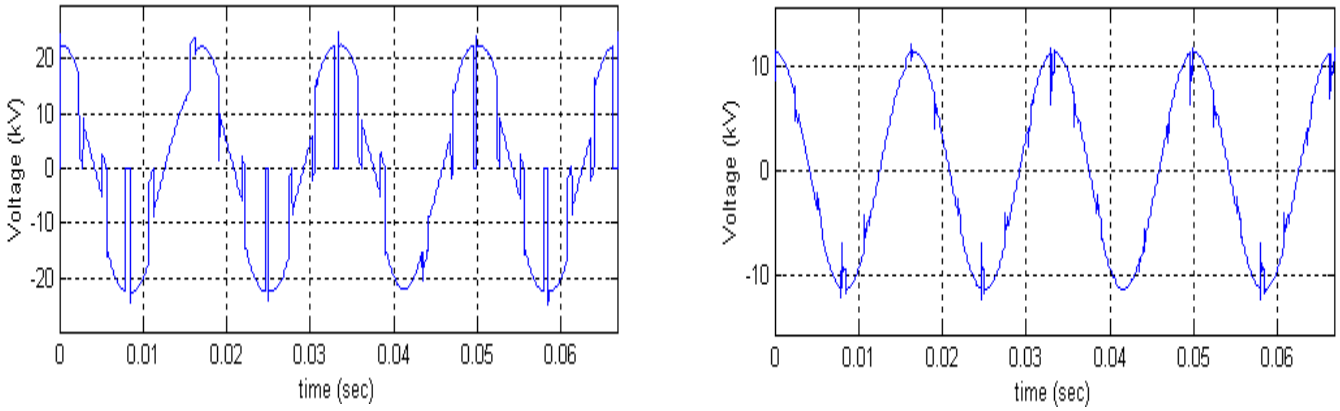

Figure B.13 Voltage waveforms during forced commutation (a) Vsab Line-line voltage at the SFC input side (b) Vna Line-ground voltage at the primary side of the auxiliary transformer 13.8 kV

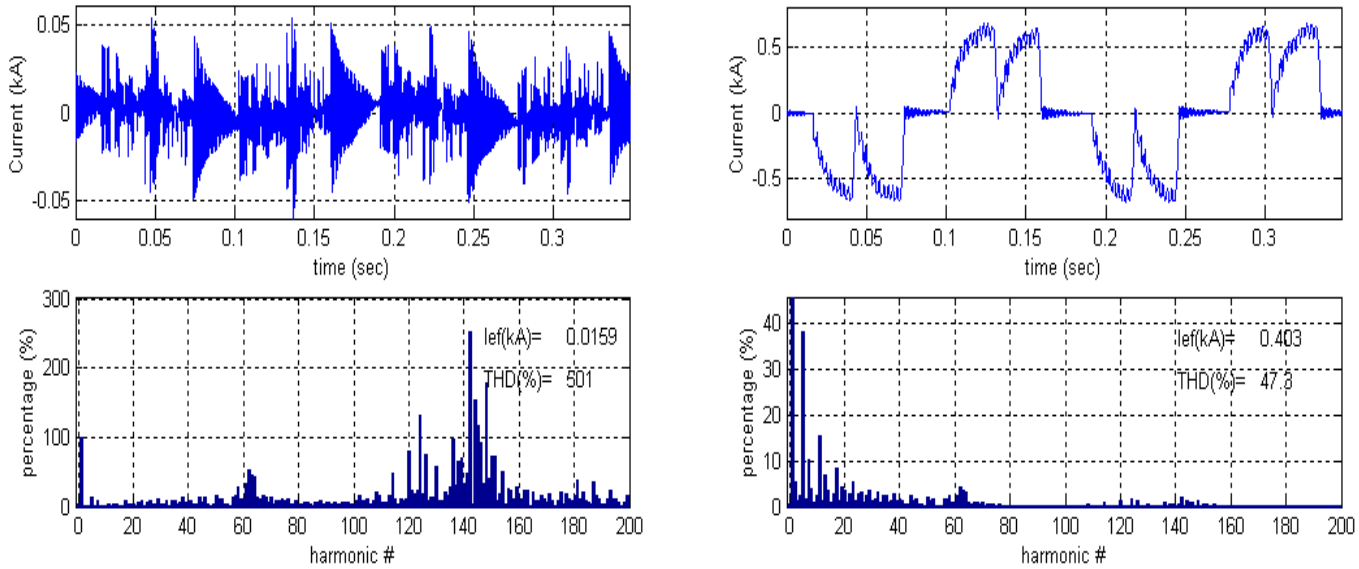

Figure B.14 Current waveforms during forced commutation operation (a) Iat Line current at the transformer LV side (b) Iag current taken by the generator

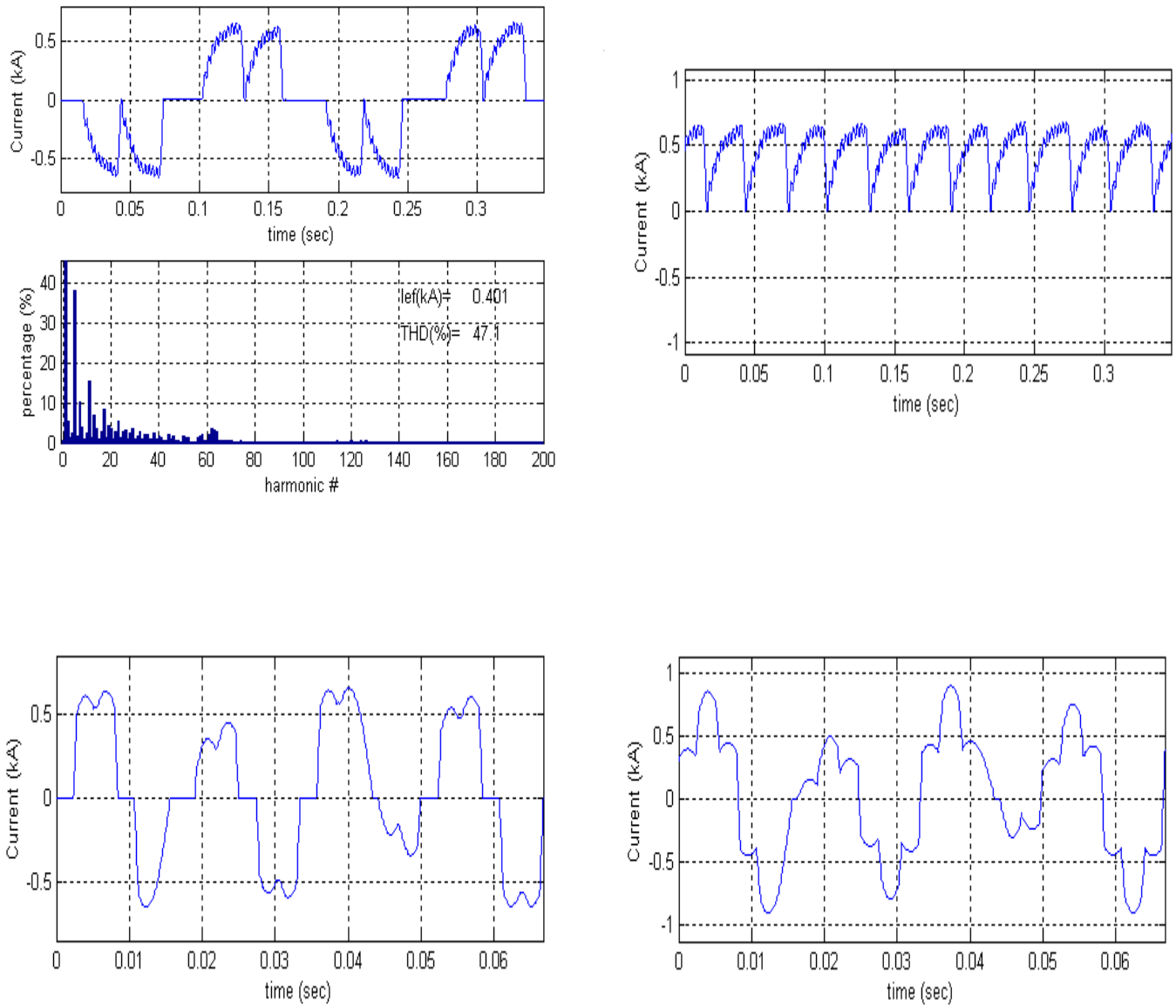

Figure B.15 Current waveforms at forced commutation operation (a) Iato SFC output current, it is observed the absence of higher order components which are absorbed by the generator (b) Irect Current in the DC interface (c) Isa current at the SFC input (d) Isa2 current at the primary side of the auxiliary transformer, 13.8 kV

B.6 Snubber circuit not operative

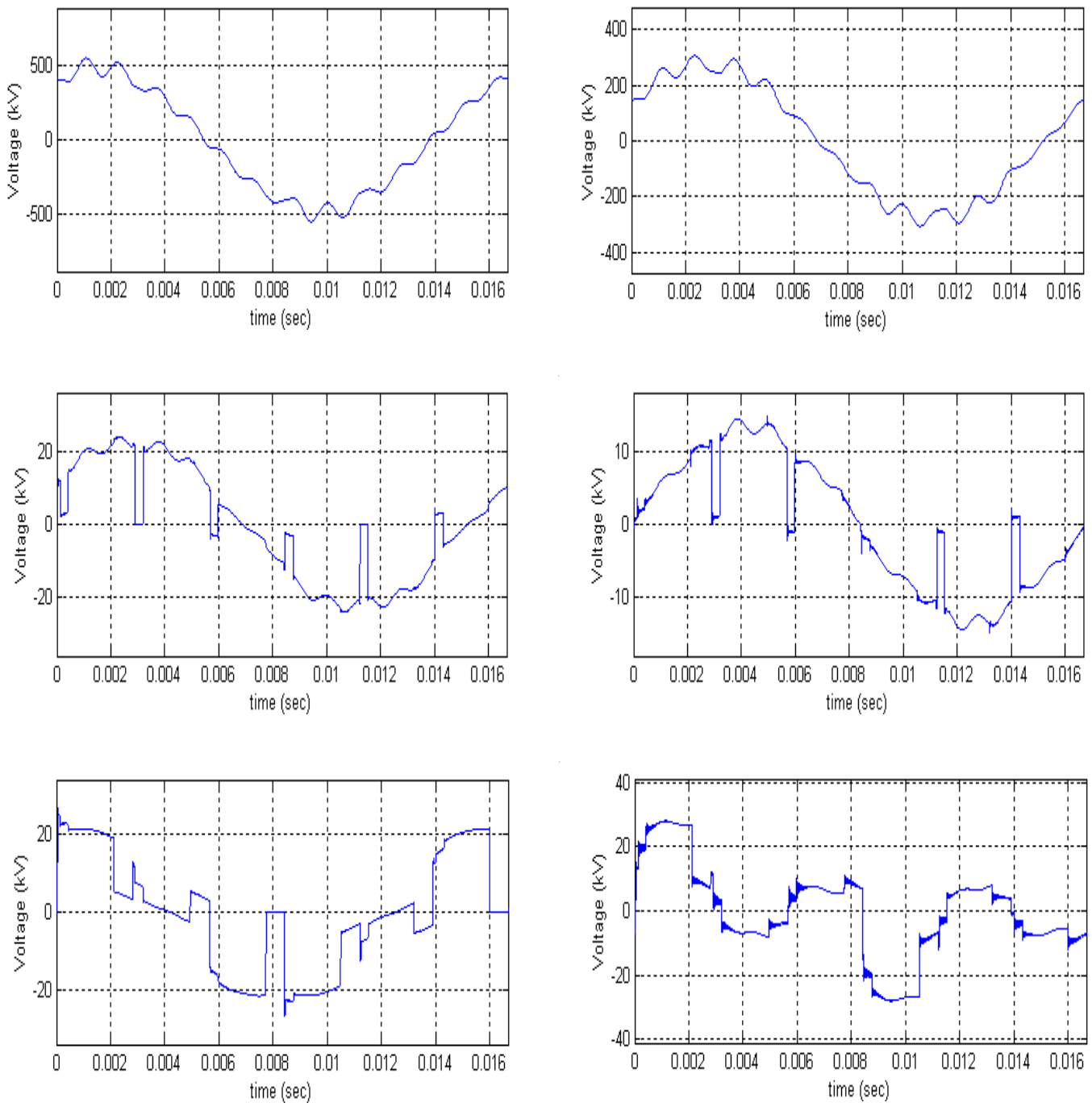

Figure B.16 Voltage waveforms for the study of the commutation transient without snubber circuit (a) Vtab line-line voltage at the transformer HV side (b) Vta line-ground voltage at the transformer HV side (c) Vab line-line voltage at the SFC output (d) Va line-ground voltage at the SFC output side (e) Vsab line-line voltage at the SFc input side (f) Vsa line-line voltage at the SFC input side

B.7 Snubber Circuit Operative

B.7.1 Natural Commutation

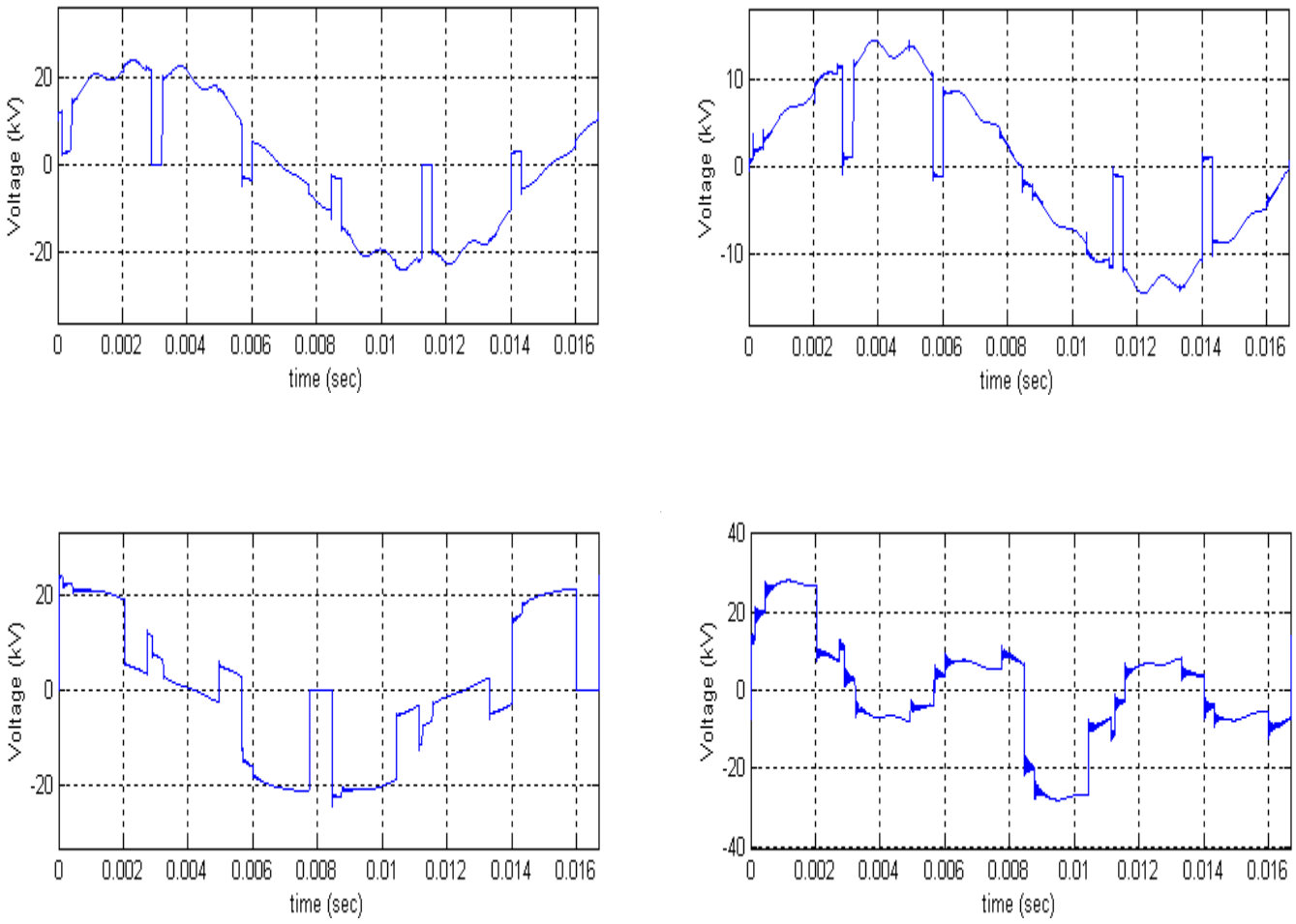

Figure B.17 Voltage waveforms at natural commutation for the study of the commutation transient with snubber circuit in operation (a) Vab line-line voltage at the SFC output (b) Va line-ground voltage at the SFC output (c) Vsab line-line voltage at the SFC input side (d) Vsa line-ground voltage at the SFC input side

B.7.2 Forced Commutation

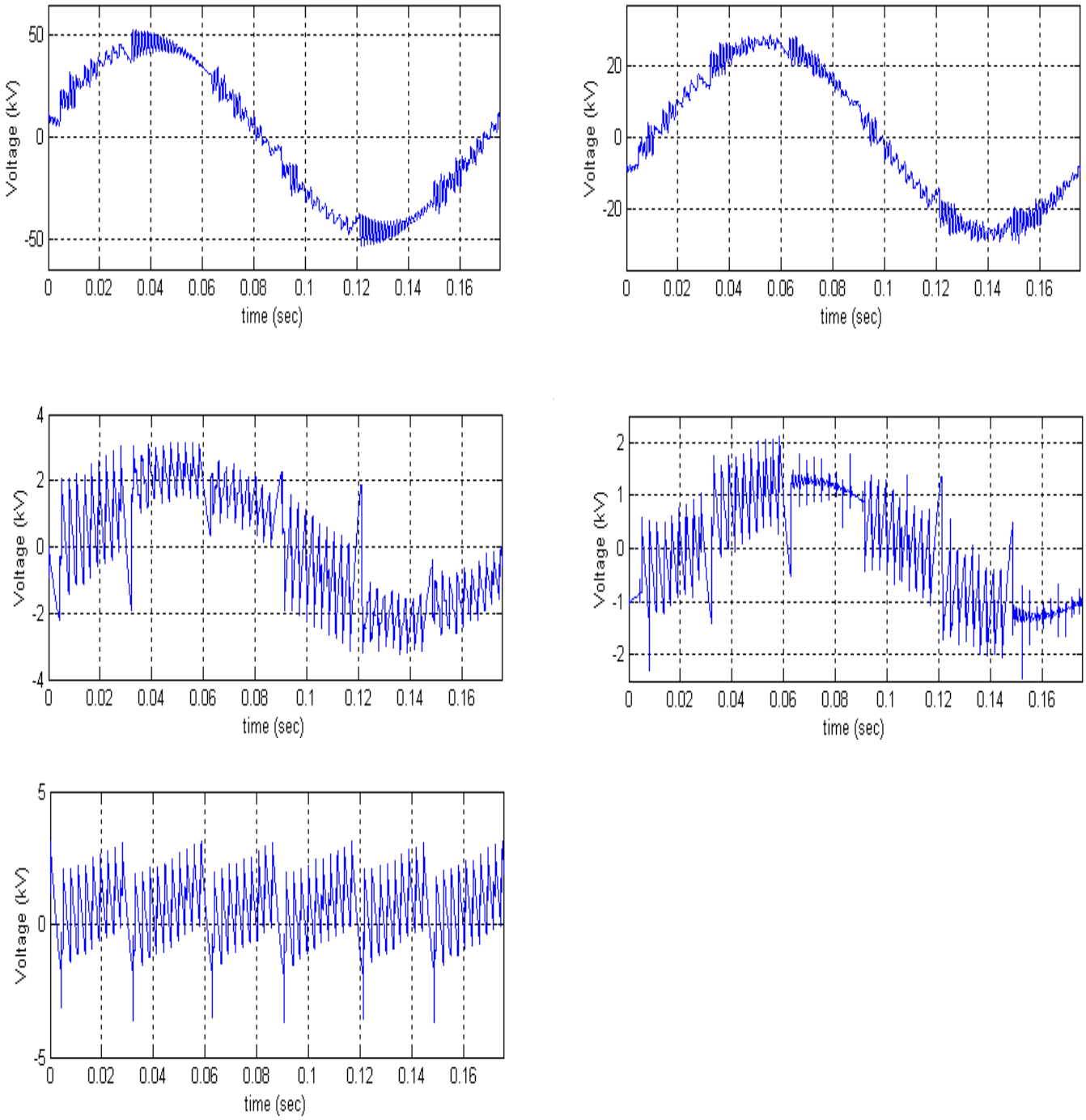

Figure B.18 Voltage waveforms at forced commutation for the study of the commutation transient with snubber circuit in operation (a) Vtab line-line voltage at the HV side of the transformer (b) Vta line-ground voltage at the HV side of the GSU transformer (c) Vab line-line voltage at the SFC output (d) Va line-ground voltage at the SFC output (e)Vis voltage at the DC interface

B.8 Failure in the Firing Sequence

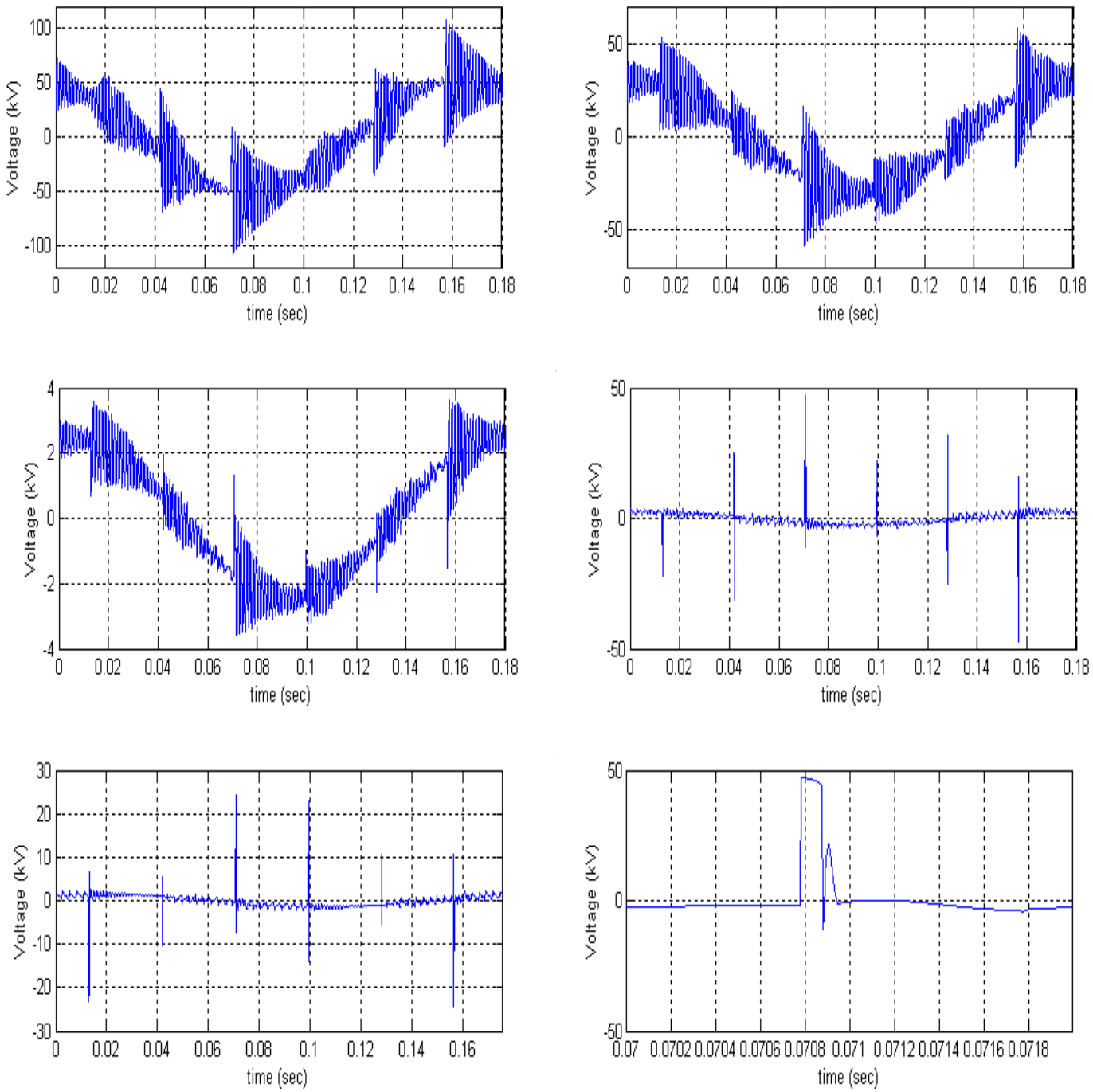

Figure B.19 Voltage waveforms for the study of the transient produced by a miss-synchronization of the firing pulses (a) Vtab line-line voltage at the transformer HV side (b) Vta line-ground voltage at the transformer HV side (c) Vtlab line-line voltage at the transformer LV side (d) Vab line-line voltage at the SFc output (e) Va line-ground voltage at the SFC output (f) Enlargement of Vab to observe the details of the spike

References

[1] G. Magsaysay et al., "Use of a Static Frequency Converter for Rapid Load Response in Pumped-Storage Plants," IEEE Trans. Energy Conversion, Vol. 10, No. 4, December 1995

[2] R. Rudenberg, *Transient performance of Electric power systems*, M.I.T., London, UK, 1970

[3] A. Greenwood, *Electrical Transients in Power Systems* 2nd ed., Wiley, New York, 1991

[4] Elkins et al, Transients During 138KV SF6 Breaker Switching of Low Inductive Currents. IEEE Trans. on Industry Applications, vol. 29, no.4, July 1993.

[5] CIGRE Working group 33/13-09, "Very Fast Transient Phenomena Associated with Gas Insulated Substations", CIGRE Report 33-13, 1988

[6] Y. Shibuya et al, "Effects of Very Fast Transient Overvoltages on Transformer", IEE Proc. Gener. Transm. Distrib., vol. 146, no. 4, July 1999

[7] IEEE working group report, "Estimating lightning performance of transmission lines. II. Updates to analytical models", IEEE Transactions on Power Delivery, vol.8, no.3, July 1993, pp.1254-67

[8] J. Arrillaga, D. Bradley, P. Bodger, *Power System Harmonics,* John Wiley & Sons, 1985

[9] A. Arsoy et al. *Modeling and Simulation of Power System Harmonics,* IEEE Press, Piscataway NJ, 1998

[10] R. Dugan et al., *Electrical Power Systems Quality*, McGraw-Hill, 1996

[11] R. Tessendorf, "Application of Arresters and Surge Protective Devices to DC Drives", Conf. Rec. of 1986 Annual Pulp and Paper Industry Technical Conference, IEEE, pp.66-70, 1986

[12] K. Harada et al, "Optimum Design of RC Snubbers for Switching Regulators", IEEE Transactions on Aerospace and Electronic Systems, vol. AES-15, no. 2, March 1979

[13] J. Olivier, G. Stone, "Implications of the Application of Adjustable Speed Drive Electronics to Motor Stator Winding Insulation", IEEE Electrical Insulation Magazine, pp.32-36, 1995

[14] C. Lanier, "A novel Technique for the Determination of Relative Corona Activity within Inverter-Duty Motor Insulation Systems Using Steep-Fronted Voltage Pulses", Conf. Record of the 1998 Int. Sym. On Electrical Insulation, pp. 229-236, 1998

[15] CIGRE Joint Working Group 12/14.10, "HVDC converter transformers", CIGRE 1996: 12-202

[16] X. Dong et al., "Simulation of switching, SFC, and lightning transients in Mingtan pumped storage plant (Final Report)", unpublished work

[17] S. P. Kennedy, C.L. Ivey, "Application, Design and Rating of Transformers Containing Harmonic Currents", Pulp and Paper Industry Technical Conference, 1990, Conference Record pp: 19-31

[18] E. Fuchs, R. Fei, "A New Computer-Aided Method for the Efficiency Measurement of Low-loss Transformers and Inductors Under Non-sinusoidal Operation", IEEE Trans. On Power Delivery, Vol. 11, No.1, January 1996

[19] E. Emmanuel, X. Wang, "Estimation of loss of life of Power Transformers Supplying Non-linear Loads", IEEE Trans. On Power Apparatus and Systems, Vol PAS-104, no.3, March 1985

[20] IEEE Transformers Committee, "Standard Test Code for Liquid-Immersed Distribution, Power and Regulating Transformers", ANSI/IEEE std. C57.12.90, 1987

[21] M. A. Masoum, E. F. Fuchs, D. J. Roesler, "Impact of Nonlinear Loads on Anisotropic Transformers", IEEE Trans. On Power Delivery, October 1991, Vol. PWRD-6, pp. 1781-1778

[22] A. Kelley et al. "Transformer Derating for Harmonic Currents: A Wide-Band Measurement Approach for Energized Transformers", IEEE Trans. On Industry Applications, vol. 35, no. 6, Nov/Dec 1999

[23] IEEE Transformers Committee, "IEEE Recommended Practice For Establishing Transformer Capability When Supplying Nonsinusoidal Load", Std C57.110-1998, 1998

[24] Underwriters Laboratory, "Dry Type General Purpose and Power Transformers", Standard UL 1561, Apr. 22, 1994

[25] D. Yildrim, E. Fuchs, "Measured Transformer Derating and Comparison with Harmonic Loss Factor (F_{HL}) Approach", IEEE Trans. On Power Delivery, vol. 15, no.1, Jan 2000

[26] A. Delaiba et al., "The Effect of Harmonics on Power Transformers Loss of Life", Proceedings of the 38th Midwest Symposium on Circuits and Systems, 1995, pp 933-936 vol.2

[27] P. Krause, *Analysis of electric Machinery*, McGraw-Hill, 1986

[28] B. K. Bose, *Power Electronics and AC Drives*, Prentice-Hall, New Jersey, 1986

[29] U. de Martinis, et al., "On the Evaluation of the Harmonic Impedances in AC/DC Systems," ICHPS V Int. Con. on Harmonics in Power Systems. IEEE, pp.102-6. New York, 1992

[30] J. Eggleston at al. "Harmonic Norton Equivalent of the Synchronous Generator," Journal of Electrical and Electronic Eng., Australia, Vol. 7, No. 1, March 1987

[31] P. Hart, J. Bonwick, "Harmonic Modeling of Synchronous Machines," IEE Proceeedings, vol. 135, Pt. B, No. 2, March 1988

[32] X. Zhang, E. Handschin, "Frequency-Dependent Simple Harmonic Model of Synchronous Machines," IEEE Power Engineering Review, vol.20 No.5, May 2000

[33] E. W. Kimbark, *Power System Stability*, Vol. 3, Synchronous Machines, IEEE Press, New York, 1995.

[34] P. Anderson, A. Fouad *Power System Control and Stability*, Iowa State University Press, 1986

[35] J. Martinez-Velasco, "ATP Modeling of Power Transformers," European EMTP-ATP Users Group News, pp. 63-76, Aug-Nov 1998

[36] W. Dugui, X. Zheng, "Harmonic Model of Power Transformer", 1 Harmonic model of power transformer", Proceedings. POWERCON '98. Int. Con. Power System Technology, Vol. 2, pp. 1045 –1049, 1998

[37] Task Force on Harmonic Modeling & Simulation "Modeling and Simulation of the Propagation of Harmonics in Electric Power Networks – Part I", IEEE Trans. Power Delivery, Vol. 11, No. 1, January 1996

[38] Manitoba HVDC Research Centre, *EMTDC Theory Manual*, Winnipeg, 1994

[39] T-H. Liu et al. "Modeling and Performance of a Static Frequency Converter Starting a 300MVA Synchronous Machine", Electric Power Systems Research, vol.37, pp.45-53, 1996.

[40] K.V. Rao et al., “Static Frequency Converter Starting of Microsynchronous Motor,” Journal of the Institution of Engineers (India), Part El, vol.64, pp.241-7, April 1984

[41] B. Mueller et al. “Static Variable Frequency Starting and Drive System for Large Synchronous Motors”, Conf. Rec. IEEE/IAS Annual Meeting, pp. 429-438, 1979

[42] J. Murphy, F. Turnbull, *Power Electronic Control of AC Motors,* Pergamon Press, Oxford, 1988

[43] Le-Huy et al., “Microprocessor Control of a Current-fed Synchronous Motor Drive”, Report from the IEEE/IAS Annual Meeting, pp. 873-880, 1979

[44] R. Krishnan, *Electronic Control of Machines*, Virginia Tech, Blacksburg VA, 1999

[45] A. Trzynadlowski, “Introduction to Modern Power Electronics”, John Wiley &Sons, 1998

[46] G. Heydt, “Power System Quality”, Stars in a Circle Publications, 1991

[47] D. Rice, “Adjustable Speed Drive and Power Rectifier Harmonics-Their Effect on Power System Components”, IEEE Transactions on Industry Applications, vol. IA-22, no.1, pt. 1, Jan-Feb 1986, pp 161-77

[48] L. X. Bui, G. Morin, “Some Experiences in Power System Simulation Using Electromagnetic Transient Programs”, Canadian Conference on Electrical and Computer Engineering, Vol. 2, pp 647–650, 1996

[49] T-H. Liu et al. “Modeling and Harmonics Elimination for a Static Frequency Converter Driving a 300MVA Synchronous Machine”, Proc. of the IEEE Int. Symposium on Industrial Electronics ISIE '96, IEEE. Part vol.2, pp.602-7, New York, 1996

[50] J-C. Chiang et al. “Mitigation of Harmonic Disturbance at Pumped Storage Power Station with Static Frequency Converter”, IEEE Tans. Energy Conversion, Vol.12, No. 3, Sep. 1997

Vita

Sebastian Rosado was born in Rosario, Argentina, on March 14th 1968. He got his electrical engineering degree from the National University of Rosario on March 1994. From 1994 to 1999 he worked as an electrical engineer at Acindar, a steel making company in Argentina. His work there dealt with the generation and distribution electric system of the company, a major consumer of electricity. From 1991 to 1999 he also worked as an assistant and teacher at the Polytechnic Institute of the National University of Rosario. On August 1999 he came to Virginia Tech to pursue his Masters degree in Electrical Engineering.